Government of Western Australia

Department of
Mines and Petroleum

REPORT
127

DEPOSITION, PROVENANCE, INVERSION HISTORY AND MINERALIZATION OF THE PROTEROZOIC EDMUND AND COLLIER BASINS, CAPRICORN OROGEN

by HN Cutten, SP Johnson, AM Thorne, MTD Wingate, CL Kirkland, EA Belousova, OA Blay, and H Zwingmann

EXPLORATION INCENTIVE SCHEME

CCFS

Curtin University

GEMOC

Geological Survey of Western Australia

Government of **Western Australia**
Department of **Mines and Petroleum**

REPORT 127

DEPOSITION, PROVENANCE, INVERSION HISTORY AND MINERALIZATION OF THE PROTEROZOIC EDMUND AND COLLIER BASINS, CAPRICORN OROGEN

by
HN Cutten, SP Johnson, AM Thorne, MTD Wingate, CL Kirkland[1], EA Belousova[2], OA Blay, and H Zwingmann[3]

1 Centre for Exploration Targeting — Curtin Node, Department of Applied Geology, Western Australian School of Mines, Curtin University, Bentley WA 6102

2 GEMOC, Department of Earth and Planetary Sciences, Macquarie University, Sydney NSW 2109

3 Department of Geology and Mineralogy, Graduate School of Science, Kitashirakawa Oiwakecho, Sakyo-ku, Kyoto University, Kyoto, 606-8502, Japan

Perth 2016

Geological Survey of Western Australia

REFERENCE
The recommended reference for this publication is:
Cutten, HN, Johnson, SP, Thorne, AM, Wingate, MTD, Kirkland, CL, Belousova, EA, Blay, OA and Zwingmann, H 2016, Deposition, provenance, inversion history and mineralization of the Proterozoic Edmund and Collier Basins, Capricorn Orogen: Geological Survey of Western Australia, Report 127, 74p.

National Library of Australia Cataloguing-in-Publication entry:

Creator:	Cutten, H.N., author.
Title:	Deposition, provenance, inversion history and mineralization of the proterozoic Edmund and Collier basins, Capricorn orogen / HN Cutten, SP Johnson, AM Thorne, MTD Wingate, CL Kirkland, EA Belousova, H Zwingmann.
ISBN:	9781741686913 (ebook)
Subjects:	Siliceous rocks--Western Australia--Capricorn Range Region. Mines and mineral resources--Western Australia--Capricorn Range Region. Geological surveys--Western Australia--Capricorn Range Region. Geology, Stratigraphic--Proterozoic. Capricorn Range Region (W.A.)
Other Authors/Contributors:	Johnson, S. P., author. Thorne, A. M., author. Wingate, M. T. D. (Michael Thomas David), author. Kirkland, C. L., author. Belousova, E. A., author. Zwingmann, H., author. Geological Survey of Western Australia, issuing body.
Dewey Decimal Classification:	552.509941

ISSN 0508–4741

U–Pb measurements were conducted using the SHRIMP II ion microprobes at the John de Laeter Centre at Curtin University in Perth, Australia. Isotope analyses were funded in part by the Western Australian Government Exploration Incentive Scheme (EIS). Lu–Hf measurements were conducted using LA-ICPMS at the ARC National Key Centre for Geochemical Evolution and Metallogeny of Continents (GEMOC), via the ARC Centre of Excellence in Core to Crust Fluid Systems (CCFS), based in the Department of Earth and Planetary Sciences at Macquarie University, Australia.

Grid references in this publication refer to the Geocentric Datum of Australia 1994 (GDA94). Locations mentioned in the text are referenced using Map Grid Australia (MGA) coordinates, Zone 50. All locations are quoted to at least the nearest 100 m.

Published 2016 by Geological Survey of Western Australia
This Report is published in digital format (PDF) and is available online at <www.dmp.wa.gov.au/GSWApublications>.

Further details of geological publications and maps produced by the Geological Survey of Western Australia are available from:
Information Centre | Department of Mines and Petroleum | 100 Plain Street EAST PERTH WESTERN AUSTRALIA 6004
Telephone: +61 8 9222 3459 Facsimile: +61 8 9222 3444 | **www.dmp.wa.gov.au/GSWApublications**

Cover photograph: Landscape view of the southern end of the Four-T Syncline, Uaroo 1:100 000 scale geological map, with fine-grained sandstone of the Kiangi Creek Formation, Edmund Group, in the foreground and silicified siltstone in the background (photograph by HN Cutten)

Contents

Appendices

Figures

Tables

Deposition, provenance, inversion history and mineralization of the Proterozoic Edmund and Collier Basins, Capricorn Orogen

by

HN Cutten, SP Johnson, AM Thorne, MTD Wingate, CL Kirkland[1], EA Belousova[2], OA Blay and H Zwingmann[3]

Abstract

The 1679–1067 Ma Edmund and Collier Basins, which comprise about 4–12 km of siliciclastic sedimentary rocks, are the youngest depositional elements of the Proterozoic Capricorn Orogen — the collision zone between the Archean Pilbara and Yilgarn Cratons. The Edmund Basin was deposited within a half-graben structure, produced during 7–8% regional-scale extension by the reactivation of pre-existing basement faults. The architecture and tectonic setting of the overlying Collier Basin is still poorly understood. Paleocurrent directions within rocks of the Edmund Basin indicate a northerly source for sediment detritus, although the ages and Lu–Hf isotope compositions of detrital zircon grains suggest they were ultimately derived from the Gascoyne Province basement to the south. These results imply that detritus was recycled many times, first from the Gascoyne Province into the northern Capricorn Orogen basins, and then as a second cycle into the Edmund Basin. The detrital zircon record of the Collier Basin suggests that most material was sourced from the uplifted and eroded Edmund Basin. Regional-scale basin inversion and shortening averages about 21%, and resulted from orogenwide deformation during both the 1321–1171 Ma Mutherbukin Tectonic Event and the 1026–954 Ma Edmundian Orogeny. The Edmund and Collier Groups are host to a wide range of mineral occurrences, including the polymetallic Abra deposit in the Edmund Basin. Although little is known about the mineral systems setting of these occurrences, many of them, including Abra and the supergene Ilgarari and Butcherbird deposits in the Collier Basin, are directly associated with major crustal-scale faults that have been reactivated many times.

KEYWORDS: compression, cross sections, deformation (structural geology), extension, faults, folds, geochronology, mineralization, orogeny, Proterozoic, sedimentary basins

Introduction

The Proterozoic Edmund and Collier Basins contain about 4–12 km of siliciclastic, carbonate, and minor volcaniclastic low-grade metasedimentary rocks that were deposited in a variety of fluvial to deep-marine environments (Martin and Thorne, 2004). They form the youngest depositional elements of the Proterozoic Capricorn Orogen and extend for over 600 km in a convex northwest- to west-trending belt between the Pilbara and Yilgarn Cratons (Fig. 1). The rocks have been extensively folded and faulted, and subject to low-grade metamorphism during numerous intracontinental reworking events (Martin and Thorne 2004; Sheppard et al., 2010b; Zi et al., 2015; Korhonen et al., 2015). Although the depositional settings of the Edmund and Collier Basins are well known (Martin and Thorne, 2004; Martin et al., 2008), the timing and style of basin formation, provenance, and subsequent history of structural inversion are far less constrained.

The Capricorn Orogen is a 1000 km-long by 500 km-wide belt of deformed meta-igneous and metasedimentary rocks between the Archean Pilbara and Yilgarn Cratons (Cawood and Tyler, 2004). The orogen records the collision of the Pilbara and Yilgarn Cratons during the 2215–2145 Ma Ophthalmia and 2005–1950 Ma Glenburgh Orogenies (Johnson et al., 2011b), as well as over one billion years of intracratonic reactivation and reworking (Sheppard et al., 2005, 2010a,b; Johnson, 2013; Johnson et al., 2013; Korhonen et al., 2015). The two oldest reworking events,

1 Centre for Exploration Targeting — Curtin Node, Department of Applied Geology, Western Australian School of Mines, Curtin University, Bentley WA 6102

2 GEMOC, Department of Earth and Planetary Sciences, Macquarie University, Sydney NSW 2109

3 Department of Geology and Mineralogy, Graduate School of Science, Kitashirakawa Oiwakecho, Sakyo-ku, Kyoto University, Kyoto, 606-8502, Japan

the 1817–1772 Ma Capricorn Orogeny (e.g. Sheppard et al., 2010a) and the 1680–1620 Ma Mangaroon Orogeny (e.g. Sheppard et al., 2005) were characterized by widespread deformation and sedimentation, regional metamorphism, and voluminous granite magmatism. Subsequent episodes of tectonic reactivation resulted in deformation and metamorphism with little or no granite magmatism or sedimentation, as exemplified by the 1321–1171 Ma Mutherbukin Tectonic Event (e.g. Korhonen et al., 2015), the 1026–954 Ma Edmundian Orogeny (e.g. Sheppard et al., 2007; Thorne et al., 2016) and the c. 570 Ma Mulka Tectonic Event (e.g. Sheppard et al., 2010b). Importantly, the Edmund and Collier Groups were deposited between major tectonic episodes, after the cessation of all major granite magmatism in the orogen. The significance of this major switch in style of tectonic reworking is currently unknown. Despite these differences, the underlying collisional architecture, imparted during the Ophthalmia and Glenburgh Orogenies, appears to have fundamentally controlled the location and orientation of all the subsequent reworking events, including the depositional architecture and inversion history of the basins (Johnson et al., 2013). Reactivation of these major faults and shear zones also appears to have controlled the location of major gold and base-metal deposits, highlighting the importance of major crustal-scale structures and fluid flow to mineral systems (Johnson et al., 2013; Johnson, 2014).

Geological mapping (1:100 000 scale) and zircon and baddeleyite geochronology by the Geological Survey of Western Australia (GSWA) has provided a wealth of data on the depositional history of the Edmund and Collier Basins, particularly in the western part of the orogen, as well as an initial evaluation of their deformation history (e.g. Martin and Thorne, 2004; Martin et al., 2008). However, more recent geological mapping in the eastern part of the basins (Blay and Thorne 2015; Blay et al., 2014, 2012a,b; Blay and Thorne 2015; Cutten et al., 2013, 2010; Thorne and Cutten, 2010, 2011), combined with in situ phosphate geochronology (Zi et al., 2015; Korhonen et al., 2015; Rasmussen et al., 2010), and a deep crustal seismic reflection survey across the entire Capricorn Orogen (Fig. 2; Johnson et al., 2011a, 2013), has significantly advanced our understanding of the structural evolution of these basins, including the timing and setting of base-metal and gold mineralization. In this Report, we provide a comprehensive outline of the Edmund and Collier Basin stratigraphy, including the spatial distribution and thickness variations of individual units, as well as constrain the sedimentary source components from the U–Pb and Lu–Hf isotope compositions of detrital zircons. These factors provide critical information on the growth history of the basins, including the location and identity of uplifted source regions, and the timing of movement and downdrop on individual faults and

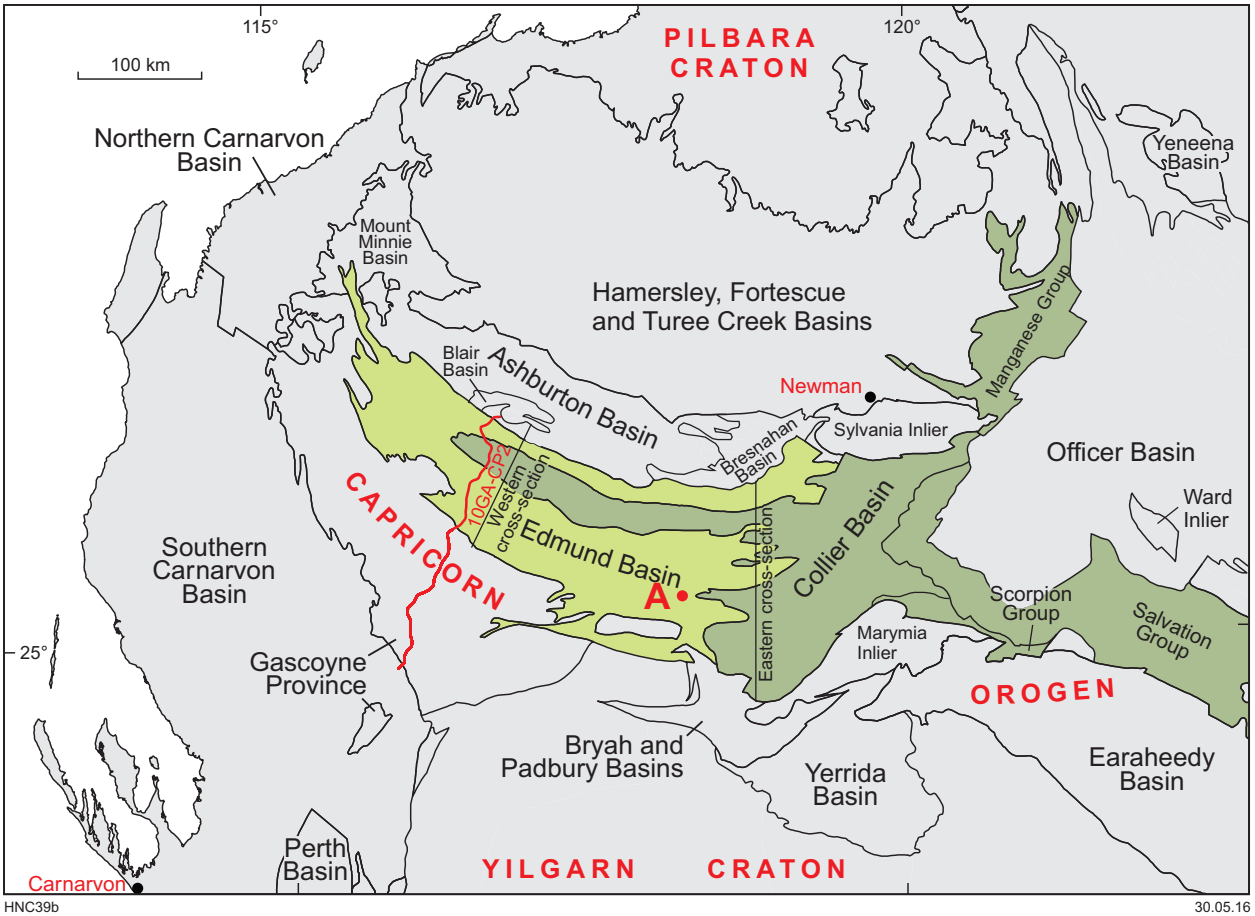

Figure 1. Location of the Edmund and Collier Basins and older sedimentary basins in the Capricorn Orogen. Note the location of the Capricorn Orogen deep crustal seismic reflection survey 10GA-CP2, the Abra polymetallic deposit (A), and the western and eastern cross-sections.

intervening fault blocks. We also resolve the amount of regional-scale extension that accompanied basin formation and the amount of shortening that took place during each of the intracontinental reworking events. This improved understanding of basin formation, and inversion provides the critical geological framework for evaluating the mineral prospectivity of these two basins.

Edmund and Collier Groups

The Edmund and Collier Groups were divided by Martin and Thorne (2004) into six depositional packages (Fig. 3). Depositional Packages 1–4 comprise the Edmund Group and Depositional Packages 5 and 6, the Collier Group. These packages are defined by basal unconformities or major marine flooding surfaces and are the result of differential fault movements or fluctuations in sea level (Martin and Thorne, 2004). The ages of the Edmund and Collier Groups are relatively poorly constrained, but the Edmund Group was probably deposited some time between c. 1679 and 1452 Ma, and the Collier Group some time between c. 1171 and 1069 Ma. Multiple generations of dolerite sills intrude both the Edmund and Collier Groups, and these may have inflated the stratigraphic thickness by as much as 60% (Morris and Pirajno, 2005). These sills include the 1517–1505 Ma Waldburg Dolerite (Wingate et al., 2012b, 2013a; Blay et al., 2015) and the 1465–1452 Ma Narimbunna Dolerite (Wingate, 2002), both of which intrude only the Edmund Group, and the 1084–1067 Ma Kulkatharra Dolerite, which intrudes both the Edmund and Collier Groups (Wingate, 2002).

Edmund Group

The Edmund Group (Thorne, 2015a) is a mixed siliciclastic and carbonate sedimentary unit made up of (in ascending stratigraphic order) four depositional packages including the Yilgatherra and Irregully Formations (Depositional Package 1), the Gooragoora, Blue Billy, and Cheyne Springs Formations (Depositional Package 2), the Kiangi Creek and Muntharra Formations (Depositional Package 3), and the Discovery, Devil Creek, Ullawarra, and Coodardoo Formations (Depositional Package 4).

The maximum depositional age of the Edmund Group is poorly constrained. On the Edmund 1:250 000 map sheet (Martin et al., 2005), the Edmund Group unconformably overlies older tectonic units of the Gascoyne Province, including granitic rocks of the 1680–1620 Ma Durlacher Supersuite, specifically the 1675–1660 Ma Dingo Creek, Pimbyana, and Yangibana Granites (Sheppard et al., 2010b). Although the 1644–1619 Ma Discretion Granite on Marquis is the youngest granite phase in the Durlacher Supersuite (Sheppard et al., 2010b), the boundary between the Discretion Granite and the overlying Edmund Group is faulted and the true nature of the contact, whether it is intrusive or unconformable, cannot be determined. The Edmund Group is interpreted to overlie the Mount Augustus Sandstone, which contains detrital zircons as young as c. 1679 Ma (Martin et al., 2008) but the contact is either faulted or not exposed. This age is used as a conservative older age limit for the Edmund Group.

The minimum age for the lower part of the Edmund Group (Yilgatherra to Gooragoora Formations) is given by the timing of the earliest phase of mineralization in the Irregully and Gooragoora Formation host rocks at the Abra polymetallic deposit. This event has been dated to between c. 1610 and 1590 Ma, based on the U–Pb age of hydrothermal xenotime within the deposit (Zi et al., 2015; Johnson et al., 2015a). The younger limit for mineralization at c. 1590 Ma also provides a maximum age for the Kiangi Creek Formation in the middle part of the group, because this unit unconformably overlies the mineralized rocks. Sills belonging to the Waldburg Dolerite (Blay et al., 2015) have been emplaced into the Kiangi Creek Formation and lower parts of the Edmund Group on Mount Augustus, Mangaroon, and Candolle. These sills have igneous crystallization ages of 1517–1505 Ma (Wingate et al., 2015a,b; 2012b) and provide a younger age limit for the Blue Billy, Cheyne Springs and Kiangi Creek Formations.

The minimum age of c. 1452 Ma for the Edmund Group is derived from the ages of felsic volcaniclastic rocks within the Ullawarra Formation near the stratigraphic top of the succession, and also from the age of the c. 1465 Ma Narimbunna Dolerite, which intrudes the Edmund Group. Wingate et al. (2010a, 2012a) obtained maximum depositional ages of 1463 ± 8 Ma and 1455 ± 9 Ma from felsic volcaniclastic units within the Ullawarra Formation on Milgun and Calyie, which are interpreted as being close to depositional ages. In addition, Wingate (2010b) acquired an age 1461 ± 7 Ma from the youngest group of detrital zircons in a sandstone sample, taken from the Ullawarra Formation on Peedawarra. The dates obtained from the Ullawarra Formation are within uncertainty of the c. 1465 Ma Narimbunna Dolerite (Wingate, 2002; Martin et al., 2005) and indicate that dolerite intrusion, felsic volcanism, and sedimentation were essentially coeval.

Depositional Package 1

Depositional Package 1 (Thorne, 2015b; Fig. 3) is the basal package of the Edmund Group and comprises the Yilgatherra Formation and the overlying Irregully Formation. The Yilgatherra Formation unconformably overlies basement rocks of the Gascoyne Province, the Wyloo, Capricorn and Padbury Groups, and is in unconformable or in fault contact with the Mount Augustus Sandstone. Deposition of Package 1 was initially influenced by movement on the Deadman, Tringadee, and adjacent Turner Faults in the south of the basin and later by the Talga and Mount Vernon Faults (Figs 4 and 5) that separated the shallow-marine Pingandy Shelf (Muhling and Brakel, 1985a) to the north from a block-faulted terrain to the south (Martin and Thorne, 2004).

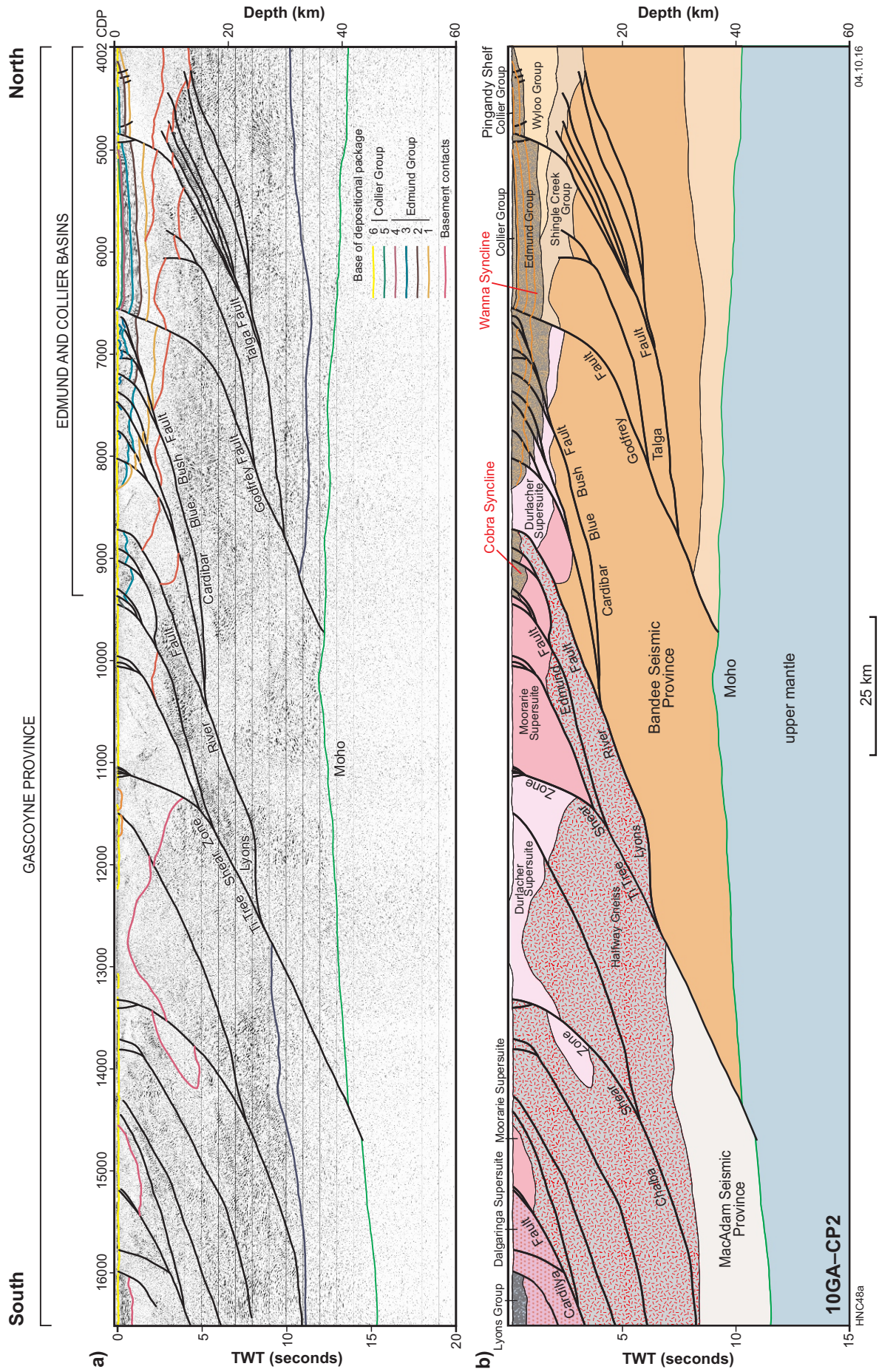

Figure 2. Part of the Capricorn Orogen deep crustal seismic reflection survey 10GA-CP2 showing the Edmund and Collier Basins (top right), basement architecture and the major faults including the Talga, Godfrey, Cardibar-Blue Bush, and Lyons River Faults. The Lyons River Fault – Ti Tree Shear Zone extends down to, and offsets, the Moho.

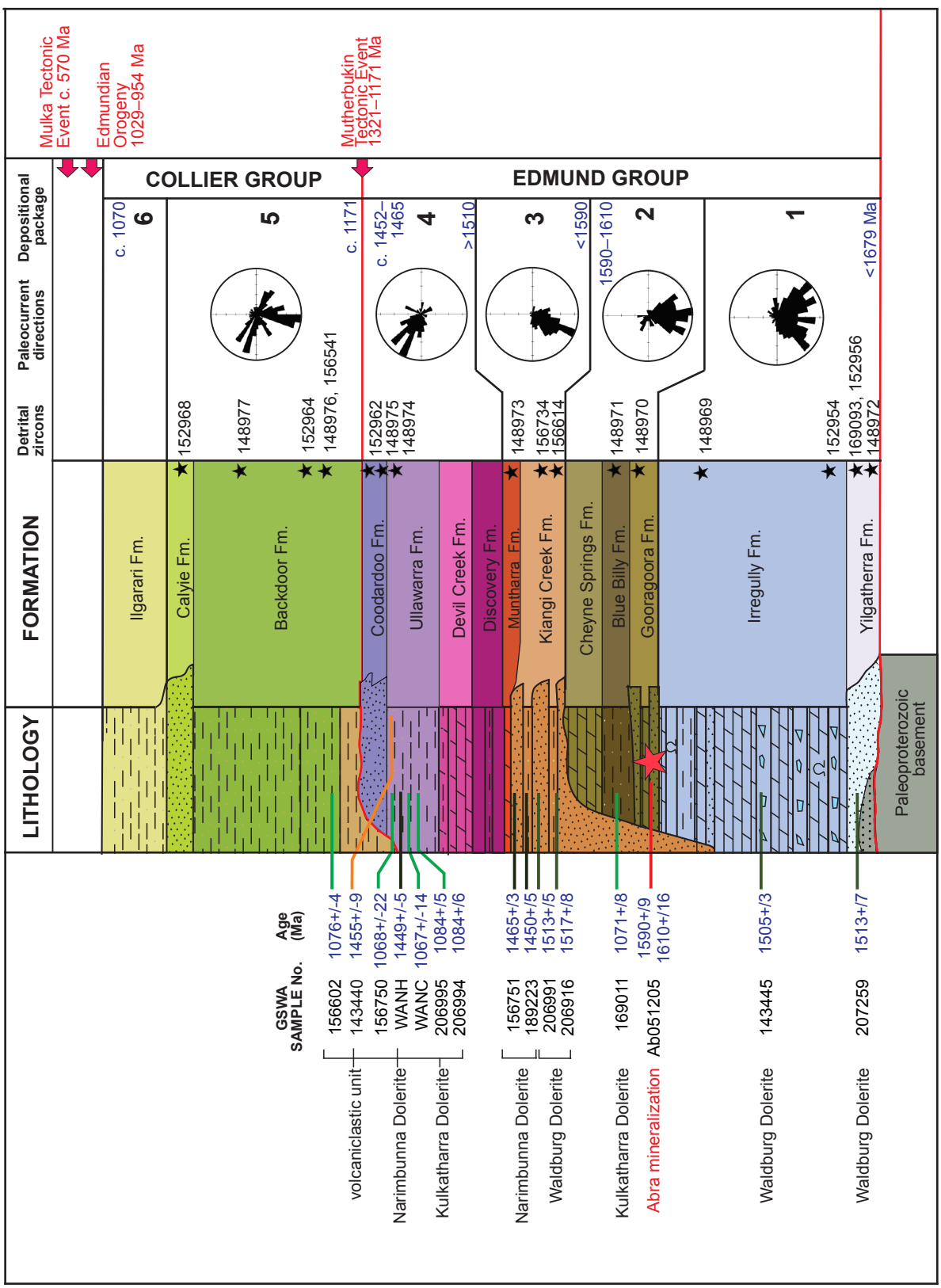

Figure 3. **Stratigraphy of the Edmund and Collier Groups showing subdivision into formations and depositional packages and the timing of tectonic events. The relative position in the stratigraphy of a dated volcaniclastic unit and Abra mineralization is indicated. The highest stratigraphic level of the intruding Kulkatharra, Narimbunna and Waldburg Dolerites provides minimum ages for units below, although these dolerite intrusions also occur lower in these units. The stratigraphic position of the detrital zircon samples is shown, as well as paleocurrent direction rose diagrams for each of the depositional packages.**

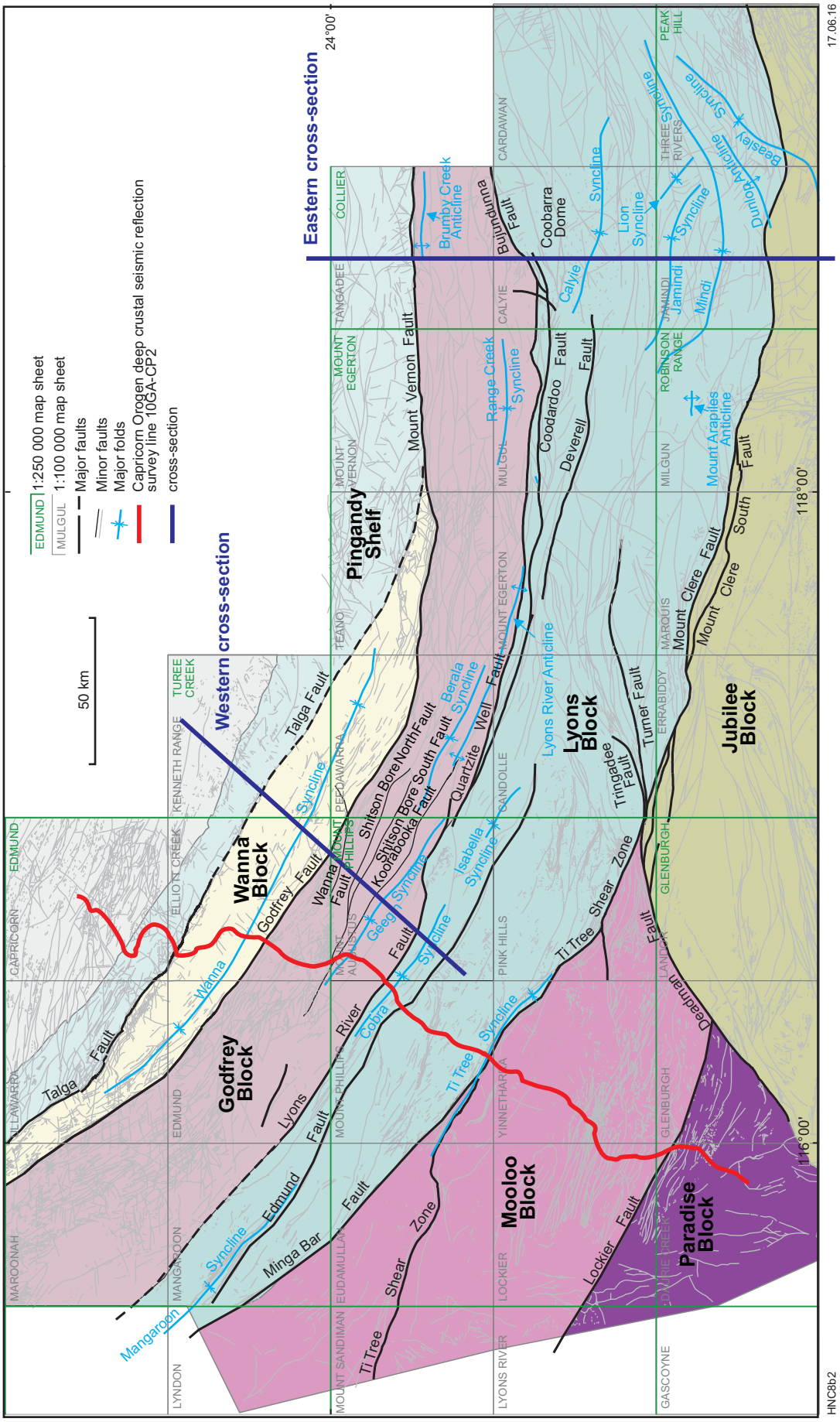

Figure 4. Named half-graben and marginal fault blocks of the study area, most of which are downthrown by normal movement on the northern margin of the fault block adjacent to each boundary fault (see also Fig. 11). The Capricorn Orogen deep crustal seismic reflection survey 10GA-CP2 is marked by the red line and the western and eastern cross-sections by heavy blue lines (see Figs 19 and 20).

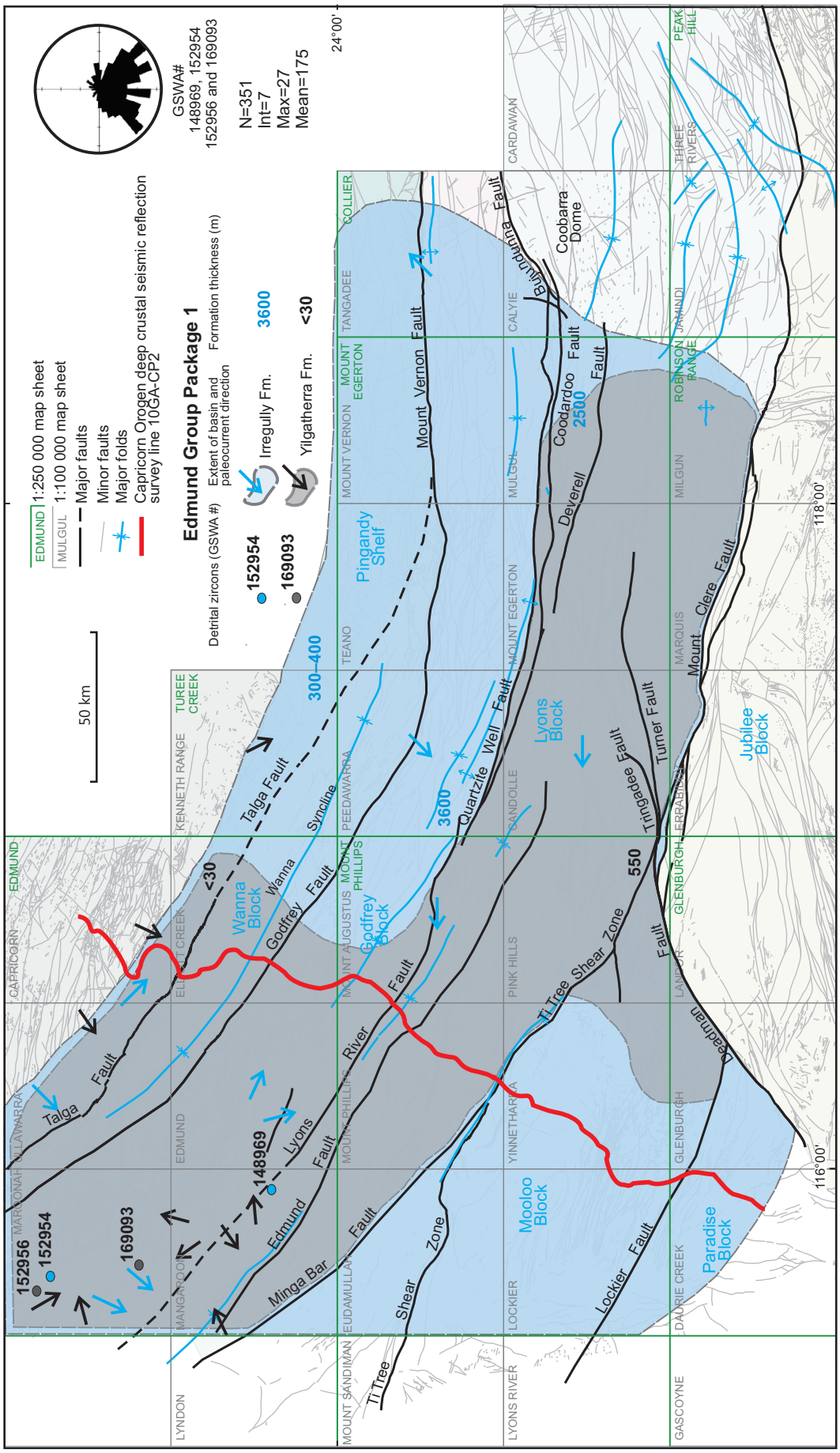

Figure 5. The extent and thickness of the Yilgatherra (dark grey), and Irregully Formations (pale blue) of Depositional Package 1, lower Edmund Group. The western and northwestern geographical extent (straight line margins) of Depositional Package 1 is currently unknown. Paleocurrent direction rose diagram is from Martin et al. (2008) and paleocurrent direction arrows are from Martin and Thorne (2004). The locations of detrital zircon geochronology samples are colour coded for the sampled formation and identified with their GSWA sample number. The sediment thicknesses in various parts of the basin are similarly colour coded.

Yilgatherra Formation

The Yilgatherra Formation (Daniels, 1970; Martin and Thorne, 2000; Thorne, 2015c) is an upward-fining succession of mainly fluvial to shallow-marine conglomerate and sandstone overlain by deeper marine siltstone. Low-grade, schistose metasandstones and metasiltstones form part of the Yilgatherra Formation in the Woodlands Dome area on Mulgul. The formation is thin (<30 m) and discontinuous in the Pingandy Shelf area, northeast of the Talga and Mount Vernon Faults on the Edmund and Turee Creek 1:250 000 map sheets (Figs 4, 5). Elsewhere, the formation is more continuous and forms extensive outcrops, particularly on Pink Hills and Candolle in the vicinity of the Deadman, Tringadee, and Turner Faults, where it attains its maximum thickness of 550 m. The Yilgatherra Formation is absent from the Coobarra Dome on Calyie (Cutten et al., 2010; Fig. 5), where the Irregully and Kiangi Creek Formations disconformably overlie granitic rocks of the 1820–1775 Ma Moorarie Supersuite. On the Pingandy Shelf, conglomerate and sandstone are locally interbedded with stromatolitic dolomite and planar-laminated siltstone. The conglomerates are tabular bedded with poorly to moderately developed parallel stratification in the lower levels that is transitional into parallel-stratified interbedded conglomerate and sandstone. The sandstones that overlie, and are interbedded with, the conglomerates are trough cross-stratified, and commonly contain disseminated pebbles. South of the Talga Fault, where conglomerates are generally thinner, the Yilgatherra Formation consists of an upward-fining succession, ranging from coarse- to very coarse-grained sandstone to planar-laminated siltstone. In the vicinity of the Deadman and Tringadee Faults, the lower part of the formation comprises medium- to very thick-bedded, medium- to very coarse-grained feldspathic or lithic quartz sandstones interbedded with subordinate conglomerate and pebbly sandstone. Middle to upper levels of the formation are dominated by fine- to medium-grained quartz sandstone and siltstone, interbedded with relatively minor amounts of coarse- to very coarse-grained sandstone and pebbly sandstone. Fluvial paleocurrent directions on the Pingandy Shelf are directed towards the southwest, but south of the Talga and Mount Vernon Faults are highly variable, towards the northwest, west, southwest, and southeast, suggesting they were influenced by local topographic highs (Fig. 5). The thick succession in the vicinity of the Deadman and Tringadee Faults records variable paleocurrent directions. The Yilgatherra Formation is intruded by, and therefore older than, a 1513 ± 4 Ma dolerite sill of the Waldburg Dolerite (Wingate et al., 2013a), emplaced at or near the contact with underlying basement rocks. The upper part of the Yilgatherra Formation and the overlying Irregully Formation is intruded by a Waldburg Dolerite sill dated at 1505 ± 3 Ma (Wingate et al., 2012b). The age of the Yilgatherra Formation at 1679–1610 Ma is based on the maximum age of the underlying Mount Augustus Sandstone and the age of mineralization in the overlying Irregully and Gooragoora Formations at the Abra polymetallic deposit in the eastern part of the basin (Zi et al., 2015).

Irregully Formation

The Irregully Formation (Daniels, 1966; Thorne, 2015d) either conformably overlies the Yilgatherra Formation or else unconformably overlies the Wyloo, Capricorn, and Bresnahan Groups, and basement rocks of the Gascoyne Province. On the Pingandy Shelf, northeast of the Talga and Mount Vernon Faults, the Irregully Formation is generally 300–400 m thick and consists mostly of peritidal shelf carbonates and stromatolitic shelf dolomites, interbedded with minor siliciclastic deposits. To the south and southwest of these faults, the formation markedly increases in thickness to over 3000 m, and contains slope carbonates as well as thick accumulations of fluvial to shallow-marine siliciclastic sedimentary rocks. These facies and thickness variations reflect active growth faulting and also suggest that much of the Irregully Formation on the Pingandy Shelf was subaerially exposed and eroded during times when areas south of the Talga and Mount Vernon Faults experienced fluvial and shallow-marine sedimentation. The Irregully Formation has a maximum thickness of 3600 m in the area of the Lyons River Anticline on Peedawarra and the Tringadee Fault on Candolle (Figs 4 and 5). Immediately south of the Quartzite Well Fault, the formation is up to 2500 m thick. Paleocurrent directions from cross-stratified sandstones on Edmund (1: 250 000 map sheet) are mostly directed towards the southwest, but are variable on central Edmund, with flow towards the west on Mount Augustus and Candolle, flow towards the southwest on Peedawarra, and flow towards the northeast on Tangadee (Fig. 5). The Irregully Formation is intruded by a dolerite sill of the Waldburg Dolerite dated at 1505 ± 3 Ma (Wingate et al., 2012b). The age of the Irregully Formation at 1679–1610 Ma is based on the maximum age of the underlying Mount Augustus Sandstone and the age of extensive hydrothermal alteration and mineralization of this unit within the Abra polymetallic deposit in the eastern part of the basin (Zi et al., 2015).

Depositional Package 2

Depositional Package 2 (Thorne, 2015e; Fig. 3) includes the Gooragoora, Blue Billy, and Cheyne Springs Formations (Martin and Thorne, 2004). The contact with Depositional Package 1 is a flooding surface resulting from a rise in sea level. The contact shows no sign of significant erosion. Outcrop is confined to the northwestern and northern parts of the Edmund Basin, but most likely extended farther to the south, with deposits removed by erosion prior to deposition of Depositional Package 3.

Gooragoora Formation

The Gooragoora Formation (Thorne, 2015f) is mostly composed of fine-grained to very coarse-grained quartz sandstone, feldspathic sandstone and siltstone, together with minor conglomerate and dolomite and has only been recognized on the Edmund and Winning Pool 1:250 000 map sheets and on Kenneth Range (Figs 4

and 6). Mineralized and hydrothermally altered sandstone units intersected in drillcore from the Abra polymetallic deposit on Calyie have been tentatively correlated with the Gooragoora Formation (Johnson et al., 2015a). Generally, the Gooragoora Formation is up to 250 m thick and has a sharp conformable contact with the underlying Irregully Formation. It is thought to have been deposited in a deltaic to shallow-marine shelf environment, at a time when the Edmund Basin experienced a rise in sea level and drowning of the Pingandy Shelf. In contrast to the underlying Irregully Formation, basement structures such as the Talga Fault had little influence on Gooragoora Formation sedimentation. Paleocurrent directions indicate flow towards the south, with some towards the northeast and northwest. The age of the Gooragoora Formation at 1679–1610 Ma is based on the maximum age of the underlying Mount Augustus Sandstone and the age of extensive hydrothermal alteration and mineralization of this unit at the Abra polymetallic deposit in the eastern part of the basin (Zi et al., 2015; Johnson et al., 2015a).

Blue Billy Formation

The Blue Billy Formation (Thorne, 2015g) is composed of a distinctive parallel-planar laminated, black, pyritic, carbonaceous, fissile to flaggy siltstone, interbedded with subordinate sandstone, dolomitic siltstone, and chert. Thicker deposits of medium- to coarse-grained quartz sandstone, dolomitic sandstone, and pebbly sandstone are found on Ullawarra, Maroonah and Edmund (Figs 4 and 6). The formation is up to 800 m thick, but is generally less than 200 m thick. The formation is thickest in the vicinity of Irregully Gorge on Capricorn and Ullawarra, and thins out to the south and to the east where it extends as far as Tangadee. It either has a sharp conformable lower contact with the Gooragoora Formation or a disconformable contact with the Irregully Formation. The Blue Billy Formation is interpreted as a basinwide deposit of mostly deep-marine anoxic mudstone that records transgression and expansion of the Edmund Basin beyond the preserved limits of the Pingandy Shelf. During this time, major basement structures such as the Talga Fault had little influence on Blue Billy Formation sedimentation. Thick-bedded sandstone in the upper part of the Blue Billy Formation is interpreted to represent turbiditic and mass-flow deposits (Martin and Thorne, 2004). The age of the Blue Billy Formation is poorly known, but was probably deposited in a similar time frame to the underlying Gooragoora Formation. A sill of Kulkatharra Dolerite emplaced near the top of the Blue Billy Formation yielded a combined zircon and baddeleyite date of 1072 ± 8 Ma (Nelson, 2001; Wingate, 2002).

Cheyne Springs Formation

The Cheyne Springs Formation (Thorne, 2015h) conformably overlies the Blue Billy Formation. The formation was named by Chuck (1984) and modified by Martin and Thorne (2002). Most of the Cheyne Springs Formation is made up of dololutite, dolarenite, dolorudite, mudstone, siltstone and minor sandstone. The formation ranges in thickness from 50 to 300 m, but only locally exceeds 200 m, and is largely confined to the Pingandy Shelf on Ullawarra, Capricorn, Elliott Creek, Kenneth Range, Teano, Boggola and Mount Vernon, and also on the southwestern margin of the Wanna Syncline on Maroonah, Mangaroon and Edmund (Figs 4 and 6). It is thickest immediately adjacent to the Talga Fault on Ullawarra and thins rapidly to the south and southeast beneath a disconformity at the base of the Kiangi Creek Formation. The Cheyne Springs Formation is interpreted as an assemblage of shelf and pelagic deposits that mark a slight shallowing of the Edmund Basin following the Blue Billy Formation transgression. Data from sandstone units indicate a broadly southwest-sloping shelf with paleocurrent directions in a broad sector towards the south and to the northwest. The age of the Cheyne Springs Formation is poorly known, but it was probably deposited in a similar time frame to the underlying Blue Billy and Gooragoora Formations.

Depositional Package 3

Depositional Package 3 (Thorne, 2015i; Fig. 3) comprises the Kiangi Creek Formation and the Muntharra Formation. Deposition followed an extended period of erosion that, in the eastern part of the Edmund Basin, has truncated and removed parts, or all, of Depositional Packages 1 and 2 (Martin and Thorne, 2004).

Kiangi Creek Formation

The Kiangi Creek Formation (Martin and Thorne, 2002; Thorne, 2015j) is up to 2600 m thick and forms extensive outcrops throughout the Edmund Basin. In most areas, the formation disconformably overlies lower units of the Edmund Group, except in the Coobarra Dome area on Calyie, where it is unconformable on granitic rocks of the 1820–1775 Ma Moorarie Supersuite of the Gascoyne Province (Figs 4 and 7). The main rock types in the Kiangi Creek Formation are siltstone, fine-grained to very coarse-grained sandstone, and dolomite, together with minor conglomerate, chert and felsic volcanic rock (Tangadee Rhyolite Member). On the Pingandy Shelf, northeast of the Talga and Mount Vernon Faults, the formation comprises stromatolitic and non-stromatolitic dolomite, dolomitic siltstone, siltstone and sandstone. These were deposited in fluvio-deltaic and shallow-marine environments. This succession ranges in thickness from about 600–700 m on Ullawarra and Elliott Creek, to about 400 m on Kenneth Range. It also outcrops on Boggola, Teano and Mount Vernon. Farther east, the formation thickens to about 1000 m on Tangadee. Southwest of the Talga Fault on Maroonah, Mangaroon and Edmund, the Kiangi Creek Formation varies in thickness from 200 m to about 650 m and comprises mostly interbedded siltstone and sandstone. Farther to the southwest in the Mangaroon Syncline, a predominance of silicified siltstone indicates a transition to a deeper marine environment. Mixed sandstone and siltstone units of similar thickness also make up most of the formation in the Ti Tree and Cobra Synclines on Mount Phillips.

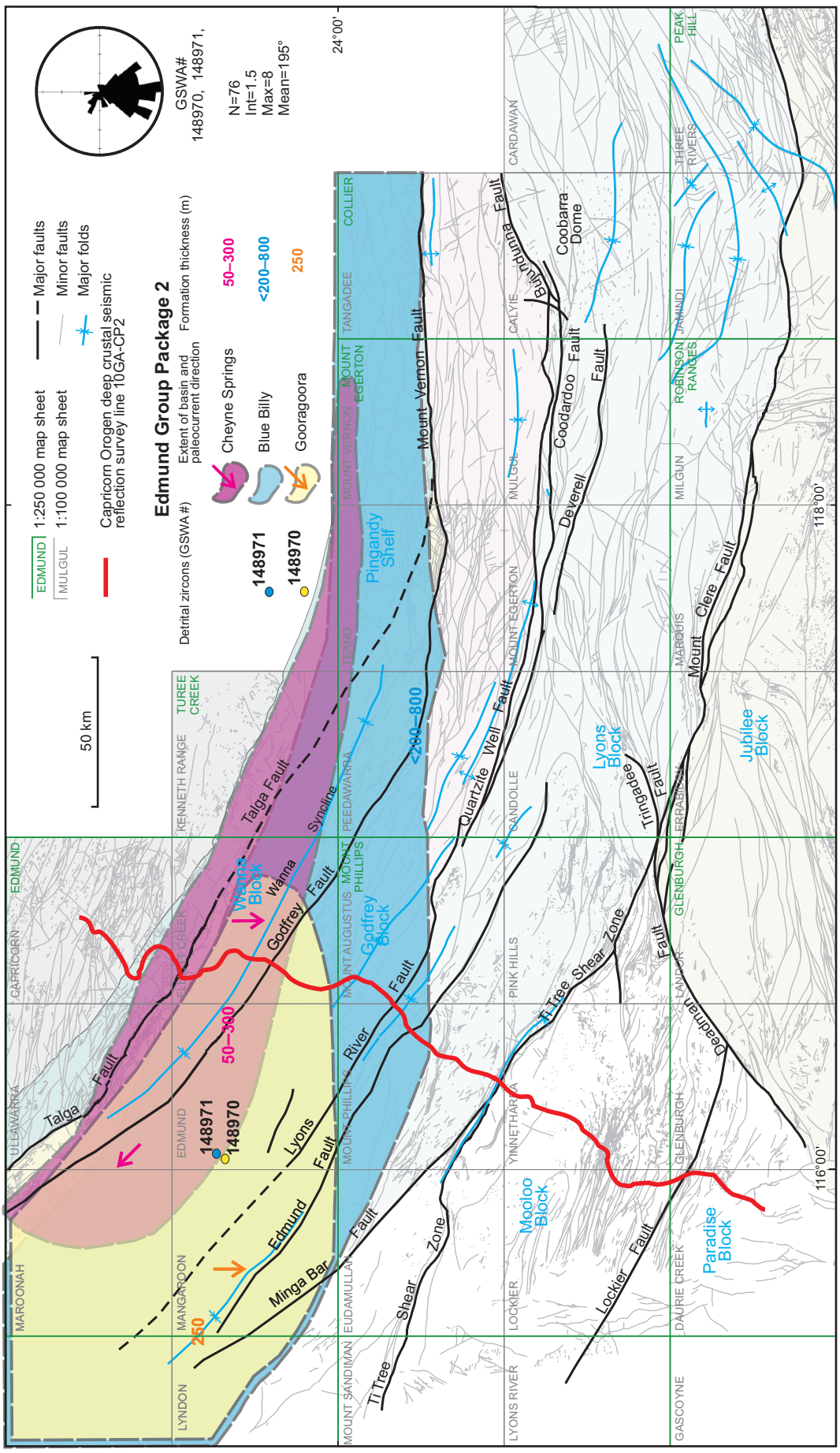

Figure 6. The extent and thickness of the Gooragoora (yellow), Blue Billy (blue) and Cheyne Springs Formations (purple) of Depositional Package 2, Edmund Group. The northwestern and eastern geographic extent (straight line margins) of the Depositional Package 2 is currently unknown. Paleocurrent direction rose diagram is from Martin et al. (2008) and paleocurrent direction arrows are from Martin and Thorne (2004). Note the overlap of successive formations. The locations of detrital zircon geochronology samples are colour coded for the sampled formation and identified with their GSWA sample number. The sediment thicknesses in various parts of the basin are similarly colour coded.

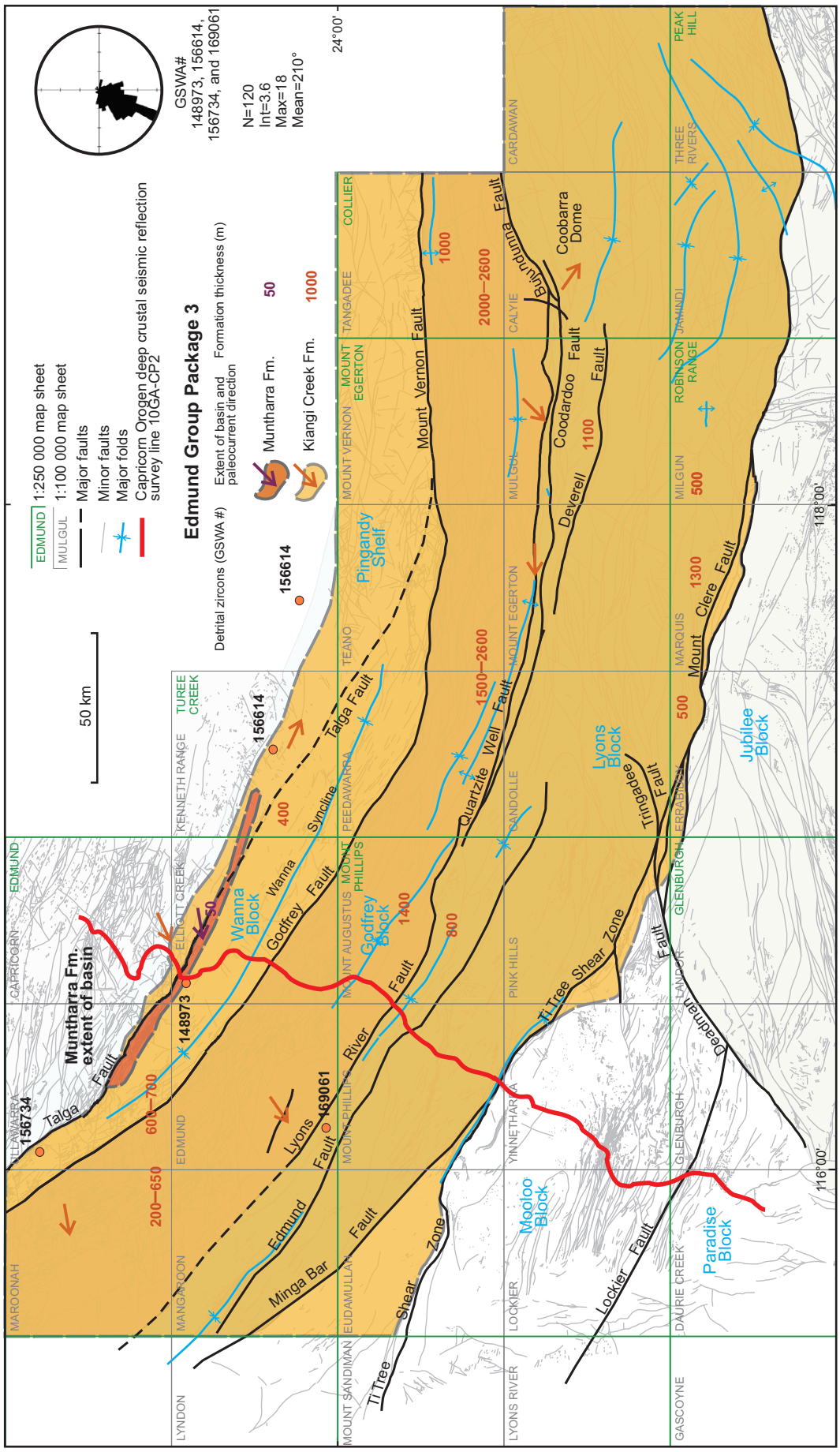

Figure 7. The extent and thickness of the Kiangi Creek (orange) and the Muntharra Formations (brown) of Depositional Package 3. The extent of the Kiangi Creek Formation basin to the north and northwest and east and northeast (straight line margins) is currently unknown. Paleocurrent direction rose diagram is from Martin et al. (2008) and paleocurrent direction arrows are from Martin and Thorne (2004). The location of detrital zircon geochronology samples are colour coded for the sampled formation and identified with their GSWA sample number. The sediment thicknesses in various parts of the basin are similarly colour coded.

The Kiangi Creek Formation thickens markedly to the southeast on Mount Augustus. It is about 800 m in the eastern part of the Cobra Syncline and about 1400 m thick in the nearby Geegin Syncline. The eastward thickening trend is maintained on Peedawarra and Mount Egerton with 1500–2600 m of mixed sandstone units. The succession is slightly thinner (~1100 m) on Mulgul, but thickens to 2000–2600 m in the area around the Budjundunna Fault on Calyie. In these areas, coarse-grained siliciclastic units dominate the lower part of the stratigraphy whereas finer grained rocks are more abundant in upper levels. These represent a proximal fluvial and alluvial fan, and a younger later deltaic environment. In the eastern part of the Edmund Basin, close to the Abra deposit, fluvial and alluvial fan units previously identified as a lower Kiangi Creek facies (Martin and Thorne, 2004; Martin et al., 2008) are now tentatively correlated with the Gooragoora Formation (Johnson et al., 2015a). A rapidly subsiding, fault-bounded marine depocentre was located farther to the west. Small occurrences of felsic volcanic rock belonging to the Tangadee Rhyolite are also present in lower parts of the formation around the Coobarra Dome. The Kiangi Creek Formation is estimated to be about 500 m thick on Errabiddy and Milgun, thickening to about 1300 m near the Mount Clere Fault on Marquis. Regional and stratigraphic lithological variation suggests that Kiangi Creek Formation stratigraphy records the infill and burial of a horst-and-graben basin architecture by alluvial and shallow- to deep-marine shelf deposits. On western Calyie, the rocks preserve southeasterly directed paleocurrents, with westerly flow observed on Mount Egerton and southwesterly flow in the western part of the basin, except on Kenneth Range where southeasterly paleocurrents are recorded (Fig. 7). On the Edmund 1:250 000 map sheet, paleocurrents are towards the southwest.

A sill of Waldburg Dolerite emplaced into the Kiangi Creek Formation on Mount Augustus yielded a U–Pb zircon age of 1517 ± 8 Ma (Wingate et al., 2015a), which provides a minimum age for the deposition of the unit. Hydrothermal alteration and mineralization at the Abra polymetallic deposit, dated between c. 1610 and 1590 Ma (Zi et al., 2015), does not extend above an unconformity into the overlying Kiangi Creek Formation, indicating that deposition of the unit was younger than c. 1590 Ma. These data also imply that the unconformity at the base of the formation may record a depositional hiatus of c. 20 Ma (Johnson et al., 2015a).

Muntharra Formation

The Muntharra Formation (Martin, 1999; Martin and Thorne, 2002; Thorne, 2015k) is exposed in a small area confined to the western part of the Pingandy Shelf adjacent to the Talga Fault on Ullawarra, Elliott Creek and Kenneth Range, where it attains a maximum thickness of about 50 m (Figs 4 and 7). It conformably overlies the Kiangi Creek Formation and consists mainly of dolomite and stromatolitic dolomite, together with sandstone, dolomitic sandstone and siltstone. Deposition occurred under quiet-water conditions below storm wave-base, although there were localized periods of high-energy carbonate and siliciclastic sedimentation. Paleocurrent directions are towards the west-southwest (Martin and Thorne, 2004). The age of the Muntharra Formation is poorly known, but was probably deposited in a similar time frame to the Kiangi Creek Formation, between c. 1590 and 1517 Ma.

Depositional Package 4

Depositional Package 4 (Thorne, 2015l; Fig. 3) includes the Discovery, Devil Creek, Ullawarra and Coodardoo Formations (Martin and Thorne, 2004).

Discovery Formation

The Discovery Formation (Thorne, 2015m) is recognized throughout the Edmund Basin and has been regarded as a major regional marker horizon (Muhling and Brakel, 1985b). The formation consists predominantly of massive or laminated chert, together with silicified mudstone and siltstone (Daniels, 1966; Martin, 1999). There are also minor occurrences of silicified sandstone and conglomerate at the base of the succession in western parts of the basin. The Discovery Formation is divided into a lower dark grey to black chert and an upper silicified siltstone. On the Pingandy Shelf, on Elliott Creek, Kenneth Range, Teano and Mount Vernon, its thickness generally ranges from 30 to 70 m, but in the southwestern, southern and southeastern parts of the basin it ranges from 280 to 300 m (Figs 4 and 8). The formation is thickest in areas close to the Mount Clere, Louisa Bore and Turner Faults on Errabiddy, Candolle, Marquis and Milgun, and south of the Coodardoo Fault on Calyie. The lower chert of the Discovery Formation is characterized by very strong, undulatory bedding that results in a pinch-and-swell appearance. In extreme cases, this can result in a boudinaged effect where detached, irregular lenses of black chert are enclosed in an envelope of black carbonaceous siltstone. A non-silicified siltstone unit may separate the upper and lower divisions. The formation appears to have been deposited in a starved anoxic environment below storm wave-base and the silicification was probably an early diagenetic feature. Evidence of an erosive basal contact for the Discovery Formation appears to be confined to the Pingandy Shelf. Here, silicified sandstone and conglomerate at the base of the formation, along the southwestern margin of the Pingandy Shelf, are possible remnants of a ravinement surface developed during the initial marine transgression (Martin and Thorne, 2004). Over most of the remaining part of the Edmund Basin, the basal contact appears conformable and gradational (Daniels, 1966; Muhling and Brakel, 1985a). The Discovery Formation marks a major marine transgression that crossed the region from southwest to northeast. The age of the formation is poorly constrained, but it was probably deposited between c. 1590 and 1465 Ma, based on the ages of underlying and overlying stratigraphic units.

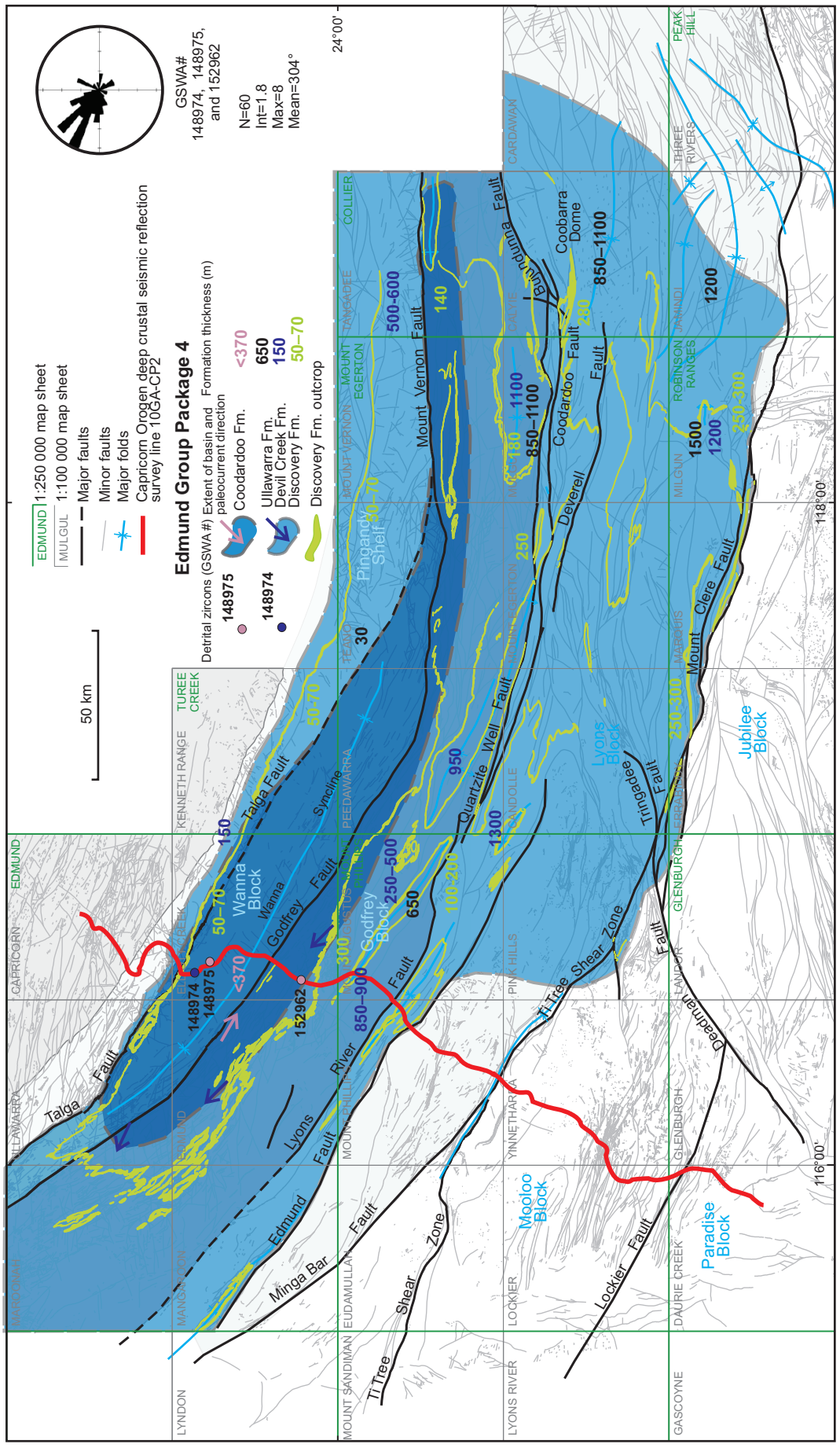

Figure 8. The extent of the Discovery, Devil Creek and Ullawarra Formations of Depositional Package 4 are shown in blue. Thicknesses of these formations are marked and colour coded. Present-day outcrop of the Discovery Formation, a distinctive marker bed, is shown in green highlight. The extent of the Coodardoo Formation of Depositional Package 4 is shown in dark blue with thickness indicated (pink). Paleocurrent direction rose diagram is from Martin et al. (2008) and paleocurrent direction arrows are from Martin and Thorne (2004). The location of detrital zircon geochronology samples are colour coded for the sampled formation and identified with their GSWA sample number.

Devil Creek Formation

The Devil Creek Formation (Daniels, 1966; Thorne, 2015n) is widely distributed throughout the Edmund Basin and generally has gradational, conformable contacts with the underlying Discovery Formation. It is present on the Edmund, Turee Creek, Mount Phillips, Robinson Range, Mount Egerton and Collier 1:250 000 map sheets (Fig. 8) and has a maximum thickness of about 1300 m. Principal rock types include non-stromatolitic and stromatolitic dolomite, dolomite breccia, dolomitic siltstone and siltstone, and minor diagenetic chert. Significant thicknesses of chert breccia are present on Kenneth Range and major occurrences of siltstone are recorded south of the Talga and Mount Vernon Faults in central and eastern parts of the basin. Platform carbonates occur on the Pingandy Shelf north of the Talga and Mount Vernon Faults, where thickness ranges from 150 m on northern Elliott Creek and Kenneth Range to 500–600 m in the area farther east on Teano and Tangadee. South of the Talga Fault, finer grained basinal deposits include thin- to medium-bedded dolomitic siltstone and siltstone with varying proportions of thin-bedded dololutite, fine- to medium-grained dolarenite, and siltstone. These reach a thickness of 250–500 m around the southern margin of the Wanna Syncline, to 850–900 m in the Cobra and Geegin Synclines on Mount Phillips and Mount Augustus, and 950 m in the Berala Syncline on Peedawarra. The Devil Creek Formation thickens to the east and south, with 1300 m in the Isabella Syncline on Candolle, 1100 m in the Range Creek Syncline on Mulgul, and about 1200 m in the vicinity of the Mount Arapiles Anticline on Milgun. The Devil Creek Formation on the Pingandy Shelf is interpreted to be a platform carbonate (Martin et al., 2005). South of the Talga and Mount Vernon Faults, finer grained basinal deposits may have been rimmed by a stromatolite reef. The alignment of the columnar stromatolites was interpreted as reflecting a paleoslope towards the southwest, perpendicular to the Talga Fault (Thorne, 2015n), although Daniels (1966) documented a preferential orientation with tops towards 124°, which he interpreted as the result of a current from the south-southeast. Southwest of the Talga and Mount Vernon Faults, the slope facies pass into thick, fine-grained mixed siliciclastic–carbonate basinal deposits that are uniform across the southern part of the basin, suggesting little influence from other basement structures in this part of the region. Paleocurrent data suggest a regional deepening towards the west and northwest. The age of the Devil Creek Formation is poorly constrained but it was probably deposited between c. 1590 and 1463 Ma, based on the ages of underlying and overlying stratigraphic units.

Ullawarra Formation

The Ullawarra Formation (Daniels, 1966; Thorne, 2015o) is exposed across most of the Edmund Basin where it conformably overlies the Devil Creek Formation (Fig. 8). The Ullawarra Formation is composed of siltstone, with subordinate fine-grained sandstone, dolomite, and chert and is commonly intruded by numerous dolerite and gabbro sills. The formation ranges in thickness from a minimum of about 30 m on the Pingandy Shelf, where siltstone is dominant, to about 1800 m in the south-central parts of the basin. More significant occurrences of sandstone are interbedded with siltstone in areas south of the Talga and Mount Vernon Faults. Ferruginous and manganiferous siltstone, dolomite and felsic volcanic rock are only locally present. South of the Talga Fault on the northern and southern limbs of the Wanna Syncline and in the Geegin Syncline, the formation thickens to about 650 m. Farther east, the formation contains significantly less sandstone, and is about 1500 m thick in the Mount Arapiles Anticline and 850–1100 m in the Range Creek and Calyie Synclines on Calyie, and in the Brumby Creek Anticline on Tangadee. The formation is about 1250 m thick on Jamindi, where it is largely composed of ferruginous and manganiferous siltstone.

The Ullawarra Formation was likely deposited in a deep-marine shelf environment, given the fine-grained nature of most of the rock types, their range of sedimentary structures, and general lack of shallow-water facies or evidence of wave-reworking. Sandstones were probably deposited from distal, relatively dilute, turbidity currents, whereas siltstones were laid down during the final stages of turbidity current deposition and also from suspension settling in the intervening quiet-water periods. Paleocurrent data, dominated by flow towards the northwest and west, indicate that deposition took place in response to relative uplift in the area to the southeast of the exposed Edmund Basin, with a depocentre located on the Mount Egerton and Robinson Range 1:250 000 map sheet areas.

Felsic volcaniclastic units within the Ullawarra Formation yielded youngest detrital zircon age components at 1463 ± 8 Ma (Wingate et al., 2010) and 1455 ± 9 Ma (Wingate et al., 2012a), providing a maximum depositional age for the upper part of formation. The unit is also intruded by sills of Kulkatharra Dolerite, one of which yielded a weighted mean $^{207}Pb^*/^{206}Pb^*$ baddeleyite age of 1068 ± 22 Ma (Wingate, 2002). The Ullawarra Formation was therefore deposited sometime between c. 1590 and 1455 Ma.

Coodardoo Formation

The Coodardoo Formation (Daniels and Halligan, 1969; Thorne, 2015p) is the uppermost formation of the Edmund Group and is exposed mainly around the core of the Wanna Syncline in the western part of the Edmund Basin, where it attains a maximum thickness of 370 m. It is also recorded from small outcrops south of the Mount Vernon Fault on Mount Vernon and Tangadee (Figs 4 and 8). The formation has a conformable, gradational contact with the underlying Ullawarra Formation and an unconformable boundary with the overlying Collier Group. The Coodardoo Formation is composed of thin- to very thick-bedded, fine- to very coarse-grained lithic quartz sandstone and pebbly sandstone, interbedded with siltstone. Martin and Thorne (2004) and Martin et al. (2005) interpreted the Coodardoo Formation as a deep-marine shelf submarine fan deposit with the sandstones probably deposited from turbidity currents, and the siltstones deposited during the final stages of turbidity current deposition and also from suspension settling in the

intervening quiet-water periods. The limited paleocurrent data available indicate that sediment was supplied from a southeastern source, although there was also an increasing contribution from an upland area to the northwest. Considering the conformable relationship with the underlying Ullawarra Formation, this unit was probably deposited in a similar time frame, close to the age of the underlying volcaniclastic units at c. 1455 Ma.

Depositional hiatus

The Collier Group is separated from the Edmund Group by a depositional hiatus during which extensive erosion of the Edmund Group took place. Based on the time difference between the youngest detrital zircons in the Backdoor Formation of the Collier Group at c. 1397 Ma, and the minimum age of the Edmund Group, this lacuna must have lasted at least 65 Ma (Martin and Thorne, 2004). Peperite structures were identified in the Backdoor Formation (Martin, 2003) in association with mafic sills of the 1084–1067 Ma Kulkatharra Dolerite. Peperites are commonly interpreted to be the result of the interaction between magma and wet sediments (Skilling et al., 2002), so this suggests that deposition of the Collier Group may have taken place closer to c. 1070 Ma, indicating that this lacuna may have lasted for as long as 370 Ma.

Collier Group

The Collier Group (Thorne, 2016a) is predominantly a siliciclastic sedimentary unit made up (in stratigraphically ascending order) of two depositional packages including the Backdoor and Calyie Formations (Depositional Package 5), and the Ilgarari Formation (Depositional Package 6). The Collier Group was deposited following a major marine transgression that led to deep-marine shelf sedimentation (lower Backdoor Formation) prevailing across the region. This was followed by a period of delta progradation (upper Backdoor Formation and Calyie Formation), and finally by delta abandonment and a return to deep-marine shelf conditions (Ilgarari Formation).

The age of the Collier Group is poorly constrained. The group does not appear to have been deformed during the 1321–1171 Ma Mutherbukin Tectonic Event (Johnson et al., 2011d; Korhonen et al., 2015) and so the sediments were deposited after c. 1171 Ma. Mafic sills of the 1084–1067 Ma Kulkatharra Dolerite were emplaced throughout the Edmund and Collier Basins, thus providing a minimum age for the deposition of the group. Most sills are characterized by planar upper and lower chilled margins, implying they were emplaced into a lithified host (Martin, 2003); however, on the northern flank of the Wanna Syncline on Kenneth Range, a mafic sill emplaced into the lower part of the Backdoor Formation, at the base of the Collier Group, contains peperites (Martin, 2003), suggesting the deposits were wet and unconsolidated. The upper contact of the sill is marked by either a sediment-matrix dolerite breccia or a thin unit of mixed and remobilized sedimentary rock, which separates the dolerite sill from the overlying intact host rocks (Martin, 2003). This sill yielded a weighted mean $^{207}Pb^*/^{206}Pb^*$ zircon date of 1076 ± 4 Ma (Wingate and Bodorkos, 2007), suggesting that deposition of the Backdoor Formation may have occurred shortly before c. 1076 Ma.

Depositional Package 5

Depositional Package 5 (Thorne, 2016b; Fig. 3) is the lower package of the Collier Group, deposited unconformably on the Edmund Group, and includes the Backdoor and Calyie Formations.

Backdoor Formation

The Backdoor Formation (Brakel and Muhling, 1976; Martin et al., 1999; Thorne, 2016c) comprises siltstone, mudstone, thin- to thick-bedded sandstone, and minor chert and dolomite. The formation outcrops around the core of the Wanna Syncline and extends north of the Talga and Mount Vernon Faults on Kenneth Range, Teano, Mount Vernon and Tangadee (Figs 4 and 9). In the southeastern part of the Collier Basin, the Backdoor Formation is exposed on Calyie, Cardawan, Milgun, Jamindi and Three Rivers. In most areas, the Backdoor Formation has an unconformable lower contact with the Coodardoo and Ullawarra Formations of the Edmund Group, except on Jamindi where it has an unconformable lower contact with the Paleoproterozoic Bryah Group. The Backdoor Formation ranges in thickness from 1400 to 1750 m in the Wanna Syncline on Peedawarra and Kenneth Range, but thins to 400–600 m in the east, north of the Mount Vernon Fault on Mount Vernon and Teano. The formation thickens in the southeastern part of the basin to as much as 1400 m on Calyie and 1700 m on Milgun. The anomalously thick succession (~3000 m) that appears to be present southwest of the Thomson Fault on Jamindi (Cutten et al., 2013) may be due to a combination of structural repetition and limited exposure in this area, and a thickness of about 1500 m is more likely. The Backdoor Formation records a progradation from distal shelf to proximal shelf and distal delta-front depositional environments (Martin et al., 2005). Southwesterly to southerly directed paleocurrent data recorded on Kenneth Range, Peedawarra and Teano, both north and south of the Talga Fault (Fig. 9) suggests a source area to the northeast. In the eastern part of the basin on Tangadee, paleocurrent directions are towards the southwest on the Pingandy Shelf north of the Mount Vernon Fault, but south of the fault on Tangadee and Calyie they are towards the northwest, west and southwest, suggesting a source area to the east. The Backdoor Formation was deposited some time after the 1321–1171 Ma Mutherbukin Tectonic Event (Korhonen et al., 2015) but before the emplacement of dolerite sills belonging to the 1086–1067 Ma Kulkatharra Dolerite; however, the local presence of peperites (Martin, 2003) suggests that sediment deposition may have taken place closer to c. 1076 Ma.

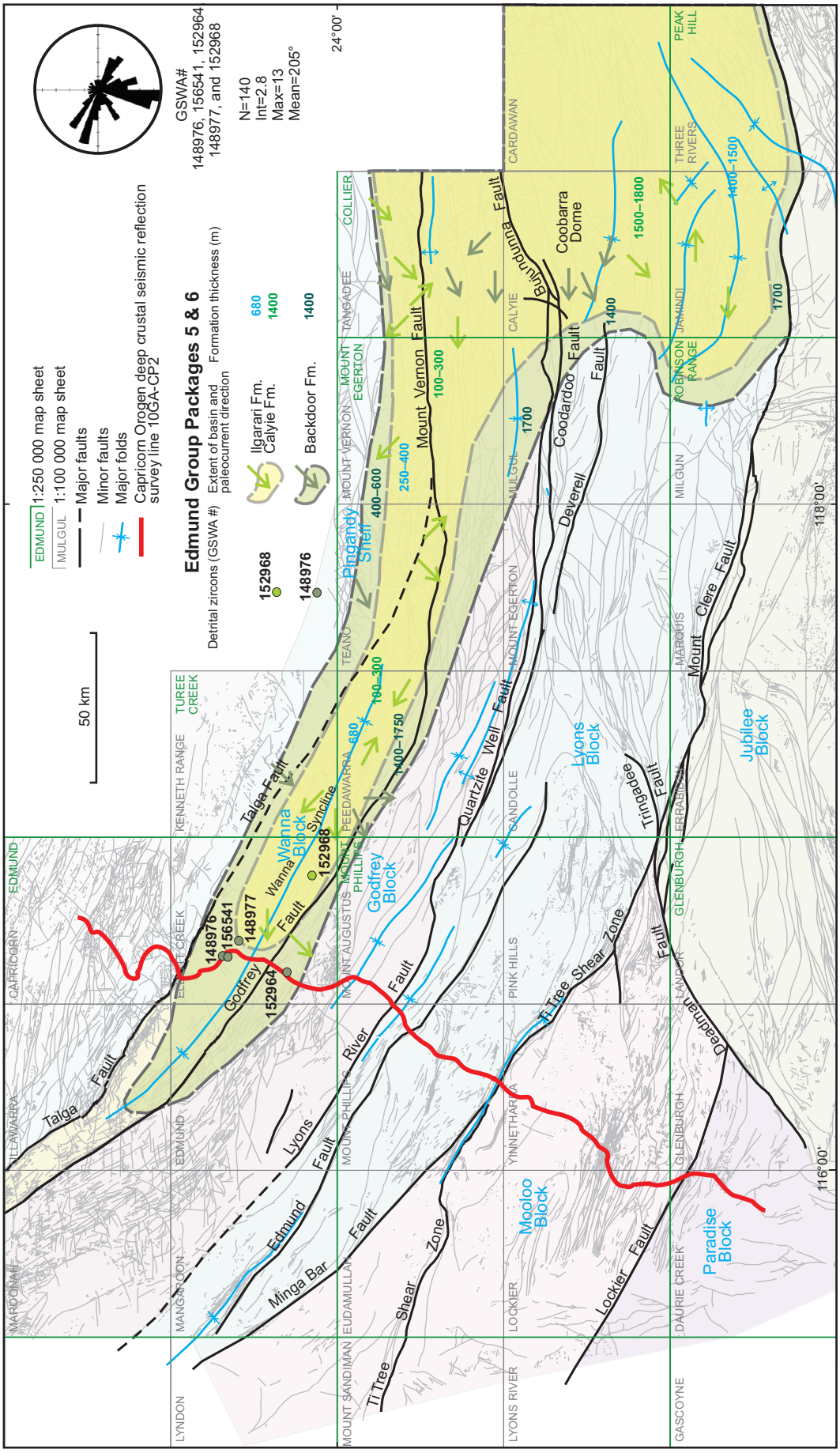

Figure 9. The extent of the Backdoor Formation of Depositional Package 5 is shown in green. The extent of the Calyie and Ilgarari Formations, shown in yellow, are similar, although they comprise separate Depositional Packages, 5 and 6, respectively. Formation thicknesses are indicated and colour coded. Paleocurrent direction rose diagram is from Martin et al. (2008) and sediment supply arrows are indicated. The location of detrital zircon geochronology samples are colour coded for the sampled formation and identified with the GSWA sample number. The sediment thicknesses in various parts of the basin are similarly colour coded.

Calyie Formation

The Calyie Formation (Martin et al., 1999; Thorne, 2016d) consists of thin- to very thick-bedded quartz sandstone and subordinate siltstone, together with minor conglomerate, and has a gradational conformable contact with the underlying Backdoor Formation. It outcrops in the core of the Wanna Syncline between Elliott Creek and Teano and extends north of the Mount Vernon Fault on Teano, Mount Vernon and Tangadee. Like the Backdoor Formation, it is also exposed on Calyie, Cardawan, Jamindi, Milgun and Three Rivers. The formation generally ranges in thickness from 100 to 300 m in the Wanna Syncline and Mount Vernon Fault area but thickens to about 1500–1800 m in the Calyie and Jamindi Synclines. The Calyie Formation was probably laid down in a delta-front to delta-top depositional environment. Paleocurrent directions in the Calyie Formation on the southern margin of the Pingandy Shelf north of the Mount Vernon Fault on Mount Vernon and Tangadee show flow towards the southwest and northwest. In the Wanna Syncline, flow was towards the northwest and southeast parallel to the trend of the basin with some flow to the southwest and west. To the east on Calyie, Jamindi and Three Rivers, paleocurrent directions are variable, towards the east, west, northeast and southwest. Based on the conformable relationship with the underlying Backdoor Formation, the Calyie Formation is interpreted to have been deposited in a similar time frame.

Depositional Package 6

Depositional Package 6 (Thorne, 2016e; Fig. 3) comprises the uppermost unit of the Collier Group, the Ilgarari Formation.

Ilgarari Formation

The Ilgarari Formation (Martin et al., 1999; Thorne, 2016f) conformably overlies the Calyie Formation and outcrops in the core of the Wanna Syncline on Elliott Creek, Kenneth Range and Peedawarra, extending north of the Mount Vernon Fault on Teano, Mount Vernon and northwestern Tangadee. It is also exposed in the Calyie Syncline on Calyie, and the Mindi and Beasley Synclines and the Dunlop Anticline on Jamindi and Three Rivers. The Ilgarari Formation is up to 680 m thick in the Wanna Syncline, 250–400 m thick north of the Mount Vernon Fault, and farther southeast on Jamindi and Three Rivers is as much as 1400–1500 m thick. Exposure is controlled by fold structures although the basin was likely more extensive, possibly similar in extent to that of Package 5. The Ilgarari Formation is primarily composed of parallel planar-laminated pyritic and carbonaceous siltstone with thin beds of massive to planar-laminated fine-grained sandstone and interbedded siltstone towards the top of the formation. Limestone and calcareous siltstone and chert are minor constituents. These rocks represent marine-shelf facies deposits, and were laid down following a basinwide marine transgression. Based on the conformable relationship with the underlying Calyie Formation, the Ilgarari Formation is interpreted to have been deposited in a similar time frame.

Intraplate reworking and inversion of the Edmund and Collier Basins

The Edmund Group was inverted and deformed during the 1321–1171 Ma Mutherbukin Tectonic Event, the 1026–954 Ma Edmundian Orogeny, and by the c. 570 Ma Mulka Tectonic Event. Because the Collier Group was deposited after the Mutherbukin Tectonic Event, it was only affected by the Edmundian Orogeny and the Mulka Tectonic Event. All three reworking events produced near-coaxial structural features that trend northwest-southeast in the west and east–west in the east, and so it is difficult to differentiate between them. However, some features, such as faulting or folding, are more prevalent in the Edmund Group than in the Collier Group that directly overlies it, indicating that the major movement on these structures must have occurred during the Mutherbukin Tectonic Event.

Fault plane exposure in the Edmund and Collier Basins is not common, and only occasionally do they contain fault gouge (Fig. 10a) or show well-developed slickenlines (Fig. 10b). Most of the faults are characterized by offset ridges of steeply dipping sandstones separated by valleys filled with regolith, or as linear outcrops of massive vein quartz or quartz–ironstone breccia (Fig. 10c).

The 1321–1171 Ma Mutherbukin Tectonic Event

In the Gascoyne Province, the 1321–1171 Ma Mutherbukin Tectonic Event (Johnson et al., 2011d, 2016; Wingate et al., 2013b; Korhonen et al., 2015) is expressed as a strong upright schistosity or crenulation schistosity in metasedimentary rocks, and a widely developed foliation or gneissic banding in metamorphosed granitic rocks (Korhonen et al., 2015; Johnson et al., 2011c). In the Edmund Group and underlying Mount Augustus Sandstone, evidence for this event is more cryptic due to the very low-grade nature of metamorphism, and coaxial nature of structures formed during subsequent events. However, these rocks not only contain abundant Mutherbukin-age hydrothermal monazite and xenotime (Rasmussen et al., 2010; Zi et al., 2015; Korhonen et al., 2015), but major faults that developed in the Edmund Group show only minor (reactivated) offsets within the Collier Group (Thorne, 2016a). Also, on the southern limb of the Wanna Syncline on Edmund, there is a greater intensity of faults within the Edmund Group. These faults are shown on the Capricorn Orogen deep crustal seismic reflection survey to be reverse faults with accompanying hanging-wall anticlines (Johnson et al., 2011a, 2013). Because these are not replicated in the overlying Collier Group, the deformation is considered to be related to the Mutherbukin Tectonic Event.

During the Mutherbukin Tectonic Event, the Edmund Group and Mount Augustus Sandstone were subjected to intense localized hydrothermal alteration, possibly related to fault reactivation (Zi et al., 2015). Hydrothermal monazite from a single sample of the Mount Augustus Sandstone on Mount Augustus yielded a U–Pb

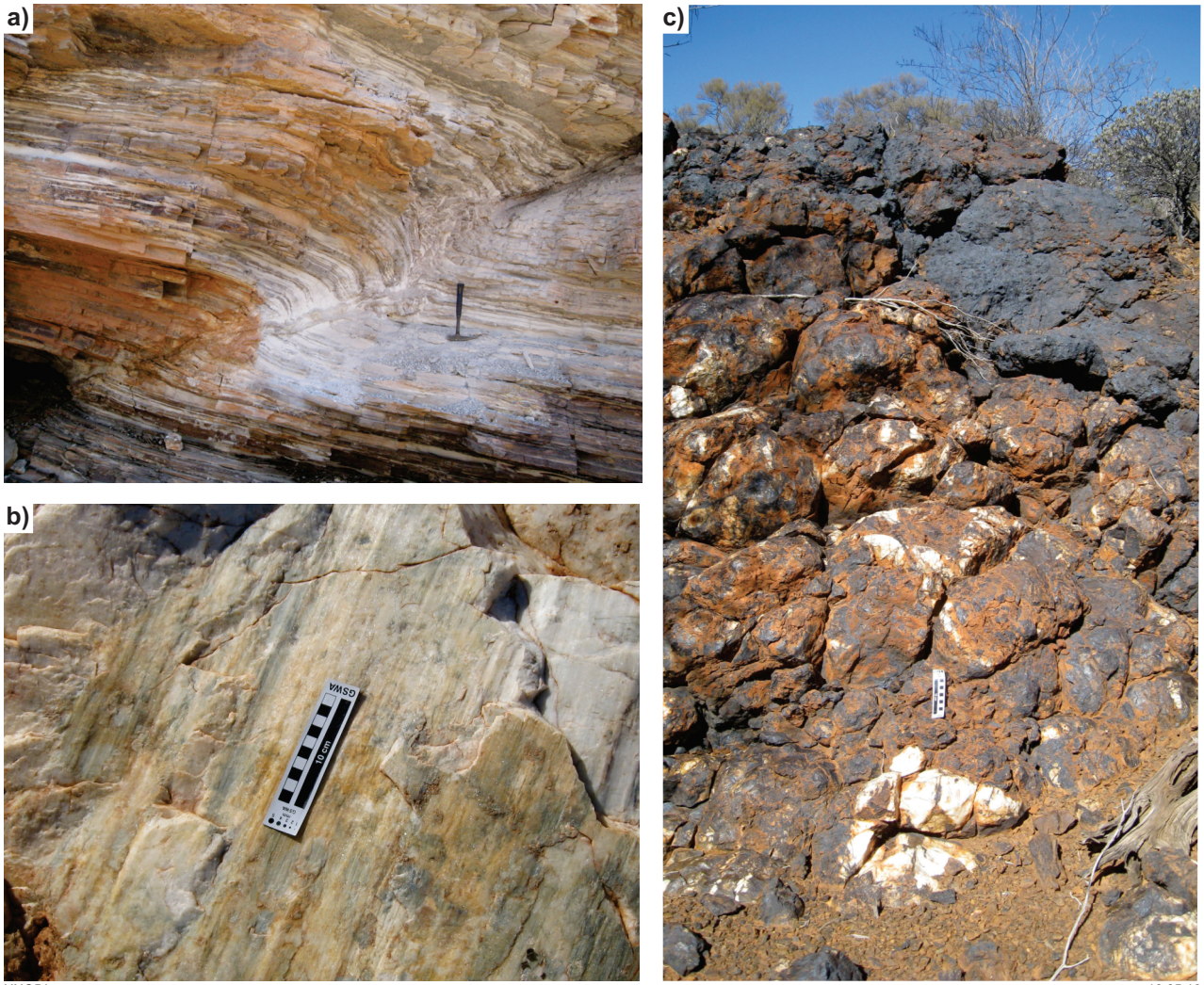

HNC54 10.05.16

Figure 10. a) A small reverse fault, attitude 35° dip to 10° azimuth, displacing Kiangi Creek Formation siltstone beds by 50 cm, on the TANGADEE 1: 100 000 map sheet, near a branch of the Mount Vernon Fault. Fault gouge sampled from the fault contained authigenic illite, dated by the K–Ar method at 1171 ± 25 Ma; GSWA 189218 (Zwingmann et al., 2012). Image 1658, WAROX locality HNCTGE000872, MGA coordinates, Zone 50, 679113, 7314769; b) well-developed slickenlines on the Turner Fault on the CANDOLLE 1: 100 000 map sheet, image 3359, WAROX locality HNCMTE001023, MGA coordinates, Zone 50, 548731, 7240159. Slickensides plunge 14° to azimuth 030° with a reverse sense of movement; c) brecciated quartz in an ironstone matrix, occurring on a branch of the Quartzite Well Fault. Image 3663. WAROX locality HNCMUL001177, MGA coordinates, Zone 50, 614567, 7279249 on the MULGUL 1: 100 000 map sheet.

SHRIMP date of c. 1300 Ma (Rasmussen, written comm.). Extensive U–Pb SHRIMP dating of xenotime and monazite from the Abra polymetallic deposit and surrounding rocks in the eastern part of the Edmund Basin on CALYIE, yielded numerous dates between c. 1375 and 995 Ma (Zi et al., 2015; Rasmussen et al., 2010). Hydrothermal monazite from the red zone of the Abra deposit and the overlying (and distal) unmineralized strata, are intergrown with low-grade alteration assemblages containing barite, K-feldspar, quartz and chlorite (Zi et al., 2015). Several distinct age components have been identified at c. 1375, 1221 and 995 Ma, each of which is interpreted to record the timing of a regional-scale hydrothermal alteration event associated with the reactivation of the Lyons River – Quartzite Well Fault system (Zi et al., 2015). A Re–Os model age of c. 1264 Ma was also obtained from pyrite in the red zone (Pirajno et al., 2010). Similar dates have been obtained from hydrothermal xenotime from the highly altered Tangadee Rhyolite on TANGADEE and yielded a date of c. 1235 Ma (Rasmussen et al., 2010).

Additionally, illite within fault gouge on TANGADEE, sampled from a reverse fault that displaces rocks of the Kiangi Creek Formation, yielded a K–Ar date of c. 1171 Ma (Zwingmann et al., 2012), indicating that fault movement in the Edmund Group was synchronous with events in the Gascoyne Province basement (Korhonen et al., 2015).

The 1026–954 Ma Edmundian Orogeny

The 1026–954 Ma Edmundian Orogeny was previously thought (Halligan and Daniels, 1964; Sheppard et al., 2007; Thorne et al., 2016g) to have been responsible for all the deformation and low-grade metamorphic effects in both the Edmund and Collier Groups (Martin and Thorne, 2004), and for formation of the Edmund Fold Belt (Muhling and Brakel, 1985b; Martin et al., 2005). However, in light of recent mapping in the eastern parts of the Edmund and Collier Basins, as well as extensive geochronology (Rasmussen et al., 2010; Zwingmann et al., 2012; Zi et al., 2015), much of the deformation in the Edmund Group is now attributed to the 1321–1171 Ma Mutherbukin Tectonic Event (Johnson et al., 2016). The effects of the Edmundian Orogeny are recorded principally in the Collier Group as a series of easterly to southeasterly trending, open to tight, upright folds and normal, reverse, and strike-slip faults which formed largely during north–south shortening. The effects are more pronounced in the underlying Gascoyne Province basement rocks, with the development of pervasive schistose fabrics at greenschist to amphibolite facies with the intrusion of very localized leucocratic granitic rocks and rare earth element pegmatites (Sheppard et al., 2007). U–Pb dating of monazite and xenotime by the SHRIMP, from samples of pelitic schist of the Pooranoo and Leake Spring Metamorphics, yielded dates between c. 1026 and 994 Ma (Sheppard et al., 2007), although minor granite magmatism and pegmatite intrusion continued to c. 955 Ma (Sheppard et al., 2007).

The c. 570 Ma Mulka Tectonic Event

The c. 570 Ma Mulka Tectonic Event (Johnson et al., 2015b) is responsible for a series of anastomosing shear zones or faults that cut rocks of the Gascoyne Province and Edmund and Collier Groups across the southwestern part of the Capricorn Orogen (Sheppard et al., 2010b). The largest of these fault systems are the Chalba Shear Zone – Mount Clere Fault and the Ti Tree Shear Zone. These structures display consistent dextral strike-slip kinematics where they are observed to offset mafic dykes belonging to the c. 755 Ma Mundine Well Dolerite Suite (Wingate and Giddings, 2000; Sheppard et al., 2010a). Regional-scale dextral displacements across the Chalba Shear Zone have been calculated at about 35 km or more (Sheppard et al., 2010b). White mica in the S-planes of an S–C fabric in the Chalba Shear Zone has been dated in situ using the $^{40}Ar/^{39}Ar$ method, yielding a date of c. 570 Ma (Bodorkos and Wingate, 2007).

Analytical methods

To gain a more complete understanding of the growth and inversion history of the Edmund and Collier Basins, an assessment of the structural evolution through time, including estimates of extension and subsequent shortening, and timing of fault activation, are critical. These factors have been evaluated using a variety of approaches, including the variation in spatial distribution and thickness of individual sediment packages, estimating extension and shortening from an available deep crustal seismic section, and estimating shortening during the different reworking events by line balancing two basinwide cross-sections.

Spatial distribution and sediment thickness variations

The primary distribution and thickness of sedimentary strata in sedimentary basins is directly related to the activity and timing of movement on growth faults, which accommodate space for sediment by allowing downdrop and tilting of the intervening fault blocks as well as the actual, or relative, uplift of sediment source areas. The spatial and thickness variations of sedimentary strata across the basin, and through time, record the differential movement history on the major structures (Fig. 11). Measured paleocurrent structures indicate the direction of sediment supply, which are also a guide to fault movement history. The growth history of the Edmund and Collier Basins is assessed by tracking the spatial distribution, thickness, and source variation of each formation, to determine which faults controlled sediment deposition and basin architecture, as well as the timing and movement history on these structures. However, these estimates can only be considered a minimum, since parts of the basins have been removed by subsequent erosion.

Estimating extension and shortening from the Capricorn Orogen deep crustal seismic survey

Part of the Capricorn Orogen deep crustal seismic reflection survey (the northern section of line 10GA-CP2) imaged the Edmund Basin in the central part of the orogen (Johnson et al., 2011d, 2013; Figs 1 and 2). Interpretation of this line, based on surface outcrops as well as regional-scale aeromagnetic and gravity data, reveals a regional-scale half-graben structure (Johnson et al., 2011d, 2013). Depositional packages thicken towards, and are normally offset across, the major faults (Fig. 2), features attributed to active normal fault movements during deposition, although some faults also show subsequent reverse displacements. Using trigonometry, an estimate of extension and shortening on each fault, through time, has been calculated (Fig. 12, Tables 1 and 2).

Estimation of shortening by line balancing basinwide cross-sections

Two regional-scale, north–south-trending cross-sections to 4 km depth across the Edmund and Collier Basins have been constructed by combining pre-existing cross-sections (GSWA, 2013) with additional field data (Figs 13 and 15).

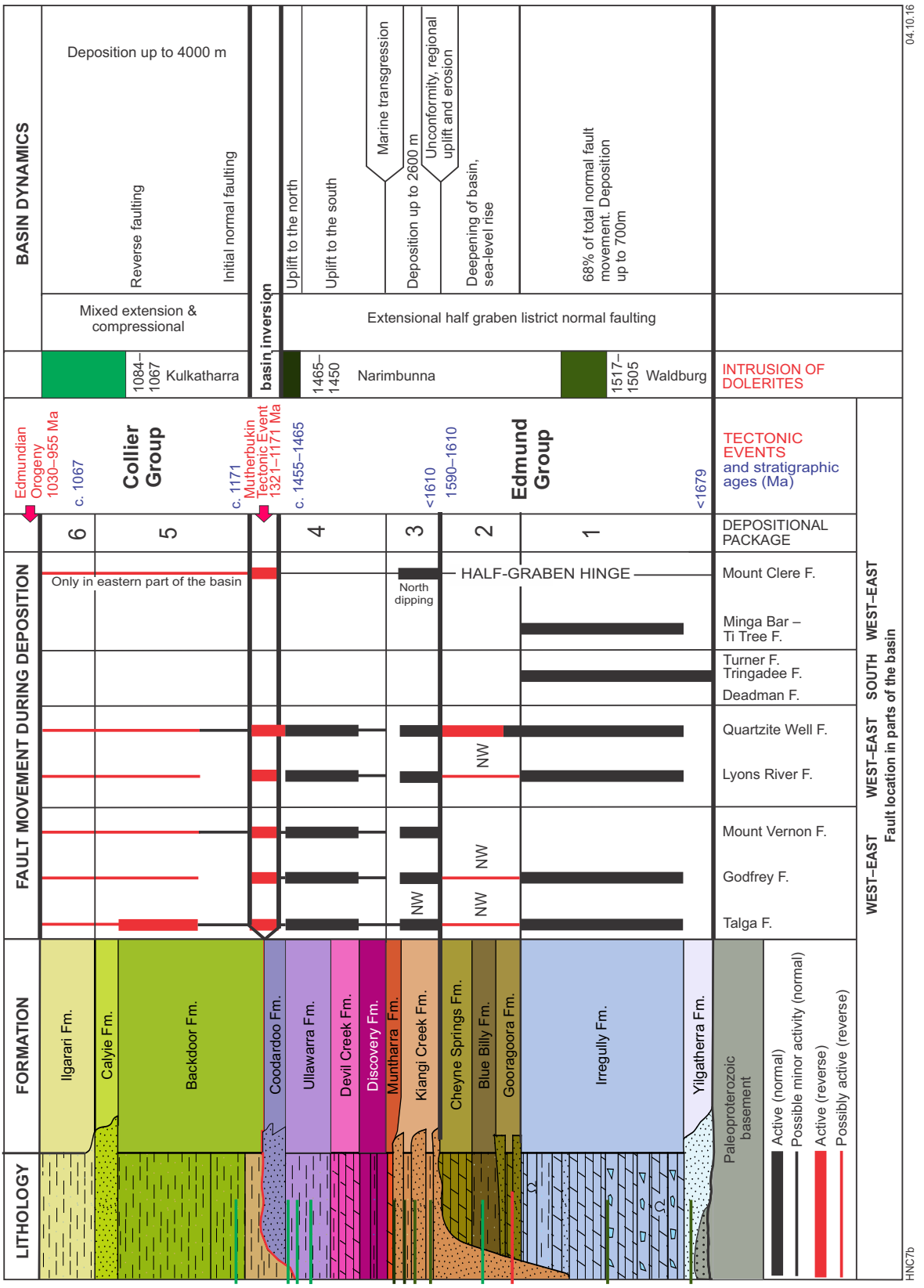

Figure 11. **Timing of fault activity. Normal fault activity (prior to the Mutherbukin Tectonic Event [MTE]) on the controlling bounding faults during deposition of the Edmund Group has been calculated from formation distribution, thicknesses and paleocurrent directions. All normal faults are south dipping, except the Mount Clere Fault, which is north dipping, and the Deadman and Tringadee Faults, which are northwest dipping. During the MTE and the Edmundian Orogeny, reverse transpressional reactivation occurred on some of these faults. Each column groups together faults that are linked and located in the western or eastern parts of the basin. For example, the Godfrey and Talga Faults in the west, both link with the Mount Vernon Fault in the east (see Fig. 4). NW signifies activity in the northwest of the Edmund Basin.**

Table 1. Extension on faults

Fault	*Cobra*	*Cobra cum.*	*Cardibar–Blue Bush*	*Cardibar–BB cum.*	*+S*	*Lyons River*	*Lyons River cum.*
Package							
3							
2							
1	0.2	0.2	4.71	4.71	0.5	≥0.16	≥0.16

Fault	*Godfrey*	*Godfrey cum.*	*Talga*	*Talga cum.*	*Basin cum.*	*Basin cum.*	*Basin width*	*Extension total*
Package								
3	0.09	0.09	0.1	0.1	0.19	0.22%		
2	>0	>0	0.05	0.15	>0.15	0.17%		
1	0.24	0.33	0.26	0.41	>6.31	7.2%	88 km	>7.2%

NOTES:
Extension calculated from faults. Figure 12 shows method of calculation with the Talga Fault example. Numbers in km except % as labelled. Cumulative (cum.) = Total of extension of each successive package base horizon. +s (= plus MTE and Edmundian O shortening), which equals the shortening on Cardibar (0.4 km) and Blue Bush (0.1 km). On the Godfrey Fault, later shortening must also have occurred, because Package 3 shows 0.09 km extension, so must Package 2 and Package 1 show at least this displacement. Yet Package 2 shows zero displacement, indicating the position of the level has been restored by later thrusting, which cannot be calculated. Therefore, measured extension is only a minimum. Probably unrecorded displacement has occurred on other smaller faults so the final 7.2% is very much a minimum. Note that fault displacement on the base of Package 1 is actually the displacement during deposition of Package 1 or immediately following and before deposition of the base of Package 2. Most of the normal fault displacement occurred during Package 1 [(7.2-0.17-0.22/7.2)=95%].

Table 2. Shortening on faults

Package	Edmund F.	Koorabooka South F.	Koorabooka North F.	Shitson Bore North F.	Terminus F.	Blue Bush F.	Cardibar F.	Total	Basin width	Shortening
Package 1 = Total	≥ 0.82	0.25	0.83	0.18	0.87	0.1	0.4	3.45	56	≥6.2%

NOTE:
Shortening between the Edmund and Cardibar Faults (56 km width) calculated from the displacement of the base of Package 1. All units are km except for shortening (%).

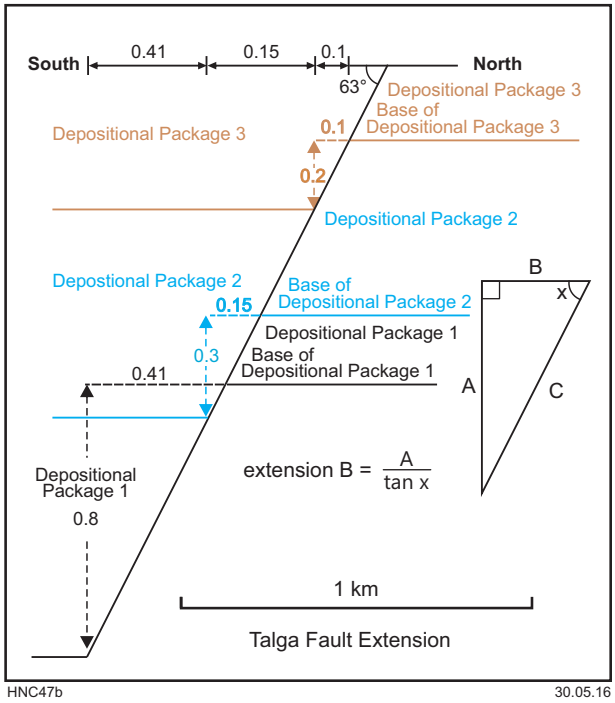

Figure 12. Trigonometric calculation of extension (B) from dip of fault (X), and downdrop (A). The example shown here is for the Talga Fault. Later uplift on some faults has been calculated by the same method.

The western cross-section closely follows the Capricorn Orogen deep crustal seismic reflection survey (Johnson et al., 2011d, 2013), and the eastern cross-section passes just to the east of the Abra deposit (Figs 1 and 4). Each section is divided into segments, which in most cases are bound by major faults (Figs 13 and 14). Shortening in each of the segments was calculated by the ratio of the original bed length (orange line, labelled E for Edmund and C for Collier) to the shortened bed length (green line; Figs 13 and 14). Some of the segments contain both Edmund and Collier Group strata, which show differing degrees of fold tightness, and hence amounts of shortening (Fig. 16). Since the Collier Group has only experienced deformation during the Edmundian Orogeny, this has provided an estimate of shortening during each of the two main reworking events, the 1321–1171 Ma Mutherbukin Tectonic Event and the 1026–954 Ma Edmundian Orogeny.

Lu–Hf isotope analyses of detrital zircons

Detrital zircons from 18 sandstone units in the northwestern part of the Edmund and Collier Basins were previously dated by SHRIMP as part of a U–Pb detrital zircon provenance study (Martin et al., 2008). The samples

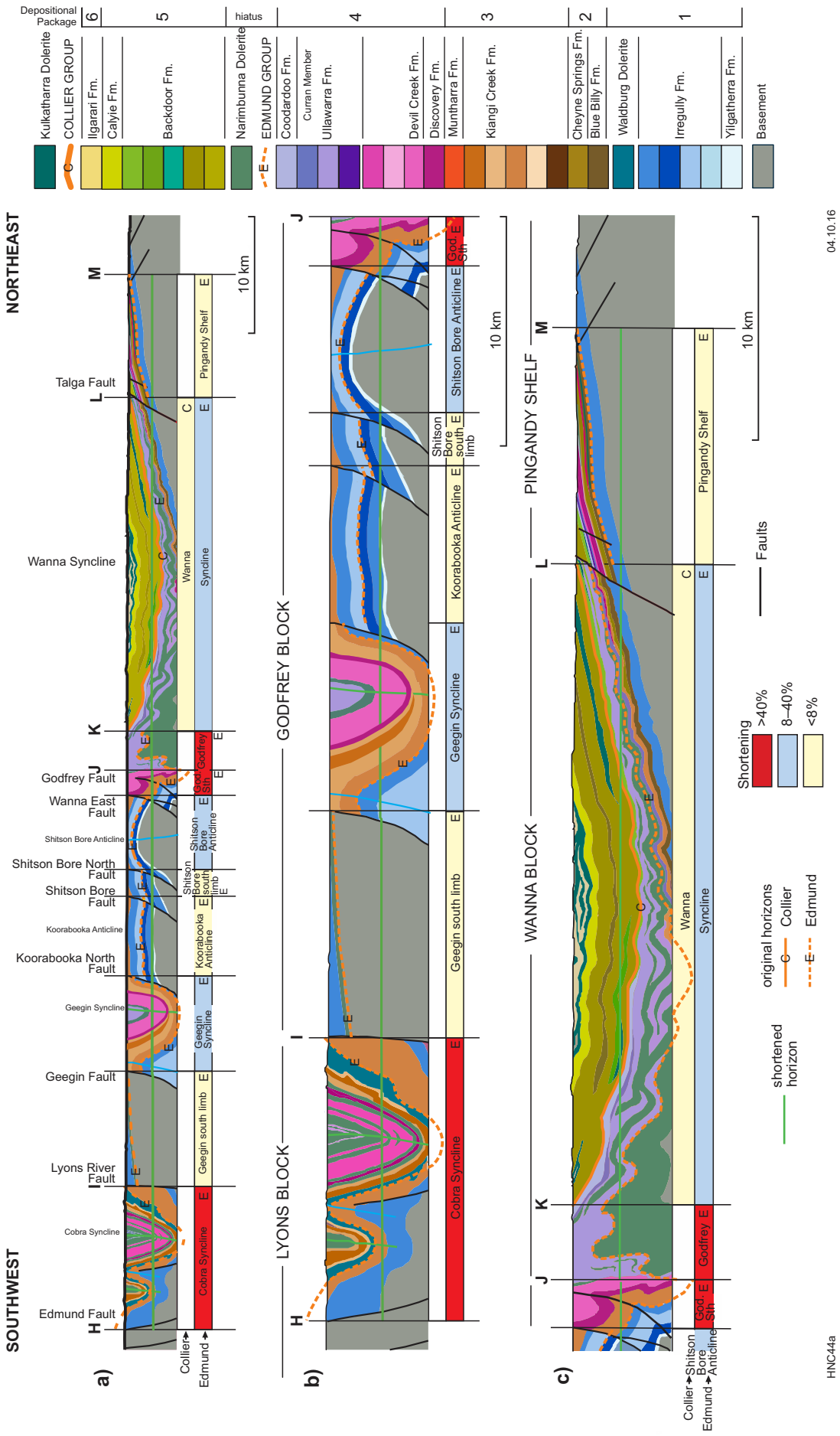

Figure 13. The western cross-section, southwest to northeast; a) complete section H–M; b) detailed enlargement of southern part of the section H–J; c) detailed enlargement of the northern part of the section J–M. Segments in which shortening has been calculated are named and the degree of shortening is colour coded. The km length of measured horizons (original orange line, shortened central green line, in Edmund Group = E, Collier Group = C), are listed in Table 3.

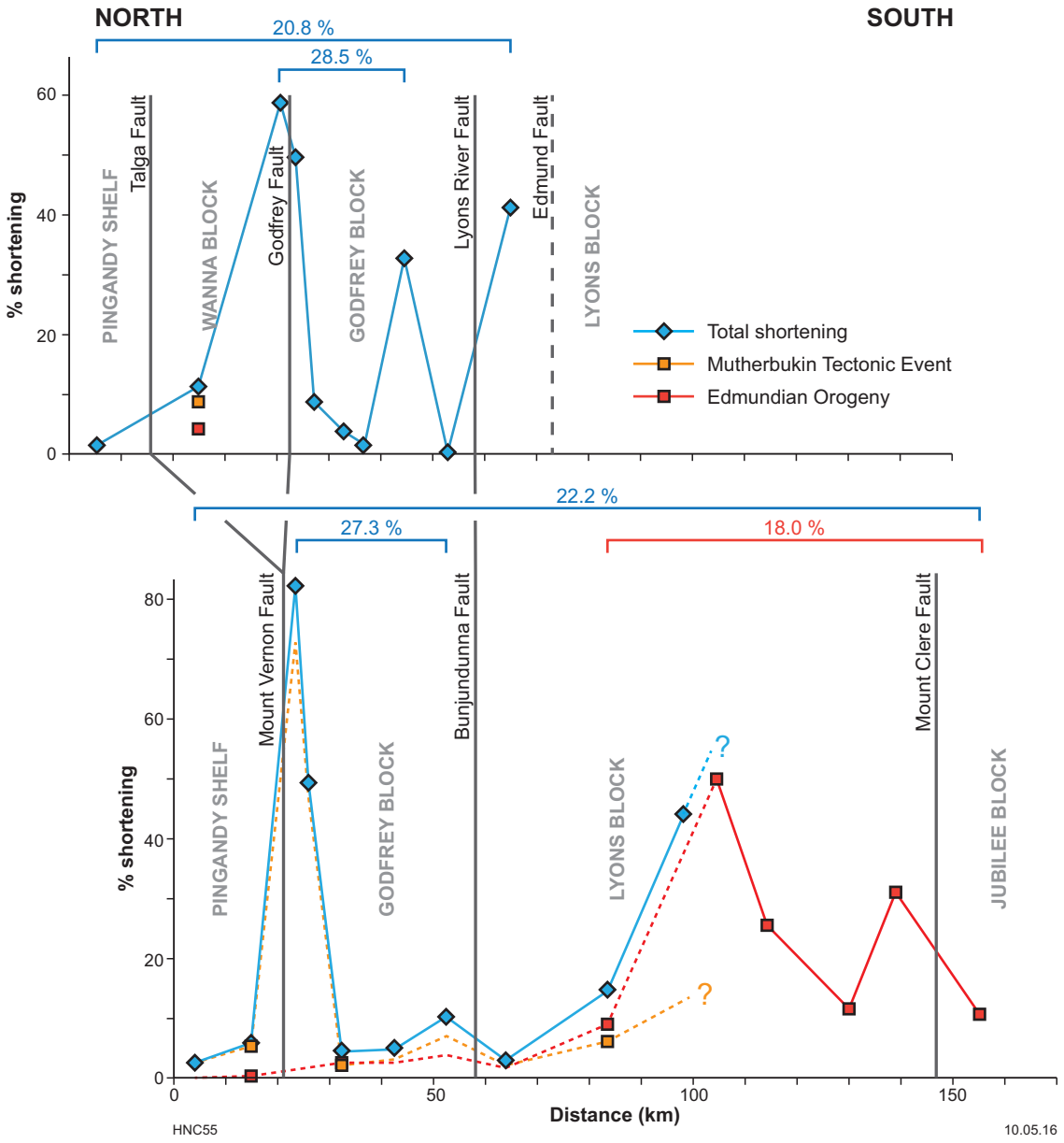

Figure 14. Estimates of shortening across the northern part of the Edmund and Collier Basins, based on line balancing of the western (a) and eastern (b) cross-sections shown in Figures 13 and 15. Differentiation between the two main deformation events is possible where both Edmund and Collier Group strata are present in the same fault segment.

were taken from each major sandstone unit throughout the stratigraphy, although no data were available from the uppermost part of the Collier Group, Depositional Package 6 (Figs 3, 5–9). Detrital zircons from 12 of these previously dated samples were selected for Lu–Hf isotope analyses.

The isotope analyses were made using a New Wave/Merchantek LUV213 laser-ablation microprobe, attached to a Nu Plasma multi-collector inductively coupled plasma mass spectrometer (LA-MC-ICPMS) at Macquarie University, Sydney, New South Wales. The analyses employed a beam diameter of about 40 µm (with ablation pits typically 40–60 µm deep), placed, where possible, over the existing SHRIMP U–Pb analysis pits in order to sample the same zircon domain. Detailed analytical conditions and measurements of standard zircons are provided in Appendix 3. The Lu–Hf data for each sample are presented in Appendix 4. Two-stage model ages were calculated assuming that the parental magma was produced from an average continental crust ($^{176}Lu/^{177}Hf$ = 0.015) that originally was derived from a depleted-mantle source with $(^{176}Hf/^{177}Hf)i$ = 0.279718 at 4560 Ma and $^{176}Lu/^{177}Hf$ = 0.0384 (Griffin et al., 2004).

Results

Fault movements during basin deposition

The Capricorn Orogen deep crustal seismic reflection survey imaged numerous, pre-existing, crustal-scale structures that controlled the depositional architecture of the Edmund and Collier Basins (Johnson et al., 2011d, 2013; Figs 2, 4). During formation of the Edmund Basin, these structures had a normal sense of movement with downdrop on the south side of each fault, producing a half-graben structure (Fig. 2). The northernmost of these faults, the Talga Fault, is one of the most significant structures in the basin, as it separates the Pingandy Shelf (Muhling and Brakel, 1985a) with its thinner, proximal sedimentary rocks, from the main part of the basin to the south. Because the seismic survey only imaged the thinnest, westernmost part of the Collier Basin (in the Wanna Syncline), the architecture and history of fault movement during the evolution of this basin are far less well constrained.

Depositional Package 1

The Yilgatherra Formation at the base of Depositional Package 1 (Thorne, 2015b) is present across most of the Edmund Basin (Fig. 5), although it is generally very thin (<30 m). There are no significant thickness variations across the Talga Fault onto the Pingandy Shelf, implying little or no movement on the fault at this time. Paleocurrent directions in this part of the basin indicate supply from local highs to the west and south, as well as from north of the Talga Fault. The thickest section is developed on the Lyons Block close to the Deadman, Tringadee and Turner Faults (Figs 5 and 11), in the southernmost part of the basin, where it is locally up to 550 m thick. This implies significant, but potentially only localized, normal, northwest-side-down movements on these structures.

The Edmund Basin expanded to its greatest extent (based on current outcrop) during the deposition of the Irregully Formation which, on the Pingandy Shelf, is generally 300–400 m thick, but to the south of the Talga Fault attains a maximum thickness of 3600 m (Fig. 5). Paleocurrent directions indicate supply of sediments from north of the Talga Fault with some flow along the axis of the basin towards the southeast. In the eastern part of the basin, paleocurrent directions indicate supply from the southeast. Deposition of the Irregully Formation resulted from large-scale normal movements on most of the major faults including the Talga – Mount Vernon, Godfrey, Lyons River – Quartzite Well, Edmund, Minga Bar, Ti Tree, Lockier, Turner, Tringadee and Deadman Faults, causing north to northeast tilting on the Wanna, Godfrey, and Lyons Blocks to form a half-graben structure. Expansion of the basin may have also been due, in part, to a sea-level rise. Marginal sag of the Pingandy Shelf in the north, and the static Jubilee and Paradise Blocks in the south, formed the northern and southern limits of the basin, respectively. On some parts of the Pingandy Shelf, the Irregully Formation was subaerially exposed, causing the development of teepee structures (Thorne, 2015d), suggesting there may have been a eustatic sea-level drop.

Depositional Package 2

The Gooragoora, Blue Billy and Cheyne Springs Formations, which make up Depositional Package 2 (Thorne, 2015e), show a very limited spatial distribution, implying deposition in a restricted depocentre (Fig. 6). They are present mostly in the northwestern part of the basin, although fluvial sandstones tentatively assigned to the Gooragoora Formation (Johnson et al., 2015a) are present in the Jillawarra Sub-basin in the east. However, it is possible that these rocks were deposited over a much wider area, with large parts of the package having been removed by erosion prior to the deposition of the disconformably overlying Kiangi Creek Formation. The contact between Depositional Package 2 and Package 1 is sharp, with no evidence of significant erosion, implying that deposition of Package 2 resulted from a gradual rise in sea level (Martin et al., 2008).

The Gooragoora Formation was deposited in a deltaic to shallow-marine setting, and is up to 250 m thick in the northwestern part of the basin. Paleocurrent directions and sedimentary structures show transport and delta progradation towards the south, indicating the presence of a topographic high somewhere to the north of the Pingandy Shelf. The overlying Blue Billy Formation is generally less than 200 m thick but locally comprises up to 800 m of deep-water carbonaceous siltstone and turbiditic sandstones. The overlying shelf to pelagic Cheyne Springs Formation comprises 50–300 m of dolomitic siltstone and sandstone, implying a slight shallowing and contraction of the basin at this time. Paleocurrent directions indicate supply from the north with flow also to the northwest along the axis of the basin with a broadly southwest-sloping shelf.

Thickness variations of the depositional package across the Talga Fault are minor, but offset of strata across the fault demonstrate that some downdrop accompanied sediment deposition. The distinct facies changes through the Gooragoora, Blue Billy and Cheyne Springs Formations probably record a relative rise in sea level and drowning of the Edmund Basin, including the Pingandy Shelf.

Depositional Package 3

Depositional Package 3 (Thorne, 2015i) comprises the Kiangi Creek and Muntharra Formations. The Kiangi Creek Formation is 200–500 m thick on the Pingandy Shelf and up to 2600 m thick in the southeastern part of the basin. The overlying Muntharra Formation is no more than 50 m thick and is restricted to the western end of the Pingandy Shelf adjacent to the Talga Fault (Fig. 7).

In the central and western parts of the basin, the Kiangi Creek Formation is dominated by deep-marine shelf siltstones and sandstones, interpreted to be part of a submarine fan system. However, on the Pingandy Shelf,

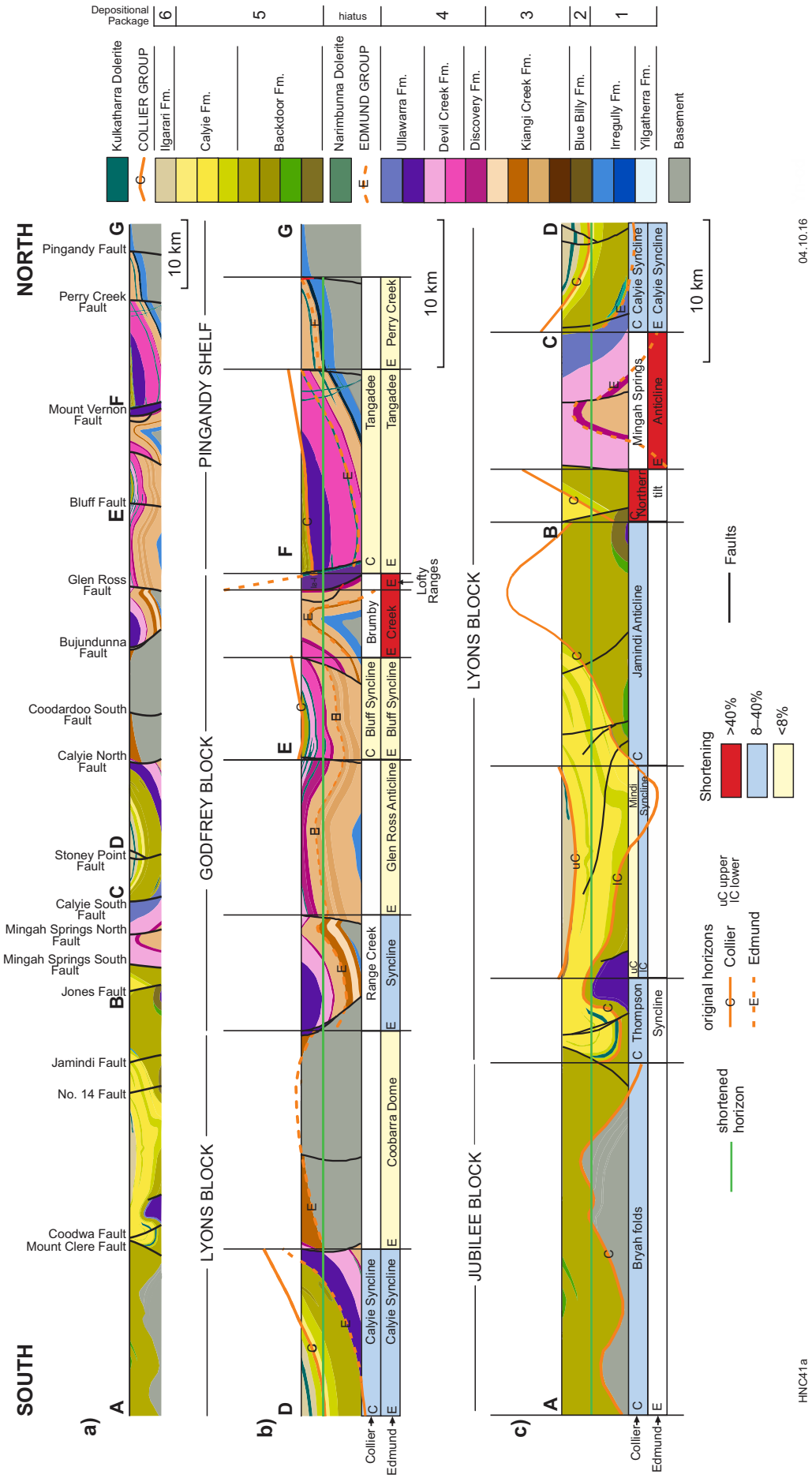

Figure 15. The eastern cross-section; a) complete section A–G; b) detailed enlargement of southern part of the section A–D; c) detail enlargement of the northern part of the section D–G. Segments in which shortening has been calculated are named and the degree of shortening is colour coded. The km length of measured horizons (original orange line, shortened central green line, in Edmund Group = E, Collier Group = C, upper Collier = uC, lower Collier = lC), are listed in Table 4.

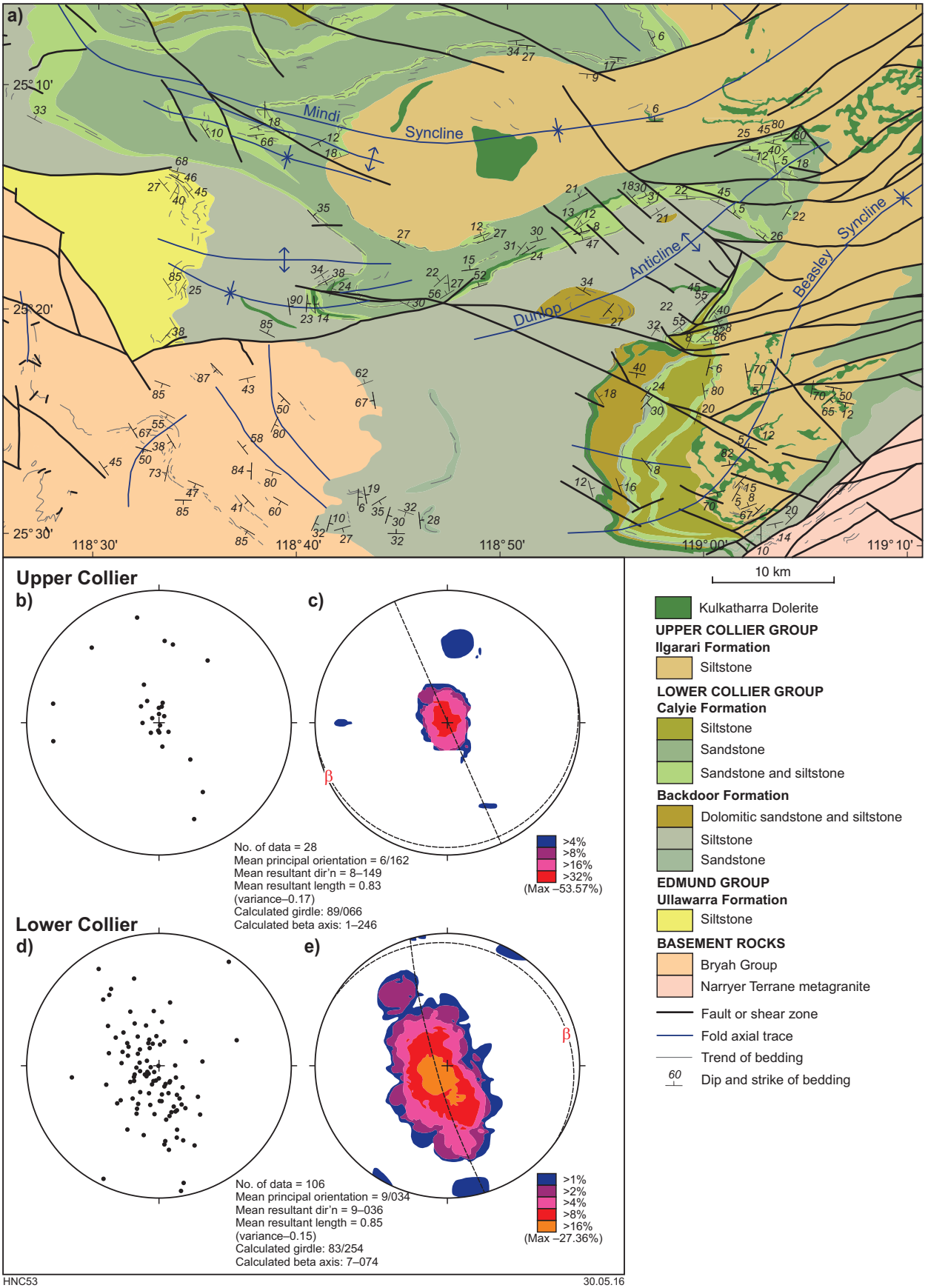

Figure 16. Comparison of folding in the upper and lower Collier Group, of the Mindi and Beasley Synclines and the Dunlop Anticline, located in the Milgun, Jamindi and Three Rivers 1:100 000 map sheets; a) geological map of structures. Stereographic projections (GEOplot) of poles to bedding of upper Collier Group (b) and (c) and of lower Collier Group (d) and (e). These show that the lower Collier Group has been more tightly folded.

and in the eastern part of the basin around the Coobarra Dome and in the Jillawarra Sub-basin, the Kiangi Creek Formation comprises predominantly fluvial-deltaic to shallow-marine shelf sandstones. Paleocurrent markers suggest a northerly source for sediment detritus throughout the basin. The base of the Kiangi Creek Formation is everywhere marked by a regional-scale, low-angle disconformity with the underlying units of Depositional Packages 1 and 2 (Martin and Thorne, 2004), and locally within the Coobarra Dome area, with granitic rocks of the 1820–1775 Ma Moorarie Supersuite of the Gascoyne Province.

The transition from Depositional Package 2 to Depositional Package 3 is interpreted as a period of uplift and erosion (Thorne, 2015e,i). In the Coobarra Dome area and Jillawarra Sub-basin in the east, the presence of a marked disconformity, which cuts through Depositional Packages 1 and 2 into the underlying Gascoyne Province basement, suggests that this part of the Edmund Basin was preferentially uplifted prior to the deposition of the Kiangi Creek Formation. Hydrothermal alteration and mineralization at the Abra polymetallic deposit in the Jillawarra Sub-basin is confined to Depositional Packages 1 and 2 (Thorne, 2015b,e). Coarse-grained sedimentary rocks of the Kiangi Creek Formation disconformably overlie the mineralized sections, indicating that hydrothermal alteration and mineralization occurred after deposition of the Gooragoora Formation during the period of uplift and erosion. Hydrothermal xenotime, intergrown with galena, hematite and magnetite, is dated between c. 1610 and 1590 Ma (Zi et al., 2015), and may suggest that the hiatus between Depositional Packages 2 and 3 may have been as long as 20 Ma. Differential uplift between the western and eastern parts of the basin may have been facilitated by minor faults between, and at a high angle to, the major northwest-southeast-trending structures.

Following the hiatus, thick (locally up to 2600 m) deposits of the Kiangi Creek Formation were deposited across the entire Edmund Basin, including the Pingandy Shelf (Fig. 7), and are associated with the infill and burial of a rapidly subsiding horst-and-graben basin architecture.

The relatively thin (<50 m) Muntharra Formation conformably overlies the Kiangi Creek Formation but is only present on the western end of the Pingandy Shelf. The formation comprises predominantly shallow-marine carbonates deposited under quiet-water conditions below storm wave-base. Paleocurrent directions indicate sediment supply from an upland area to the north (Fig. 7).

Depositional Package 4

Depositional Package 4 (Thorne, 2015l) comprises the Discovery, Devil Creek, Ullawarra and Coodardoo Formations. The package is distributed across most of the Edmund Basin, except in the far western part of the basin where it may have been removed by erosion (Fig. 8). The package attains a maximum thickness of about 3000 m in the central and southern parts of the basin and is at least 300–800 m thick on the Pingandy Shelf.

The Discovery Formation is generally 30–70 m thick on the Pingandy Shelf and locally up to 300 m thick in the main part of the basin to the south (Fig. 8). Deposition appears to have taken place mainly in a starved anoxic environment below storm wave-base. The Discovery Formation marks a major marine transgression that crossed the region from southwest to northeast.

The Devil Creek Formation is up to 600 m thick on the Pingandy Shelf and attains a maximum thickness of 1300 m in the main part of the basin. The formation comprises predominantly platform carbonates on the Pingandy Shelf, and finer grained basinal deposits to the south of the Talga – Mount Vernon Fault system. Paleocurrent data record flow towards the west and northwest.

The Ullawarra Formation ranges in thickness from 30 m on the Pingandy Shelf to about 1800 m in the central and southern parts of the basin. It is composed predominantly of turbiditic rocks with abundant Bouma Tb-c horizons with sole marks indicating paleocurrent directions towards the west and northwest. The Ullawarra Formation was sourced from a region that lay to the southeast of the present outcrop area and deposited in a deep-marine shelf environment.

The Coodardoo Formation is exposed mainly within the Wanna Syncline in the northern part of the Edmund Basin. The rocks have an unconformable contact with the overlying Collier Group and attain a maximum thickness of 370 m (Fig. 8). The relatively restricted present-day distribution more likely reflects the results of both pre- and post-Collier Basin uplift and erosion rather than deposition in a narrow, elongate depocentre. The formation comprises thin- to very thick-bedded, turbiditic rocks and was deposited within submarine fans in a deep-marine shelf environment. Limited paleocurrent data show that some sediment was supplied from a southeastern source, although there was also an increasing contribution from an upland area to the northwest.

The thick, extensive, mainly deep-marine deposits of Depositional Package 4 imply continued normal movements on most of the major faults including the Talga, Godfrey, Mount Vernon, Lyons River and Quartzite Well Faults, and that downdrop of the intervening fault blocks kept pace with, or exceeded, deposition rates. Fault activity may have been accompanied by eustatic sea-level rise.

Depositional Package 5

Depositional Package 5 (Thorne, 2016b) comprises the Backdoor and Calyie Formations of the Collier Group, which are present in the core of the Wanna Syncline and in the eastern part of the basin (Fig. 9). The distribution of lithologies prior to regional-scale folding during the 1026–954 Ma Edmundian Orogeny, however, is not known. The Backdoor Formation attains a maximum thickness of 1900 m and has an unconformable lower contact with rocks of the Edmund and Bryah Groups. The formation comprises mostly fine-grained siliciclastic rocks with minor carbonate rocks that were deposited

below storm wave-base on a distal shelf environment. The conformably overlying Calyie Formation is generally 100–300 m thick in the Wanna Syncline but thickens to 1500–1800 m in the eastern part of the basin. The sandstone-dominated formation was deposited in a delta-front to delta-top environment. In the Wanna Syncline, paleocurrent directions switch from southwesterly directed in the Backdoor Formation to northwesterly directed in the Calyie Formation (Martin et al., 2008), reflecting uplift to the southeast and erosion of the Edmund Group and progradation of the delta front away from the source area (Fig. 9). Paleocurrent data from the eastern part of the basin show northwest-, west- and southwest-directed paleocurrents in the Backdoor Formation and highly variable directions in the Calyie Formation. This suggests uplift to the east, and to the north of the Talga Fault, and even within the eastern part of the basin.

Depositional Package 6

The Ilgarari Formation of Depositional Package 6 (Thorne, 2016e) is up to 1500 m thick and has a similar spatial distribution to units in Depositional Package 5 (Fig. 9). The formation has a conformable contact with the underlying Calyie Formation and comprises fine-grained siliciclastic rocks deposited in a deep-marine anoxic environment. The transition from the Calyie to Ilgarari Formation represents a significant deepening of the basin that terminated delta progradation. No paleocurrent directions have been recorded within the Ilgarari Formation.

Estimates of extension and shortening

Capricorn Orogen deep crustal seismic reflection survey

The northern part of seismic line 10GA-CP2 (Johnson et al., 2013) imaged a near-complete (Depositional Packages 1, 2 and 3), gently folded section of Edmund Group strata up to 7 km thick, but in the Cobra Syncline in the middle part of the basin, the strata are more strongly deformed and the position of depositional package boundaries are less well defined (Fig. 2). The seismic section shows normal offset of strata across each of the major half-graben-bounding faults including the Talga, Godfrey, Lyons River and Cobra Faults. Incremental movements on the Talga and Godfrey Faults could be resolved by measuring the displacement at the base of each depositional package (in this case, Depositional Packages 1, 2 and 3) across the fault (Fig. 12; Table 1), and removing the effects of each subsequent event from the previous. The results for both faults were similar with about 1500 m, 500 m and 300 m of extension recorded during the deposition of Depositional Packages 1, 2 and 3, respectively (Table 1). The total displacement recorded by the offset on the base of Depositional Package 1 across any of the faults, is a cumulative record of all normal movement events on that fault. Despite the poor resolution of depositional package boundaries within the Cobra Syncline, minimum estimates of extension could still be calculated for the Lyons River and Cobra Faults based on the offset of the Edmund Group – Gascoyne Province basement contact, which is clearly defined in the seismic section. Extension on these faults is estimated at about 2000 m and >100 m, respectively. These results indicate a minimum net extension across the northern part of the basin (the Wanna and Godfrey Blocks) of >7–8%, of which 68% occurred during the deposition of Depositional Package 1 (Table 1). These results, despite being a minimum, are comparable to estimates of regional extension in other intracontinental basins such as the Canning Basin in Western Australia and the Basin and Range Province in the western US (Appendix 2).

Between the Godfrey and Edmund Faults, many smaller-scale structures, including the Cardibar – Blue Bush Fault, show reverse displacements of the Edmund Group – Gascoyne Province basement contact. The amount of shortening recorded on individual structures is between about 100 and 870 m, with the greatest displacements on the Edmund and Terminus Faults (Table 2). Total shortening, due to fault reactivation, in the region between the Godfrey and Edmund Faults is estimated at 6%.

Basinwide cross-sections

Western cross-section

The western cross-section is about 90 km long and extends from the Pingandy Shelf in the northeast to the Edmund Fault in the southwest (Figs 1 and 13). The Collier Group is mostly absent from the section, apart from within the Wanna Syncline segment where both Edmund and Collier Group strata are present. The tightness of folding, and thus shortening, varies greatly between adjacent segments (Table 3; Fig. 13). Total shortening, the cumulative effects of both the 1321–1171 Ma Mutherbukin Tectonic Event and the 1026–954 Ma Edmundian Orogeny, varies across the length of the section (Fig. 14a), but averages 20.8%. Total shortening is lowest across the Geegin South limb and Pingandy Shelf segments at 0.1 and 1.4%, and greatest in the Cobra Syncline, Godfrey South and Godfrey segments at 40.4, 49.6 and 58.8%, respectively (Fig. 14a). In the region between the Godfrey and Lyons River Faults, the Capricorn Orogen deep crustal seismic section (10GA-CP2) has highlighted the presence of numerous reverse faults with displacements totalling 6%. In the same region (including the footwall of the Godfrey Fault), total shortening due to folding is calculated at 28.5% (Table 3; Fig. 14a), demonstrating that strain was preferentially accommodated by folding of sedimentary strata rather than by fault reactivation.

In the Wanna Syncline segment, both the Edmund and Collier Group strata are deformed into open folds, although there is greater amount of shortening recorded in the Edmund Group succession at 11.2%, than in the overlying Collier Group at 3.7% (Table 3; Fig. 14a). This difference records the successive accumulation of strain in the Edmund Group, which was deformed during both the Mutherbukin Tectonic Event and the Edmundian

Table 3. Shortening on folds: western cross-section

Fault segment (north to south)	*Group*	*Shortened length (km)*	*Original length (km)*	*Difference (km)*	*Shortening (%)*
Pingandy Shelf	Edmund	10.56	10.71	0.15	1.4
Wanna Syncline	Collier	28.63	29.75	1.12	3.77
Wanna Syncline	Edmund	28.63	32.25	3.62	11.22
Godfrey	Edmund	3.36	8.17	4.81	58.87
Godfrey south	Edmund	2.16	4.29	2.13	49.65
Shitson Bore Anticline	Edmund	6.34	6.94	0.6	8.65
Shitson Bore south limb	Edmund	2.33	2.42	0.09	3.72
Koorabooka Anticline	Edmund	6.8	6.88	0.08	1.16
Geegin Syncline	Edmund	8.21	12.19	3.98	32.64
Geegin south limb	Edmund	9.87	9.88	.01	0.1
Cobra Syncline	Edmund	12.29	20.65	8.36	40.48
Average shortening (%) Collier = Edmundian Orogeny					3.77
Average shortening (%) Edmund = Mutherbukin Event					20.78
True ratio (Mutherbukin/Edmundian)					4.5:1

NOTES:
Calculated shortening across named segments of the western cross-section. Averaged across the complete basin, the Mutherbukin Event was more active than the Edmundian Orogeny with a ratio of 4.5:1 derived from (20.78-3.77)/3.77. However, only one segment includes the Collier Group, which increases the uncertainty in this value.

Orogeny, compared to the Collier Group, which was deformed only during the younger event. Thus, 3.7% of the total shortening recorded in the Edmund Group can be attributed to the Edmundian Orogeny. In the Wanna Syncline, most of the shortening/folding (~10.7%) took place during the Mutherbukin Tectonic Event (Fig. 14a). Because Collier Group strata are only present in the Wanna Syncline segment, differentiating between the effects of the two deformation events from the total accumulated strain across the section is not possible.

Eastern cross-section

The eastern cross-section is 166 km in length and passes just to the east of the Abra deposit (Figs 1 and 15). The section contains three segments, which contain both Edmund and Collier Group strata, and eight segments that contain Collier Group strata alone, allowing for a more robust estimation of shortening across the basins during each of the deformation events.

Similar to the western cross-section, fold tightness differs markedly between segments (Table 4) but results in a similar average total shortening across the section of 22.2% (Fig. 14b). Total shortening is lowest across the Perry Creek, Bluff Syncline, Glen Ross Anticline, and Coobarra Dome segments at 2.5, 4.5, 4.8 and 2.9%, and greatest in the Loft Range Tilt, Brumby Creek, Mingah Springs Anticline, and Northern Tilt segments at 82.5, 49.8, 44.1 and 49.9%, respectively (Fig. 14b). In the three segments where both Edmund and Collier Group rocks are present, the proportion and intensity of shortening due to the 1026–954 Ma Edmundian Orogeny generally increases to the south (Fig. 14b), particularly to the south of the Calyie Syncline where strongly deformed Collier Group strata are present. In this zone, shortening during the Edmundian Orogeny is estimated at 18.0% (Fig. 14b). Total shortening in this zone is not known, because no Edmund Group strata are present.

In the northern part of the section, intense shortening in the Lofty Range Tilt and Brumby Creek segments occurs in a similar geographical position to folding and reverse fault movement in the western part of the basin, that is, between the Godfrey and Lyons River Faults (Figs 13 and 14b). Total shortening due to folding in this zone is estimated at 27.3%, similar to that for the western cross-section (Fig. 14b). Due to the lack of abundant Collier Group strata in this zone, it is not possible to precisely differentiate between the effects of the different deformation events. However, because the effects of the Edmundian Orogeny appear to increase significantly towards the south, it is possible that most of the shortening in this zone may be attributable to the 1321–1171 Ma Mutherbukin Tectonic Event.

In the Mindi Syncline segment, there appears to be a difference in shortening between strata of the lower and upper Collier Group (Depositional Packages 5 and 6), estimated at 11.5 and 1.9%, respectively (Fig. 15). This difference is also reflected in the measured dip and strike of strata in the Mindi and Beasley Synclines and the Dunlop Anticline on Jamindi and Three Rivers (Cutten et al., 2013, Blay et al., 2014), where the lower Collier Group shows a greater range of orientations than the upper Collier Group (Fig. 16). Despite the apparent conformable relationship between the Calyie (lower Collier Group) and Ilgarari (upper Collier Group) Formations across most of the Collier Basin, these relationships imply that deposition of each unit was separated by a period of deformation, at least in the southernmost part of the basin.

Table 4. Shortening on folds: eastern cross-section

Fault segment (north to south)	*Group*	*Shortened (km)*	*Original (km)*	*Difference (km)*	*%*
Perry Creek	Edmund	7.0	7.18	0.18	2.5
Tangadee	Collier	15.37	15.41	0.04	0.26
Tangadee	Edmund	15.37	16.36	0.99	6.05
Lofty Range tilt	Edmund	1.25	7.13	5.88	82.47
Brumby Creek	Edmund	5.11	10.17	5.06	49.75
Bluff Syncline	Collier	7.62	7.8	0.18	2.31
Bluff Syncline	Edmund	7.62	7.98	0.36	4.51
Glen Ross Anticline	Edmund	11.66	12.25	0.59	4.82
Range Creek Syncline	Edmund	8.74	9.73	0.99	10.18
Coodardoo Dome	Edmund	16.39	16.88	0.49	2.9
Calyie Syncline	Collier	19.98	21.94	1.96	8.93
Calyie Syncline	Edmund	19.98	23.42	3.44	14.69
Mingah Springs Anticline	Edmund	9.23	16.5	7.27	44.06
Northern tilt	Collier	3.6	7.19	3.59	49.93
Jamindi Anticline	Collier	16.5	22.14	5.64	25.47
Mindi Syncline	Upper Collier	14.39	14.67	0.28	1.91
Mindi Syncline	Lower Collier	14.39	16.26	1.87	11.50
Thompson Syncline	Collier	5.76	8.34	2.58	30.94
Bryah folds	Collier	24.0	26.85	2.85	10.62
Average % shortening Collier = Edmundian Orogeny					17.5
Average shortening (%) of Edmund Group by the Mutherbukin Event					22.19
Ratio of shortening of the Edmundian Orogeny to Mutherbukin Event					3.7:1
Ratio of shortening of early Edmundian Orogeny to late Edmundian Orogeny					5:1

NOTES:
Calculated shortening across named segments of the eastern cross-section. All units are km, except % and ratios. Averaged across the complete basin, the Edmundian Orogeny was more active than the Mutherbukin Event with a ratio of 3.7:1 derived from (17.5/22.19-17.5). Calculated from the Mindi Syncline, the early Edmundian Orogeny was more active than the late Edmundian with a ratio of 5:1 derived from (11.5-1.91)/1.91.

Lu–Hf isotope compositions and ages of detrital zircons

The age distribution of previously dated (Martin et al., 2008) detrital zircons from 18 sandstone units throughout the Edmund and Collier stratigraphy (Fig. 3) are plotted as a series of Kernel Density Estimation plots (KDE) (Fig. 17a; Vermeesch 2012). These plots are constructed, and work, in a similar way to the more commonly produced probability density distribution plots (PPD). Unlike the PPD, the KDE do not suffer from the over-representation of precise data or artificial smoothing of data when the sample set is large (Vermeesch, 2012). The total dataset includes 1089 analyses of zircons that are less than 10% discordant. Detrital zircons from the 18 samples yield a range of dates from c. 4291 to 1325 Ma (Fig. 17a). Major age components are defined at c. 3475, 3160, 2965, 2750, 2710–2695, 2530–2500, 2450, 2290–2250, 1995, 1950, 1795–1775 and 1680 Ma.

A total of 242 Hf isotope analyses was made on 242 previously dated (<10% discordant) detrital zircons (Appendix 4), covering the major age modes identified in the KDE (Fig. 17). The zircons have a moderate range of initial $^{176}Hf/^{177}Hf$ compositions between 0.280481 and 0.282031, leading to a range of $\varepsilon Hf_{(i)}$ values between +9.0 and –18.1 (Fig. 18a–c). The 1795–1775 and c. 1680 Ma age modes show the greatest variation in $\varepsilon Hf_{(i)}$ values, ranging from less evolved to strongly evolved compositions relative to Chondritic Uniform Reservoir (CHUR). The majority of the older grains, particularly in the 2965–2500 Ma range, are less evolved than CHUR.

Discussion

Basin architecture, deposition and provenance of the Edmund Group

The regional-scale half-graben architecture of the Edmund Basin, as imaged in the Capricorn Orogen deep crustal seismic section (Johnson et al., 2011a, 2013; Fig. 2), is also reflected by the variable distribution and thickness of sedimentary units across the basin (Figs 5–9). Each half-graben is bounded by a major crustal-scale structure that represents a normally reactivated pre-existing fault or shear zone that formed during assembly of the West Australian Craton (Johnson et al., 2011a, 2013). In the upper part of the crust, these structures are steeply dipping (Fig. 2), and thus small amounts of regional-scale extension will have resulted in large normal fault movements with the development of a deep basin. Across the northern part of the Edmund Basin, extension is estimated at 7–8%, resulting in the deposition of up to 500 m of sediment on the Wanna Block, and up to 7000 m on the Godfrey Block (Fig. 2). Most of the major structures record the greatest amount of normal movement (~68% of all extensional movements) during the deposition of Depositional Package 1 (Table 1), indicating that the half-graben architecture was initiated early in the basin history. On the Godfrey Block, this resulted in the deposition of about 3600 m of slope carbonates and fluvial to shallow-marine siliciclastic sedimentary rocks of the Irregully Formation, accounting for over half of the total basin thickness on this block. The timing of basin initiation is relatively poorly constrained, but occurred some time after c. 1679 Ma (Martin et al., 2008), the age of the youngest detrital zircon age components in the underlying Mount Augustus Sandstone, but before hydrothermal alteration and mineralization at the Abra polymetallic deposit at c. 1610 Ma (Zi et al., 2015). Most paleocurrent structures within Depositional Package 1, across the basin, indicate that sediment detritus was sourced from an area to the north of the Pingandy Shelf, although local highs may have been present in the southeast. Sediment supply must have been relatively high in order to keep pace with block downdrop, suggesting there may have been contemporaneous uplift of a northern highland region during basin initiation and subsequent growth.

Despite the restricted distribution of Depositional Package 2, due to subsequent uplift, erosion and removal prior to the deposition of Depositional Package 3, a near-continuous sequence is present in the northern part of the basin. Here, sedimentation records a progressive deepening of the basin from deltaic to shallow-marine conditions at the base, to deep-water and pelagic environments at the top. Thickness variations across the Talga Fault are minor, although at least 558 m of downdrop (or 322 m of extension) is recorded on the Talga Fault itself (Table 1) in the western part of the basin. Despite this, the facies variations most likely record a relative rise in sea level rather than significant downdrop and extension on the major faults. Paleocurrent structures, and the southwards progradation of the Gooragoora Formation delta front, indicate that sediment detritus was still being sourced from a prominent highland region to the north of the Pingandy Shelf.

A regional-scale disconformity at the base of Depositional Package 3 records a period of uplift and erosion. The disconformity is most pronounced in the eastern part of the basin, particularly the Jillawarra Sub-basin, where underlying sedimentary rocks of Depositional Packages 1 and 2 have been variably removed. In the Coobarra Dome area of the sub-basin, fluvial rocks at the base of Depositional Package 3 directly overlie basement rocks of the Gascoyne Province. Hydrothermal mineralization at the Abra polymetallic deposit is contained within rocks of Depositional Packages 1 and 2 (Zi et al., 2015; Johnson et al., 2015a) and is separated from unmineralized coarse-grained sandstones at the base of Depositional Package 3 by an unconformity, which is likely to be equivalent to the regional-scale disconformity observed elsewhere throughout the basin (Johnson et al., 2015a). This indicates that regional-scale uplift and erosion, particularly in the eastern part of the basin, occurred in a similar time frame to mineralization and hydrothermal alteration, which is dated between c. 1610 and 1590 Ma (Zi et al., 2015). These constraints indicate that deposition of Depositional Packages 1 and 2 were complete prior to hydrothermal alteration at c. 1610 Ma, and that deposition of sedimentary rocks at the base of Depositional Package 3 did not begin until after the cessation of hydrothermal activity at c. 1590 Ma.

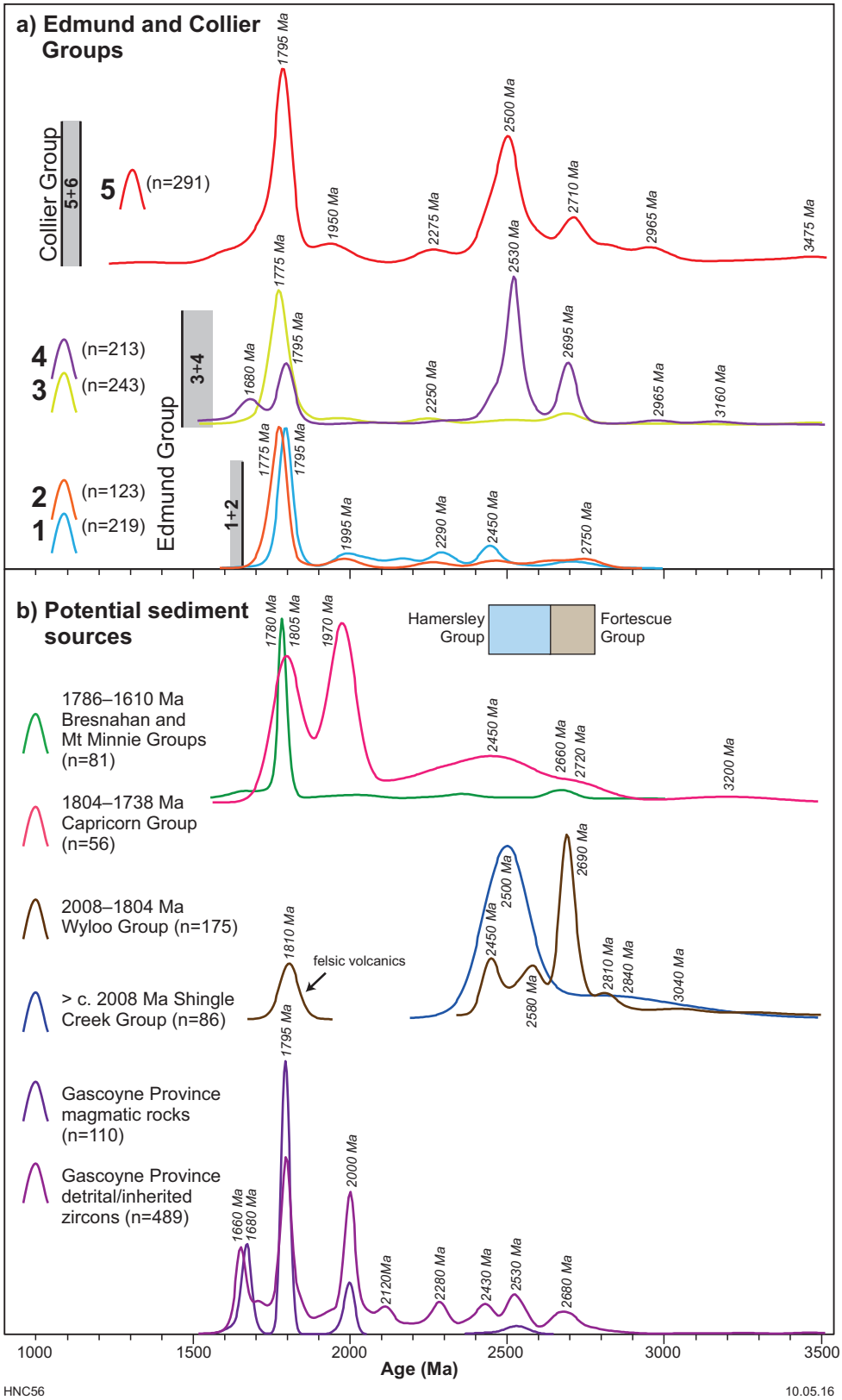

Figure 17. **Kernel density estimates (KDE, Vermeesch, 2012) for the age of: a) detrital zircons from the Edmund and Collier Groups; and b) detrital and magmatic zircons from potential source regions of the Gascoyne Province and northern Capricorn Orogen basins of the southern Pilbara region. Geochronology data available at <www.dmp.wa.gov.au/geochron>.**

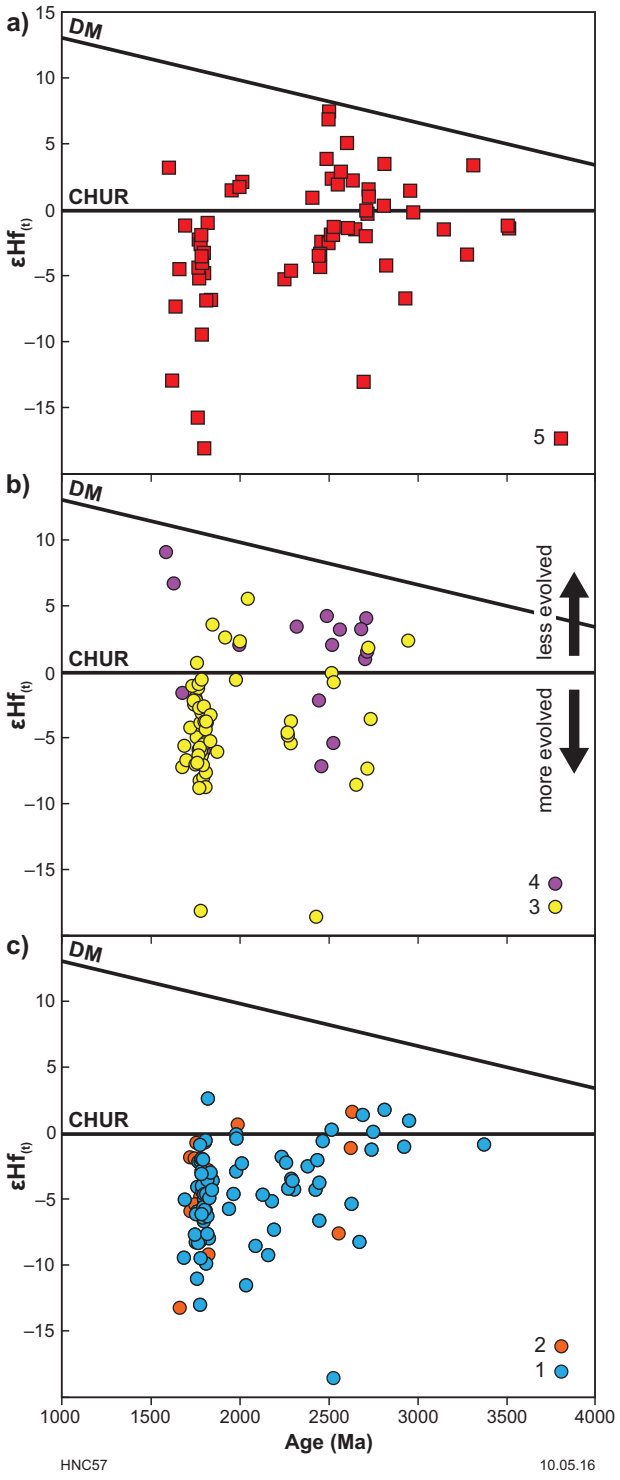

Figure 18. $\varepsilon Hf_{(i)}$ ratios of detrital zircons from the Edmund and Collier Groups, divided into: a) Depositional Package 5 of the Collier Group; b) Depositional Packages 3 and 4 of the Edmund Group; c) Depositional Packages 1 and 2 of the Edmund Group. Lu–Hf isotope data are presented in Appendix 4.

Along the Pingandy Shelf, and adjacent to the Coobarra Dome, the lowermost sedimentary rocks of Depositional Package 3 are characterized by fluvial-deltaic to shallow-marine sandstones, which transition rapidly into deeper water facies in the central and eastern parts of the basin (Cutten et al., 2010). Sediment thickness is highly variable across the basin (200–2600 m), but is thickest on the Godfrey Block, particularly in the east, where the strata are up to 2600 m thick (Fig. 7). The deep-water nature of the sedimentary rocks in the central and eastern parts of the basin imply rapid subsidence and downdrop of the horst-and-graben architecture. However, in the western part of the basin, downdrop and extension on both the Talga and Godfrey Faults was relatively limited, at about 418 m (241 m extension) and 396 m (228 m extension), respectively. To accommodate the thicker section of deep-water sedimentary rocks in the central and eastern parts of the basin, it is possible that the major faults moved differentially along strike, with significantly greater amounts of downdrop and extension taking place on the eastern parts of the fault systems. In the southeastern part of the basin, paleocurrents indicate that most sediment detritus was locally sourced from an upland area in the vicinity of the Coobarra Dome, whereas those in the northern, central, and eastern parts were sourced from the highland region north of the Pingandy Shelf. The upper parts of Depositional Package 3 were deposited in response to shallowing of the basin along the Pingandy Shelf, although deeper water sediments continued to be deposited towards the southwest (Martin and Thorne, 2004). In the central part of the basin, the Kiangi Creek Formation is intruded by numerous dolerite sills of the 1517–1505 Ma Waldburg Dolerite, indicating that the deposition of at least the lower part of Depositional Package 3 was complete by c. 1517 Ma (Wingate et al., 2015a).

The base of Depositional Package 4 is marked by a major marine transgression that appears to have crossed the region from southwest to northeast (Martin et al., 2008). Depositional Package 4 is dominated by deep-marine siliciclastic rocks, although on the Pingandy Shelf, the remnants of a ravinement surface at the base of the package, suggests a localized period of uplift and erosion prior to the marine transgression. The lower and middle parts of Depositional Package 4 are thickest in the southeastern part of the basin on the Lyons Block, totalling about 3000 m (Fig. 8). These units thin northward onto the Pingandy Shelf, suggesting that normal movements on the major fault structures were greatest in the southern part of the basin, particularly on the Lyons River – Quartzite Well, and Ti Tree – Mount Clere Fault systems (Fig. 8). Additionally, the thickening of the Discovery Formation at the base of the depositional package towards the Lyons River – Quartzite Well Fault, suggests a downdrop of the Lyons Block to the northeast (Daniels, 1966; Martin and Thorne, 2004). Most of the paleocurrent structures in the lower to middle parts of the depositional package record paleoflow from the south or flow axial to the basin (Fig. 8), although the Coodardoo Formation at the top of the package shows an increased contribution of detritus from the north of the Pingandy Shelf.

The pattern of fault movement, block downdrop and paleoflow associated with the deposition of Depositional Package 4 are in marked contrast with those in most of the underlying parts of the basin, suggesting a significant change in tectonic control on basin evolution, with the uplift of a source region to the south. Thin felsic volcaniclastic rocks within the Ullawarra Formation towards the top of the depositional package are dated between c. 1463 and 1455 Ma (Wingate et al., 2010, 2012c), providing a maximum depositional age for the upper parts of the package stratigraphy. These dates are within uncertainty of the 1465–1452 Ma Narimbunna Dolerite sills that intrude the lower and middle parts of the package (and all underlying stratigraphic units), and indicate that felsic volcanism, mafic magmatism, and sedimentation were essentially coeval and synchronous with the uplift of the southern source region and the switch in basin architecture.

Source of sediment detritus

Detrital zircons from 13 samples from the Edmund Group (Figs 3, 5–8), yield a range of individual $^{207}Pb^*/^{206}Pb^*$ dates (<10% discordant) from c. 4291 to 1497 Ma (Appendix 4). Although all the samples are dominated by 1795–1775 Ma zircons, the proportion of older zircon age components changes with stratigraphic position (Fig. 17a; Martin et al., 2008). Sandstone units of Depositional Packages 1, 2 and 3 contain only minor proportions (11–16%) of older grains, whereas those from Depositional Package 4 are dominated (55%) by Neoarchean grains (Fig. 17a). The majority of the major detrital zircon age components within Depositional Packages 1–4, are similar to the ages of magmatic zircons in granitic rocks or detrital zircon components in metasedimentary rocks in the Gascoyne Province basement, suggesting that the underlying basement could be the primary source of sediment detritus (Fig. 17b). However, paleocurrent structures throughout Depositional Packages 1–3 in the northern part of the basin, where the majority of detrital zircon samples were collected, indicate that detritus was sourced predominantly from an upland region to the north of the Pingandy Shelf, presumably the southern Pilbara region. This area consists of numerous metasedimentary and volcaniclastic rocks of various ages including the 2775–2629 Ma Fortescue, 2629–2445 Ma Hamersley, 2445–2208 Ma Turee Creek, c. 2208 Ma Shingle Creek (formerly the lower Wyloo Group), 2008–1786 Ma Wyloo (formerly the upper Wyloo Group), 1805–1738 Ma Capricorn and 1786–1610 Ma Bresnahan Groups, each of which has a unique detrital zircon signature (Fig. 17b). The oldest rocks, the Fortescue and Hamersley Groups, are mostly volcanic and volcaniclastic in origin (Thorne and Trendall, 2001), and are characterized by abundant magmatic zircons in the 2775–2450 Ma age range (Trendall et al., 2004). These rocks were recycled during uplift and erosion into the Turee Creek, Shingle Creek and Wyloo Groups, which are dominated by detrital zircons of the same age (Fig. 17b; Thorne and Seymour, 1991; Takehara et al., 2010; Martin, partial report; Thorne, partial report; Thorne, 2016h). The youngest rocks, the Capricorn and Bresnahan Groups, were sourced from an upland area in the central part of the Capricorn Orogen (Thorne and Seymour, 1991), most likely the Gascoyne Province, and are dominated by detrital zircons in the 2000–1780 Ma age range (Fig. 17b). The ages and Lu–Hf isotope compositions of detrital zircons from the possible source rocks are shown in Figure 19b and are presented in Appendix 5.

There is considerable overlap in age and isotope composition of zircons from the southern Pilbara sources with those from the Gascoyne Province, thus making it difficult to distinguish between the different source components. Despite this overlap, there are several age and isotope compositions that are unique to each region (areas i–iii in Fig. 19a). Abundant 3250–2450 Ma detrital zircons in the Shingle Creek and Wyloo Groups (sourced from the Pilbara Craton and Fortescue and Hamersley Groups) have similar ages to magmatic and inherited zircons from the 2555–2430 Ma Halfway Gneiss in the Glenburgh Terrane of the Gascoyne Province (Johnson et al., 2010). Although there is some overlap in Hf isotope composition, the majority of zircons from the Fortescue, Hamersley, Shingle Creek, and Wyloo sources are mostly less evolved than CHUR (positive $\varepsilon Hf_{(i)}$ values; area i on Fig. 19a), whereas those of similar age from the Gascoyne Province are mostly more evolved than CHUR (negative $\varepsilon Hf_{(i)}$ values). Despite the Capricorn and Bresnahan Groups being sourced predominantly from the Gascoyne Province (Fig. 19a; Thorne and Seymour, 1991), both groups lack detritus from a variably evolved 2120–2000 Ma source (area ii in Fig. 19a), and relatively radiogenic c. 1800 Ma source (area iii in Fig. 19a) that is prevalent in the Gascoyne Province. Presumably, the source areas for these zircon components were relatively localized and were not exposed during deposition of the Capricorn and Bresnahan Groups.

Paleocurrents indicate that sedimentary rocks in Depositional Packages 1–3 were sourced predominantly from north of the Pingandy Shelf. All three depositional packages show similar source contributions (Fig. 17), although sandstones from Depositional Package 1 contain some pre c. 1800 Ma grains with age components defined at c. 2750, 2450, 2290 and 1995 Ma. Most of these components are present in the Capricorn Group (Fig. 19a) and, critically, the detrital zircons with ages between c. 3250 and 2450 Ma are mostly more evolved than CHUR, suggesting they were ultimately sourced from the radiogenic Halfway Gneiss of the Gascoyne Province (i.e. via the Capricorn Group) rather than the Pilbara Craton and Fortescue and Hamersley Groups (i.e. via the Wyloo or Shingle Creek Groups; Figs 18b,c and 19b). The predominance of 1795–1775 Ma zircons suggests that the Bresnahan Group may also have been an additional sediment source (Figs 17a and 18a,b).

A major change in paleocurrent direction is recorded in the lower and middle stratigraphic units of Depositional Package 4, with most sediment being sourced from a newly formed upland area to the south of the basin. However, the Coodardoo Formation at the top of the package records a return of sediment detritus from an upland area north of the Pingandy Shelf. The analysed

samples were all collected from near the top of the stratigraphic package (Fig. 3) with samples GSWA 148975 and 152962 from the Coodardoo Formation (Martin et al., 2008) and sample GSWA 148974 from the underlying Curran Member of the Ullawarra Formation. These samples also record a major change in zircon provenance (Fig. 20). All three samples are dominated by Neoarchean zircons with prominent age modes at c. 2695 and 2530 Ma (Figs 17a and 20). These grains have less evolved $\varepsilon Hf_{(i)}$ isotope compositions than CHUR (plotting in area i on Fig. 19a), and are similar to the 3250–2450 Ma detrital zircons in the Shingle Creek and Wyloo Groups (or the Fortescue and Hamersley Groups; Fig. 19a) rather than any sources in the Gascoyne Province. Additionally, the sample from the Curran Member contains a minor age mode at c. 1680 Ma (Fig. 20), the only known source of which is the 1680–1620 Ma Durlacher Supersuite in the Gascoyne Province. With its predominantly north-directed paleocurrent directions (Fig. 8), the Curran Member shows a mixed provenance, with detritus sourced from both the Gascoyne Province and the Shingle Creek and Wyloo Groups (Figs 17b, 19b,c and 20). This is in contrast with the overlying Coodardoo Formation, which records sediment derived only from the southern Pilbara region. Additional samples from lower in the stratigraphic package or from farther south in the basin, or both, would help elaborate the major changes in sediment provenance throughout this depositional package.

The persistence of a northerly derived sediment source throughout the c. 225 Ma depositional period of the Edmund Basin, which led to a basin fill about 7 km thick, indicates that the southern Pilbara region, the predominant source of detritus, underwent significant erosion during this time. The immense volume of sediment required to fill the basin suggests that erosion of strata must have been facilitated by progressive, or at least periodic, uplift of the source region. Such a process is reflected by the significant change in zircon age modes between Depositional Package 3 and the top of Depositional Package 4, which record unroofing, incision and erosion of stratigraphically deeper strata in the southern Pilbara region (Martin et al., 2008).

Because zircon is resistant to mechanical abrasion, individual grains can pass through many cycles of erosion and sedimentation, a process that may lead to spurious interpretations of sediment provenance. First-cycle zircons are those grains eroded directly from the igneous and metamorphic basement rocks, whereas second-, or multi-cycle grains are those that have been recycled through other (meta)sedimentary rocks. Because U–Pb dating and Lu–Hf isotope compositions alone cannot distinguish first- from second- or multi-cycle grains (Campbell et al., 2005), it is generally not possible without using He–Pb double-dating techniques (e.g. Rahl et al., 2003; Campbell et al., 2005), to determine the cyclicity of the grains. However, in the case of the Edmund Group, the presence of abundant and uniform paleocurrent structures demonstrates that, despite the similarity in age and Hf isotopic composition of the detrital zircons with the Gascoyne Province basement, they were derived from a source region to the north of the Pingandy Shelf and not from the Gascoyne Province directly.

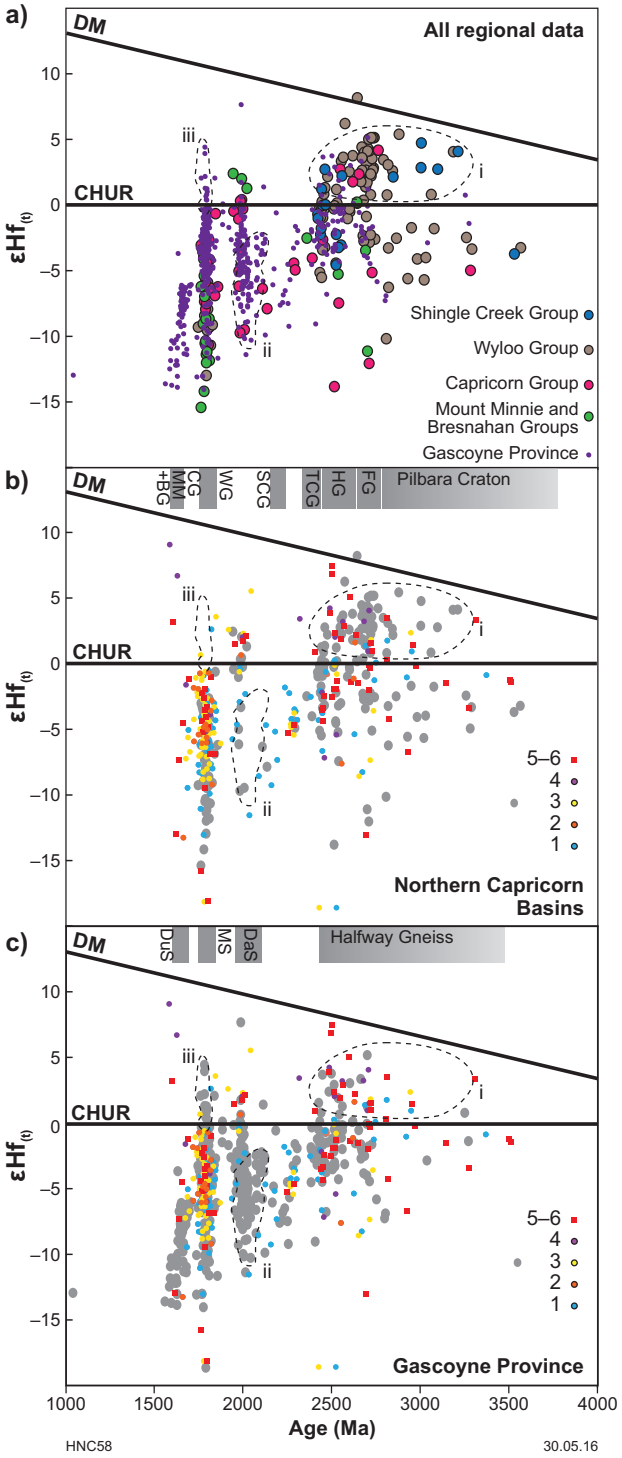

Figure 19. **a) $\varepsilon Hf_{(i)}$ ratios of detrital and magmatic zircons from potential source regions of the Capricorn Orogen. Lu–Hf isotope data are presented in Appendix 5. εHf ratios of detrital zircons from the Edmund and Collier Groups in comparison to b) detrital zircons from the northern Capricorn Orogen basins, and c) magmatic and detrital zircons from the Gascoyne Province. Note areas i, ii, and iii denote unique zircon age–isotope compositions (see main text for details). Abbreviations: BG – Bresnahan Group, CG – Capricorn Group, DaS – Dalgaringa Supersuite, DuS – Durlacher Supersuite, FG – Fortescue Group, HG – Hamersley Group, MM – Mount Minnie Group, SCG – Shingle Creek Group, TCG – Turee Creek Group, WG – Wyloo Group.**

Ultimately, however, most of the detrital zircons from Depositional Packages 1–3 were derived from igneous and metamorphic units of the Gascoyne Province, but the first-cycle detritus was transported northward and deposited and stored within sedimentary rocks of the Capricorn and Bresnahan Groups. The detrital zircons were liberated as second-cycle detritus into the Edmund Basin during the uplift and erosion of these strata. If the paleocurrent structures in the Edmund Group were poorly developed or preserved, or were obliterated during subsequent deformation and metamorphism, the first- or multi-cycle nature of the detrital zircons would not be known. Considering the detrital zircons' ultimate source is the Gascoyne Province basement, the most reasonable conclusion would be that they were derived as first-cycle detritus by the uplift and erosion of that basement rather than being derived as multi-cycle detritus from another, less-obvious source region.

Tectonic evolution of the Edmund Basin

Although the timing of basin initiation is not precisely known, the deposition of Depositional Package 1, and the formation of the half-graben basin architecture, took place in a similar time frame to the 1680–1620 Ma Mangaroon Orogeny in the underlying Gascoyne Province (Sheppard et al., 2005). In the northern part of the province, the event is relatively short lived, recording high-temperature, low-pressure metamorphism and voluminous granite magmatism between c. 1682 and 1677 Ma (Sheppard et al., 2005; Johnson et al., 2015c). In the central and southern parts of the province, deformation and metamorphism are absent, although voluminous granitic stocks and batholiths were emplaced in a slightly younger time frame between c. 1670 and 1619 Ma (Johnson et al., 2015c). The orogen principally records a period of intracratonic reworking in an extensional or transtensional tectonic setting (Johnson et al., 2015c; Sheppard et al., 2005), possibly in response to far-field plate stresses acting on the margins of the West Australian Craton (Johnson, 2013). Although the precise timing of basin initiation is not known, there does not appear to be a major switch in tectonic regime from the extension-related Mangaroon Orogeny to the formation and development of the Edmund Basin. The half-graben architecture was developed very early in the basin history, primarily controlled by extensional reactivation of pre-existing major crustal structures (Johnson et al., 2011a, 2013). The greatest amount of extension and downdrop of fault blocks also occurred early in the basin history but, as calculated in the western part of the basin, extension appears to have slowed through time (Table 1).

Detrital zircon provenance and paleocurrent studies (this study; Martin et al., 2008) demonstrate that the southern Pilbara region existed as a paleohigh throughout the formation and evolution of the basin. This suggests a regional segmentation and partitioning of strain, with the central part of the Capricorn Orogen under extension, to form the Edmund Basin, and the northern part, that is, the southern Pilbara region, mostly under compression. Within the Edmund Basin itself, sedimentation was punctuated by two main periods of basin-scale compression and uplift, both of which were associated with regional-scale hydrothermal fluid flow or the input of mantle-derived magmas into the upper crust. The first event, dated between c. 1610 and 1590 Ma (Zi et al., 2015), was responsible for uplift in the eastern and southern parts of the basin and stratabound base-metal mineralization at the Abra deposit (Pirajno, 2010). The second event was responsible for uplift of basement rocks to the south of the basin, and was synchronous with intrusion of the 1465–1452 Ma Narimbunna Dolerite sills (Wingate et al., 2013c) and extrusion of 1463–1455 Ma felsic volcaniclastic rocks (Wingate et al., 2012a). The tectonic driver for these short-lived compressional and magmatic–hydrothermal events is not known, and no similar-age events are known elsewhere in Western Australia (Johnson, 2013). However, considering the dynamic regional stress field at this time, with both compressional and extensional regimes partitioned across the orogen, small perturbations in the regional stress field could have had dramatic effects on basin evolution. Equally, the presence of hydrothermal and mafic magmatic activity during these events implies that asthenospheric and subcontinental lithospheric mantle processes may have also played a significant role.

Although the timing of basin inversion is relatively well constrained to between c. 1321 and 1171 Ma, it is not known if this event terminated sedimentation or whether deposition had ceased prior to regional-scale deformation. Estimation of extensional movements on the main fault structures in the western part of the basin show an inherent decrease in movement through time (Table 1), implying a gradual slowing of sedimentation rates. However, in parts of the basin, particularly in the south on the Lyons Block (Figs 5–8), the sedimentary packages increase in thickness through time, suggesting there may have been a southward shift in the loci of extension and deposition. However, the sedimentary rocks in this region have subsequently been strongly inverted and deeply eroded, and so it is not possible to determine if deposition continued beyond the recognized top of Depositional Package 4.

Deposition, provenance and tectonic setting of the Collier Group

Siliciclastic sedimentary rocks that make up the Collier Group were deposited across large parts of the Capricorn Orogen, although the basin is thickest in the south and east (Fig. 9). The rocks were deposited under a variety of conditions recording periods of both basin deepening, with accompanied marine transgression, and basin shallowing. Because only the peripheral parts of the basin were imaged in the deep crustal seismic section (Fig. 2; Johnson et al., 2011d, 2013), the architecture of the basin and structural controls on basin evolution remain poorly

constrained. Based on the style and intensity of folds and faults within the Edmund Group strata compared to those in the Collier Group at the regional map scale, as well as based on the line balancing of the two regional-scale cross-sections (Figs 13 and 15), it is interpreted that the Collier Group was not affected by, and was therefore deposited after, the 1321–1171 Ma Mutherbukin Tectonic Event. This interpretation is supported by the development of peperites (Martin, 2003) along the contact of a mafic sill (dated at 1076 ± 4 Ma; Wingate and Bodorkos, 2007) belonging to the 1084–1067 Ma Kulkatharra Dolerite with sedimentary rocks towards the base of the Backdoor Formation, implying that the sill was intruded into wet and unlithified sediments. Abundant mafic sills are also present throughout the entire Collier Group stratigraphy, although no other peperites have been identified. Based on their whole-rock geochemistry (Morris and Pirajno, 2005) and paleomagnetic signature (Wingate, 2002) these sills are also correlated with the 1084–1067 Ma Kulkatharra Dolerite, which would imply that the entire Collier Group may have been deposited in a relatively rapid time frame at, or around, 1080 Ma.

Paleocurrent structures throughout the basin record a distinct change in sediment transport direction between the Backdoor and Calyie Formations of Depositional Package 5 (Fig. 9; Martin et al., 2008). In the Wanna Syncline, sediment was initially sourced from the northeast, switching to the southeast, and in the eastern part of the basin it was sourced from the southeast, east and northeast, switching to highly variable directions. These changes coincide with shallowing of the basin and the formation and the west- to northwestward progradation of a major delta complex (Thorne et al., 2016b). These features are interpreted to record a period of uplift to the east of the basin. The majority of detrital zircons analysed from Depositional Package 5 are from the Backdoor Formation (262 of 291 analyses) and so, unfortunately, this change in sediment provenance is poorly recorded in the dataset. Of the 29 U–Pb zircon analyses from the Calyie Formation (GSWA 152968; Martin et al., 2008) that are <10% discordant (Appendix 4), seven define a single age component with a weighted mean $^{207}Pb^*/^{206}Pb^*$ date of 1740 ± 18 Ma (MSWD = 1.08; Martin et al., 2008); the remaining analyses scatter up to c. 3500 Ma. The c. 1740 Ma age mode is significantly younger than the prominent 1795–1775 Ma age mode present in all other depositional packages of the Edmund and Collier Groups (Fig. 17a), but the significance of these zircons is not known. Considering the statistical inadequacy of the dataset, more data are needed before any meaningful conclusions can be sought. The remaining 262 detrital zircon U–Pb analyses from the Backdoor Formation yield significant age components at c. 3475, 2965, 2710, 2500, 2275, 1950 and 1795 Ma (Fig. 17a). Similar-age detritus is present in the underlying sedimentary rocks of Depositional Packages 3 and 4 of the Edmund Group (Fig. 17a). The Lu–Hf isotope compositions of these zircons are also identical (Figs 18 and 19), suggesting that the sedimentary rocks of the Backdoor Formation were derived either from a near-identical source region to those for Depositional Packages 3 and 4, or were derived directly by the uplift, erosion and recycling of the underlying Edmund Group strata. When the detrital zircon age data for the Backdoor Formation are assessed by stratigraphic position (Fig. 20), those samples from the lowermost part of the formation contain near-identical age modes to those at the top of Depositional Package 4 (Figs 17a and 20). Within the middle and upper parts of the Backdoor Formation, the samples contain significantly fewer Archean grains and are dominated by Paleoproterozoic modes at c. 1795 Ma, similar to the age of detritus in Depositional Package 3 (Fig. 17a). These data appear to record the progressive uplift, unroofing and erosion of the underlying Edmund Group. Despite the predominantly northerly derived paleocurrent data for the Backdoor Formation in the Wanna Syncline, the detrital zircon data suggest that detritus for the lowermost part of the Collier Group was sourced directly from the recycling of the underlying Edmund Group, making the sediment a third-cycle detritus.

Despite the lack of structural control on the formation and evolution of the Collier Basin, the timing of deposition and source of detritus provides some clues into the tectonic setting of the basin. Although peperites are not pervasively developed throughout the basin, their presence along the margin of a c. 1076 Ma sill (Martin, 2003) towards the base of the Collier Group, suggests that sedimentation began shortly before this time, immediately pre-dating the intrusion of voluminous mafic magmas of the Warakurna Supersuite (Wingate et al., 2004). The basin fill is up to 4 km thick, and the stratigraphy through the lower and middle parts of Depositional Package 5 records a progressive deepening of the basin, undoubtedly implying basin formation and evolution under a mainly extensional tectonic regime. Because the basin is thickest in the south and east, it is possible that most of the regional-scale extension was accommodated by normal movements on the Mount Clere and Quartzite Well Faults. However, recycling of the underlying Edmund Group sedimentary rocks as the main source of detritus to the basin implies that parts of the orogen, initially the northern part and later, towards the top of Depositional Package 5, the eastern part, were subjected to localized uplift and erosion. The difference in shortening between strata of Depositional Packages 5 and 6 (Figs 14 and 15) suggests that parts of the Collier Basin, particularly the southern parts, were also subjected to localized uplift and inversion prior to the deposition of Depositional Package 6. The limited data available for the Collier Basin imply that basin formation took place in an intracratonic setting immediately prior to the emplacement of the Warakurna Large Igneous Province (Wingate et al., 2004) and that the basin evolved during a complex interplay between local- to regional-scale extensional and compressional (or transtensional) stresses that changed through time. A similar setting is inferred for the Edmund Group, particularly the upper part of the group where sedimentary rocks of Depositional Package 4 were deposited during a major switch in basin-scale stresses that were synchronous with the emplacement of voluminous mafic sills of the 1465–1452 Ma Narimbunna Dolerite.

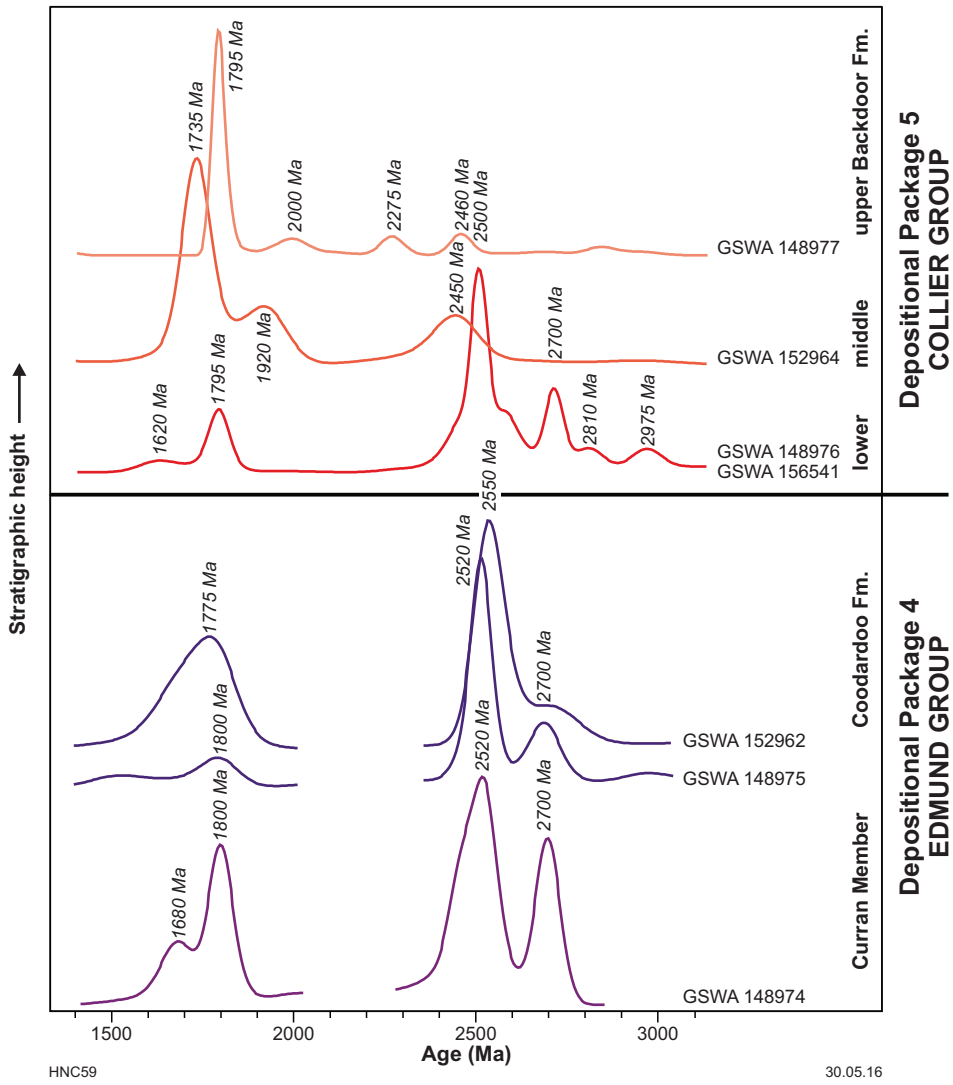

Figure 20. Kernel density estimates (KDE, Vermeesch, 2012) for the ages of detrital zircons through the top of the Edmund Group and into the base of the Collier Group. Samples are ordered by stratigraphic height. Geochronology data available at <www.dmp.wa.gov.au/geochron>.

Timing of basin inversion

Regional-scale map patterns as well as the two cross-sections through the Edmund and Collier Basins (Figs 13 and 15) show significant differences in shortening between the Edmund and Collier strata (Fig. 14). These differences can be attributed to two temporally distinct, regionally defined deformation events, the 1321–1171 Ma Mutherbukin Tectonic Event (Korhonen et al., 2015), which occurred after deposition of the Edmund Group but before deposition of the Collier Group, and the 1026–954 Ma Edmundian Orogeny (Martin and Thorne, 2004; Sheppard et al., 2007), which affected both groups.

Total shortening across the Edmund Basin, which records the cumulative effects of folding and faulting during both deformation events, is calculated at about 20%, although in detail, it is highly variable across the width of the basin (Fig. 14; Tables 3 and 4). Despite the relatively limited data, where the amount of shortening associated with each event can be resolved, the accumulated strain within each of the Edmund and Collier Groups also varies significantly across the width of the basins (Figs 13–15). In the northern part of the orogen, particularly on the Wanna and Godfrey Blocks, shortening is dominated by folding and faulting imparted during the Mutherbukin Tectonic Event. Deformation associated with the Edmundian Orogeny is predominant in the southern part of the orogen, particularly on the Lyons Block between the Bujundunna and Mount Clere Faults (Figs 4 and 14). These results suggest that strain during each event was partitioned preferentially into discrete tectonic corridors or zones. This is mirrored in the underlying Gascoyne Province basement, where higher strain deformation, during each of the medium- to high-grade crustal reworking events, has also been partitioned into discrete tectonic zones (Sheppard et al., 2010b; Aitken et al., 2014; Korhonen

and Johnson, 2015). This suggests that the distribution of strain across the orogen was controlled principally by the pre-existing crustal architecture (Johnson et al., 2013), and that there was no major decoupling between the middle and upper parts of the crust during deformation.

Although both deformation events appear to be characterized by simple, orthogonal shortening with the production of cylindrical folds and associated reverse faults (Martin and Thorne, 2004; Fig. 10a), parts of the Edmund Group that were deformed during the Mutherbukin Tectonic Event, particularly those in the southern part of the basin, show evidence for significant transcurrent or transpressional components (Cutten et al., 2010). Again, this is similar to the style and nature of deformation in the underlying Gascoyne Province basement (Korhonen et al., 2015), implying a strong coupling between the middle, upper and shallow crust.

The precise timing of folding and faulting of Edmund Group strata during the Mutherbukin Tectonic Event is poorly constrained. However, synkinematic illite from the Brumby Creek Fault, a significant splay of the Mount Vernon Fault, has been dated by the K–Ar method at 1171 ± 25 Ma (Zwingmann et al., 2012), indicating that the last movements on the fault occurred towards the end of the Mutherbukin Tectonic Event (Korhonen et al., 2015). Indirect evidence for the timing of deformation is provided by the age of hydrothermal monazite where regional- to local-scale hydrothermal fluid flow is thought to have accompanied fault movements (Zi et al., 2015). Close to the Edmund Fault in the central part of the orogen, hydrothermal monazite within the Mt Augustus Sandstone has been dated at 1300 ± 10 Ma (Rasmussen et al., written comm.). At the Abra polymetallic deposit, which lies adjacent to the Lyons River – Quartzite Well fault system, several generations of hydrothermal monazite have been dated at c. 1375, 1221 and 995 Ma (Zi et al., 2015). Additionally, in the Coobarra Dome, close to the Abra deposit, hydrothermal xenotime dated at c. 1235 Ma (Rasmussen et al., 2010) records extensive hydrothermal alteration of the Tangadee Rhyolite Member of the Kiangi Creek Formation. These dates span the entire duration of the Mutherbukin Tectonic Event and part of the Edmundian Orogeny, indicating that regional-scale hydrothermal fluid flow in the shallow crust was synchronous with medium- to high-grade metamorphism and deformation in the underlying Gascoyne Province (Sheppard et al., 2007; Korhonen et al., 2015).

Collier Group strata are mostly gently to openly folded (Figs 13 and 15), although in the southern part of the basin, on the Lyons and Jubilee Blocks, the strata are more tightly folded where shortening is estimated at 18% (Fig. 14). This zone of increased shortening lies directly along strike from the main zone of Edmundian-age deformation and medium-grade metamorphism in the underlying Gascoyne Province basement (Sheppard et al., 2007). In the basement, deformation and metamorphism is constrained between c. 1026 and 955 Ma (Sheppard et al., 2007), although the growth of most metamorphic monazite and xenotime crystals is dated between c. 1005 and 995 Ma, which may be a more precise estimate for the timing of peak metamorphism.

In the Mindi Syncline, there appears to be a difference in shortening between strata of the lower and upper Collier Group, estimated at 11.5 and 1.9%, respectively (Figs 15 and 16), suggesting that significant amounts of the total shortening in the southern part of the basin may have occurred during deposition of the lower Collier Group. Considering that the uppermost strata of the Collier Group are intruded by mafic sills of the 1084–1067 Ma Kulkatharra Dolerite, this indicates that the majority of shortening in this zone must have taken place before c. 1067 Ma. Therefore, only the very gentle folds recorded by the uppermost Collier Group strata in this zone could have been synchronous with the higher grade events in the underlying basement. It is not yet clear if this early Edmundian folding event is real or present only locally. This early Edmundian event does not correlate with any known deformation throughout the region, but might be related to the intrusion of the voluminous mafic sills associated with the Warakurna Large Igneous Province (Wingate et al., 2004).

Economic mineral endowment

Numerous mineral deposit types have been identified in the Capricorn Orogen, including world-class deposits of iron ore and base metals (Fig. 21; Department of Mines and Petroleum, 2014). Despite the relative paucity of large economic mineral occurrences within the Edmund and Collier Groups, compared with the rest of the orogen, the basins do have a long history of mining and metal production (Cooper et al., 1998). The Edmund and Collier Groups contain deposits of gold, copper and lead, and to a lesser extent silver and manganese (Fig. 21; Appendix 1).

Central to the orogen's prospectivity is the growing understanding that the formation of ore deposits is an expression of much larger Earth-system processes, which operate on a variety of scales to focus mass and energy flux. Many factors, including the geodynamic setting, architecture, metal source, fluid-flow drivers and pathways, and depositional mechanisms, influence the type, style and location of mineralization (Wyborn et al., 1994; Knox-Robinson and Wyborn, 1997; McCuaig et al., 2010; McCuaig and Hronsky, 2014). The deep crustal seismic reflection survey across the Capricorn Orogen identified numerous lithospheric-scale faults and shear zones (Johnson et al., 2011, 2013), and highlighted the coincidence between these structures, or their splays, and the spatial distribution of ore deposits (Fig. 21; Johnson et al., 2013; Johnson, 2014). It appears that reactivation of these major structures during deformation and metamorphism has greatly influenced the location and style of deposit in the orogen (Johnson, 2014). Considering that the deposition and inversion history of the Edmund and Collier Basins was intimately controlled by the pre-existing crustal architecture, it is possible that many of the mineral occurrences were formed, or remobilized, during reactivation of these lithospheric-scale structures during regional-scale deformation and metamorphic events.

The Abra polymetallic deposit is the most significant mineral occurrence in the Edmund Basin. The deposit

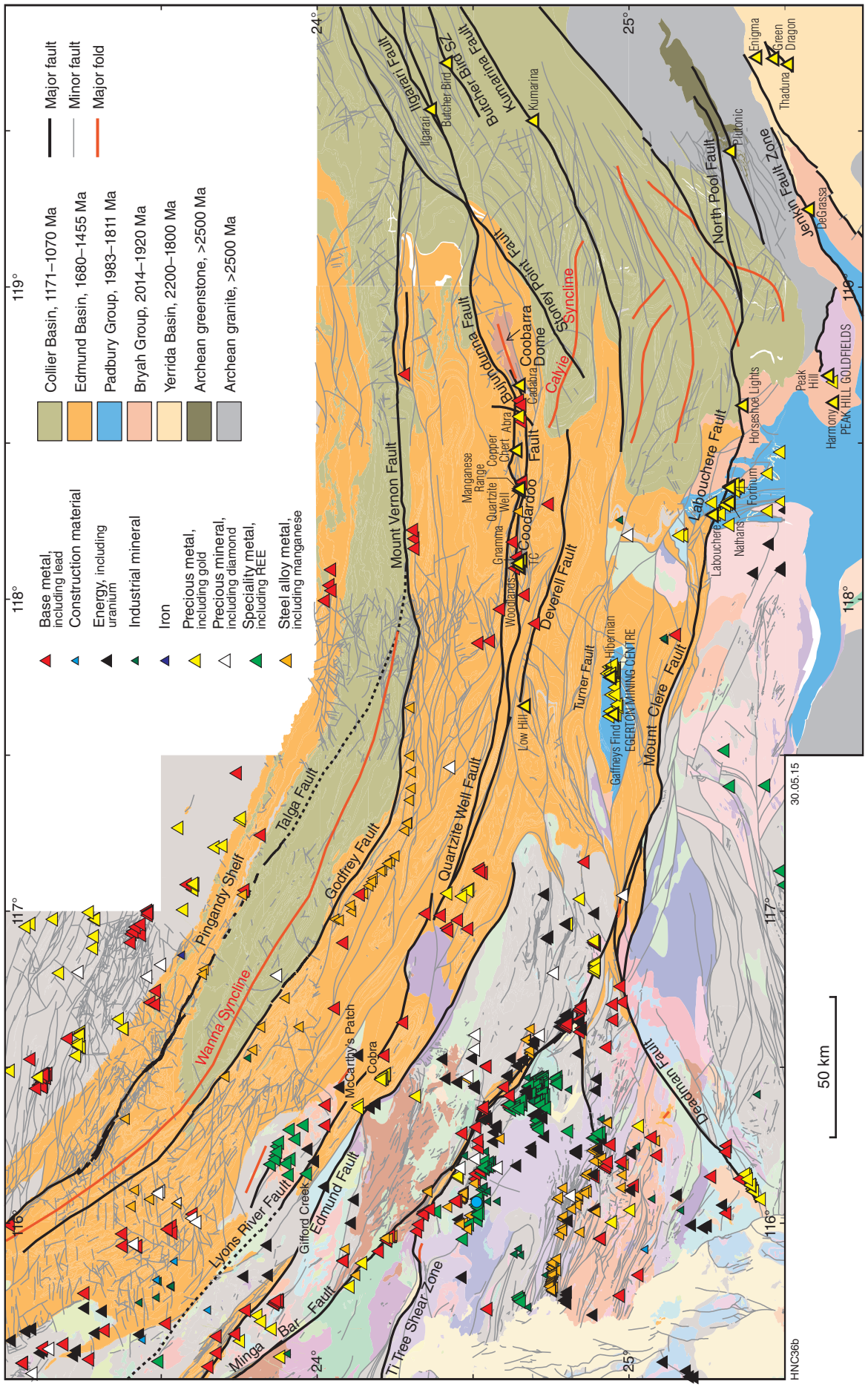

Figure 21. The distribution of mineral occurrences in the Edmund and Collier Basins, and in older Proterozoic rocks, and their spatial association with the major faults. The Plutonic mine, in Archean greenstone rocks of the Marymia Inlier, is also shown. Major deposits and major faults are named.

contains abundant lead with subordinate copper–gold–silver mineralization as well as low-grade copper–barite mineralization at TC, Gnamma and Woodlands (Fig. 21; Cooper et al., 1998). The mineralization is a stratabound deposit (Pirajno et al., 2010) hosted in the Irregully and Gooragoora Formations of Depositional Packages 1 and 2, below a regional-scale unconformity (Figs 3 and 21; Johnson et al., 2015a).

Hydrothermal xenotime, intergrown with the main ore minerals, yielded a near-continuum of dates between c. 1610 and 1590 Ma (Zi et al., 2015), indicating that hydrothermal activity and mineralization may have spanned an extended period of c. 20 Ma. Hydrothermal monazite and xenotime, as well as secondary pyrite, have been dated using a variety of techniques between c. 1284 and 995 Ma (Rasmussen et al., 2010; Pirajno et al., 2010; Zi et al., 2015), indicating that the deposit has been variably reworked by hydrothermal fluids during numerous regional-scale deformation events. The mineralization occurs close to the Lyons River – Quartzite Well fault system (Fig. 21), which is imaged on the Capricorn Orogen deep crustal seismic survey as a major lithospheric-scale structure that offsets the Moho (Fig. 2; Johnson et al., 2013). The age and stratabound nature of the deposit indicate that mineralization occurred during deposition of the lower part of the Edmund Group, but specifically during a period of localized basin inversion, uplift and erosion, which was accompanied by intense hydrothermal activity. These features suggest that the mantle-tapping fault system may have acted as a conduit for heated fluids that may have mixed with meteoric fluids enriched with base metals leached from the Edmund Group sediments (Pirajno et al., 2010).

The most significant mineralization in the Collier Basin are copper deposits at Ilgarari, Kumarina and Butcher Bird (Fig. 21; Appendix 1; Kumarina Resources, 2012; Montezuma Mining Company, 2016). These deposits are hosted in major northeast-striking transpressional structures, the Ilgarari and Kumarina Faults and Butcher Bird Shear Zone, which may be reactivated portions of older, major crustal structures. Mineralization is considered to be supergene in origin, having been reworked from older pre-existing deposits at depth (Kumarina Resources, 2012; Montezuma Mining Company, 2014). The timing of mineralization is uncertain but took place after deposition of the Collier Group and during a period of fault reactivation either during the 1026–954 Ma Edmundian Orogeny or during younger events such as the c. 570 Ma Mulka Tectonic Event (Sheppard et al., 2010b).

Despite the lack of knowledge on the timing and nature of mineralization for most deposits in the Edmund and Collier Groups, the regional-scale distribution (Fig. 21) and supergene or hydrothermal nature implies an intimate association between crustal architecture and deposit location. This is highlighted at the Abra deposit, which shows successive periods of reworking, the timing of which links medium-grade metamorphism and deformation in the underlying Gascoyne Province basement with folding, faulting and regional-scale hydrothermal fluid flow in the shallow crust.

Summary

The depositional and deformation history of the 1679–1067 Ma Edmund and Collier Basins is revealed using a variety of approaches. Initial detailed field geological mapping has documented the depositional history of 4–12 km of siliciclastic sediments, including the thickness and extent of individual formations that make up the depositional packages. Varying normal movements on listric faults, both marginal and within the basin, resulted from the reactivation of the older basement structures that accommodated the opening and growth of the Edmund Basin. A half-graben structural architecture is revealed by the Capricorn Orogen deep crustal seismic reflection survey. This survey also allowed the calculation of extension (7–8%) required to accommodate the basin fill, with 68% of this taking place during the deposition of Depositional Package 1.

Zircon U–Pb and Lu–Hf isotope analysis, together with paleocurrent information, indicate that detritus within Depositional Packages 1–3 was sourced from the Besnahan and Capricorn Groups in the southern Pilbara region, which themselves contain material originally derived from the Gascoyne Province to the south. The age and isotopic composition of detrital zircons in Depositional Package 4 indicate the incision and exposure of deeper levels of the southern Pilbara source region. Inversion of the Edmund Basin during the 1321–1171 Ma Mutherbukin Tectonic Event, and reactivation of the major faults with a reverse sense of movement, resulted in a depositional hiatus lasting as long as 370 million years. A brief period of extension is suggested by the opening of the Collier Basin. Intrusion of 1084–1069 Ma Kulkatharra Dolerite sills into the Collier Group indicates that sedimentation took place prior to mafic magmatism between c. 1084 and 1069 Ma. However, the presence of peperites, between the lowermost strata of Depositional Package 5 and a mafic sill dated at c. 1079 Ma, implies intrusion of the sills into wet sediments. Therefore, the Collier Group may have been deposited in a short period at, or around, 1069 Ma.

The Edmund and Collier Basins were then deformed during the 1026–954 Ma Edmundian Orogeny. The cumulative effect of shortening of the Edmund and Collier Basins during the regional-scale deformation events averages 21%. However, these two events are coaxial, making it difficult to apportion shortening between them. The Mutherbukin Tectonic Event deformed only the Edmund Group whereas the Edmundian Orogeny deformed both the Edmund and Collier Groups. Comparison of two cross-sections across the basins suggests that Mutherbukin Tectonic Event deformation was concentrated in the northern parts of the basin, whereas the effects of the Edmundian Orogeny increases to the south. A comparison of shortening in the lower Collier Group (Depositional Package 4) compared to the upper Collier Group (Depositional Package 5) possibly indicates a period of deformation preceding the Edmundian Orogeny. This may have taken place during a lull in sedimentation or may indicate ongoing deformation accompanying sedimentation.

Although mineral deposits are not abundant in the Edmund and Collier Basins, the underlying crustal architecture appears to have played a significant role in the formation and distribution of mineral deposits across the orogen. The stratabound Pb–Au–Ag–Cu Abra deposit, hosted in the Gooragoora Formation, is located adjacent to the Lyons River – Quartzite Well Fault, which is imaged on the Capricorn Orogen deep crustal seismic reflection survey as a major crustal structure that offsets the Moho. Hydrothermal xenotime dated at 1610–1590 Ma in the mineralized black zone of the deposit indicates that mineralization took place during a period of localized basin uplift, with reactivation of the Lyons River – Quartzite Well Fault system and was accompanied by intense hydrothermal activity. In contrast, Cu–Au mineralization at the Ilgarari and Butcherbird deposits in the Ilgarari Formation appear to be supergene deposits associated with local faults and reverse fault movements.

References

Blay, OA, Cutten, HN and Thorne, AM 2014, Three Rivers, WA Sheet 2747: Geological Survey of Western Australia, 1:100 000 Geological Series.

Blay, OA and Thorne, AM 2015, Cardawan, WA Sheet 2748: Geological Survey of Western Australia, 1:100 000 Geological Series.

Blay, OA, Thorne, AM and Cutten, HN 2012a, Mount Vernon, WA Sheet 2549: Geological Survey of Western Australia, 1:100 000 Geological Series.

Blay, OA, Thorne, AM and Cutten, HN 2012b, Teano, WA Sheet 2449: Geological Survey of Western Australia, 1:100 000 Geological Series.

Blay, OA, Johnson, SP, Thorne, AM and Cutten, HNC 2015, Waldburg Dolerite (P_-_wa-od): Geological Survey of Western Australia, WA Geology Online, Explanatory Notes extract, viewed 20 April 2016, <www.dmp.wa.gov.au/ens>.

Blichert-Toft, J and Albarède, F 1997, The Lu–Hf isotope geochemistry of chondrites and the evolution of the mantle–crust system: Earth and Planetary Science Letters, v. 148, p. 243–258.

Bodorkos, S and Wingate, MTD 2007, The contribution of geochronology to GSWA's mapping programs: current perspectives and future directions, *in* GSWA 2007 extended abstracts: promoting the prospectivity of Western Australia: Geological Survey of Western Australia, Record 2007/2, p. 10–11.

Brakel, AT and Muhling, PC 1976, Stratigraphy, sedimentation and structure in the western and central part of the Bangemall Basin, *in* Annual report for the year 1975: Geological Survey of Western Australia, p. 79–83.

Campbell, IH, Reiners, PW, Allen, CM, Nicolescu, S and Upadhyay, R 2005, He–Pb double dating of detrital zircons from the Ganges and Indus Rivers: implication for quantifying sediment recycling and provenance studies: Earth and Planetary Science Letters, v. 237, p. 402–432.

Cawood, PA and Tyler, IM 2004, Assembling and reactivating the Proterozoic Capricorn Orogen: lithotectonic elements, orogenies, and significance: Precambrian Research, v. 128, p. 201–218.

Chuck, RG 1984, The sedimentary and tectonic evolution of the Bangemall Basin, Western Australia and implications for mineral exploration: Western Australian Mining and Petroleum Research Institute, Report 6, 129p.

Colgan, JP, Dumitru, TA, Reiners, PW, Wooden, JL and Miller, EI 2006, Cenozoic tectonic evolution of the Basin and Range Province in northwestern Nevada: American Journal of Science, v. 306, p. 616–654.

Comacho, A, Hensen, BJ and Armstrong, R 2002, Isotopic test of a thermally driven intraplate orogenic model, Australia: Geology, v. 30, no. 10, p. 887–890.

Cooper, RW, Langford, RL and Pirajno, F 1998, Mineral occurrences and exploration potential of the Bangemall Basin: Geological Survey of Western Australia, Report 64, 42p.

Cutten, HN, Thorne, AM and Sheppard, S 2010, Calyie, WA Sheet 2648: Geological Survey of Western Australia, 1:100 000 Geological Series.

Cutten, HN, Blay, OA, Thorne, AM and Johnson, SP 2013, Jamindi, WA Sheet 2647: Geological Survey of Western Australia, 1:100 000 Geological Series.

Daniels, JL 1966, Revised stratigraphy, palaeocurrent system and palaeogeography of the Proterozoic Bangemall Group, *in* Annual report for the year 1965: Geological Survey of Western Australia, p. 48–56.

Daniels, JL 1970, Wyloo, Western Australia: Geological Survey of Western Australia, 1:250 000 Explanatory Notes, 19p.

Daniels, JL and Halligan, R 1969, Wyloo, WA Sheet SF50-10: Geological Survey of Western Australia, 1:250 000 Geological Series.

DeBievre, P and Taylor, PDP 1993, IUPAC Recommended Isotopic Abundances: International Journal of Mass Spectrometry and Ion Physics, v. 123, p. 149.

Department of Mines and Petroleum 2014, MINEDEX: mines and mineral deposits database: viewed 29 March 2016, <www.dmp.wa.gov.au/minedex>.

Duncan, DJ 1993, Exploration Licence E08/286 Annual report: Stockdale Prospecting Limited, Western Australia Geological Survey, M-series A38748, unpublished.

Flöttmann, T, Haines, PW, Cockshell, CD and Preiss, WV 1997, An early Palaeozoic foreland basin succession beneath Gulf St Vincent, South Australia? — implications for petroleum plays: PESA Journal, v. 25, p. 33–40.

Flöttmann, T and Hand, M 1999, Folded basement-cored tectonic wedges along the northern edge of the Amadeus Basin, central Australia: evaluation of orogenic shortening: Journal of Structural Geology, v. 21, p. 399–412.

Foden, J, Elburg, MA, Dougherty-Page, J and Burtt, A 2006, The timing and duration of the Delamerian Orogeny: correlation with the Ross Orogeny and implications for Gondwana assembly: The Journal of Geology, v. 114, p. 189–210.

Fortnam Gold Mine 2015, viewed 7 April 2016, <www.mindat.org/loc-243109.html>.

Gazley, MF, Duclaux, G, Fisher, LA, de Beer, S, Smith, P, Taylor, M, Swanson, R, Hough, RM and Cleverley, J 2012, Improving geological and metallurgical understanding of Plutonic Gold Mine, Western Australia, using three-dimensional visualisation of portable X-ray fluorescence data: The Australian Institute of Mining and Metallurgy, Applied Earth Science, Transactions of the Institute of Materials, Minerals and Mining B 120, p. 88–96.

Geological Survey of Western Australia 2013, Western Capricorn, 2013 update: Geological Survey of Western Australia, Geological Information Series.

Goleby, BR, Kennett, BLN, Wright, C, Shaw, RD and Lambert, DD 1990, Seismic reflection profiling in the Proterozoic Arunta Block, central Australia: processing for testing models of tectonic evolution: Tectonophysics, v. 173, p. 257–268.

Goleby, BR, Shaw, RD, Wright, C, Kennett, BLN and Lambeck, K 1989, Geophysical evidence for 'thick-skinned' crustal deformation in central Australia: Nature, v. 337, no. 6205, p. 325–330, doi:10.1038/337325a0.

Griffin, WL, Belousova, EA, Shee, SR, Pearson, NJ and O'Reilly, SY 2004, Archean crustal evolution in the northern Yilgarn Craton: U–Pb and Hf-isotope evidence from detrital zircons: Precambrian Research, v. 127, p. 19–41.

Griffin, WL, Pearson, NJ, Belousova, EA, Jackson, SE, O'Reilly, SY, van Achterbergh, E and Shee, SR 2000, The Hf isotope composition of cratonic mantle: LAM-MC-ICPMS analysis of zircon megacrysts in kimberlites: Geochimica et Cosmochimica Acta, v. 64, p. 133–147.

Griffin, WL, Pearson, NJ, Belousova, EA and Saeed, A 2007, Reply to "Comment to short-communication 'Comment: Hf-isotope heterogeneity in zircon 91500' by WL Griffin, NJ Pearson, EA Belousova, A, Saeed (Chemical Geology 233 (2006) p. 358–363)" by F Corfu: Chemical Geology, v. 244, p. 354–356.

Halligan, R and Daniels, JL 1964, Precambrian geology of the Ashburton Valley Region, northwest division, *in* Annual report for the year 1963: Geological Survey of Western Australia, p. 38–46.

Hancock, EA, Thorne, AM, Morris, PA, Watling, RJ and Cutten, HNC 2009, Mineralogy and trace element chemistry of lode and alluvial gold from the western Capricorn Orogen: Geological Survey of Western Australia, Record 2009/6, 29p.

Hand, M and Sandiford, M 1999, Intraplate deformation in central Australia, the link between subsidence and fault reactivation: Tectonophysics, v. 305, no. 1–3, p. 121–140.

Hawkesworth, CJ and Kemp, AIS 2006, The differentiation and rates of generation of the continental crust: Chemical Geology, v. 226, no. 3–4, p. 134–143, doi:10.1016/j.chemgeo.2005.09.017.

Johnson, SP 2013, The birth of supercontinents and the Proterozoic assembly of Western Australia: Geological Survey of Western Australia, 78p.

Johnson, SP 2014, The birth of supercontinents and the Proterozoic assembly of WA: The AusIMM Bulletin Issue no. 1, p. 53–56.

Johnson, SP, Thorne, AM and Tyler, IM (editors) 2011a, Capricorn Orogen seismic and magnetotelluric (MT) workshop 2011: extended abstracts: Geological Survey of Western Australia, Record 2011/25, 120p.

Johnson, SP, Sheppard, S, Rasmussen, B, Wingate, MTD, Kirkland, CL, Muhling, JR, Fletcher, IR and Belousova, E 2010, The Glenburgh Orogeny as a record of Paleoproterozoic continent–continent collision: Geological Survey of Western Australia, Record 2010/5, 54p.

Johnson, SP, Sheppard, S, Rasmussen, B, Wingate, MTD, Kirkland, CL, Muhling, JR, Fletcher, IR and Belousova, EA 2011b, Two collisions, two sutures: punctuated pre-1950 Ma assembly of the West Australian Craton during the Ophthalmia and Glenburgh Orogenies: Precambrian Research, v. 189, no. 3–4, p. 239–262, doi:10.1016/j.precamres.2011.07.011.

Johnson, SP, Sheppard, S, Thorne, AM, Rasmussen, B, Fletcher, IR, Wingate, MTD and Cutten, HN 2011c, The role of the 1280–1250 Ma Mutherbukin Tectonic Event in shaping the crustal architecture and mineralization history of the Capricorn Orogen, *in* GSWA 2011 extended abstracts: promoting the prospectivity of Western Australia: Geological Survey of Western Australia, Record 2011/2, p. 1–3.

Johnson, SP, Thorne, AM, Cutten, HN, Tyler, IM and Blay, OA 2011d, Geology of the Gascoyne Province, *in* Capricorn Orogen seismic and magnetotelluric (MT) workshop 2011: extended abstracts *edited by* SP Johnson, AM Thorne and IM Tyler: Geological Survey of Western Australia, Record 2011/25, p. 27–41.

Johnson, SP, Thorne, AM, Tyler, IM, Korsch, RJ, Kennett, BLN, Cutten, HN, Goodwin, J, Blay, OA, Blewett, RS, Joly, A, Dentith, MC, Aitken, ARA, Holzschuh, J, Salmon, M, Reading, A, Heinson, G, Boren, G, Ross, J, Costelloe, RD and Fomin, T 2013, Crustal architecture of the Capricorn Orogen, Western Australia and associated metallogeny: Australian Journal of Earth Sciences, v. 60, no. 6–7, p. 681–705, doi:10.1080/08120099.2013.826735.

Johnson, SP, Zi, J, Rasmussen, B, Muhling, JR, Fletcher, IR, Dunkley, DJ, Thorne, AM, Cutten, HN and Korhonen, FJ 2015a, Abracadabra — dating hydrothermal mineralization and fluid flow in a long-lived crustal structure, *in* GSWA 2015 extended abstracts: promoting the prospectivity of Western Australia: Geological Survey of Western Australia, Record 2015/2, p. 1–4.

Johnson, SP, Sheppard, S and Korhonen, FJ 2015b, Mulka Tectonic Event (MK): Geological Survey of Western Australia, WA Geology Online, Explanatory Notes extract, viewed 24 March 2016, <www.dmp.wa.gov.au/ens>.

Johnson, SP, Korhonen, FJ, Sheppard, S and Occhipinti, SA 2015c, Mangaroon Orogeny (MA): Geological Survey of Western Australia, WA Geology Online, Explanatory Notes extract, viewed 6 April 2016, <www.dmp.wa.gov.au/ens>.

Johnson, SP, Korhonen, FJ, Sheppard, S and Cutten, HNC 2016, Mutherbukin Tectonic Event (MB): Geological Survey of Western Australia, WA Geology Online, Explanatory Notes extract, viewed 24 March 2016, <www.dmp.wa.gov.au/ens>.

Kennard, JM, Jackson, MJ, Romine, KK, Shaw, RD and Southgate, PN 1994, Depositional sequences and associated petroleum systems of the Canning Basin, WA, *in* The sedimentary basins of Western Australia *edited by* PG Purcell and RR Purcell: Petroleum Exploration Society of Australia, Western Australian Branch, Perth, Western Australia, p. 657–676.

Knox-Robinson, CM and Wyborn, LAI 1997, Towards a holistic exploration strategy: using geographic information systems as a tool to enhance exploration: Australian Journal of Earth Sciences, v. 44, no. 4, p. 453–463.

Korhonen, FJ and Johnson, SP 2015, The role of radiogenic heat in prolonged intraplate reworking: The Capricorn Orogen explained?: Earth and Planetary Science Letters, v. 428, p. 22–32.

Korhonen, FJ, Johnson, SP, Fletcher, IR, Rasmussen, B, Sheppard, S, Muhling, JR, Dunkley, DJ, Wingate, MTD, Roberts, MP and Kirkland, CL 2015, Pressure–temperature–time evolution of the Mutherbukin Tectonic Event, Capricorn Orogen: Geological Survey of Western Australia, Report 146, 64p.

Kumarina Resources 2012, viewed 5 Dec 2012, </www.kumarina.com/projects-ilgarari.php>.

Maidment, DW, Hand, M and Williams, IS 2013, High grade metamorphism of sedimentary rocks during Palaeozoic rift basin formation in central Australia: Gondwana Research, v. 24, no. 3–4, p. 865–885.

Martin, DM (partial report), Turee Creek Group (P_-TK-s): Geological Survey of Western Australia, WA Geology Online, Explanatory Notes extract, viewed 19 April 2016, <www.dmp.wa.gov.au/ens>.

Martin, DM 1999, Depositional setting and implications of Paleoproterozoic glaciomarine sedimentation in the Hamersley Province, Western Australia: Geological Society of America Bulletin, v. 111, p. 189–203.

Martin, DM 2003, Peperite in the Backdoor Formation and its significance to the age and tectonic evolution of the Bangemall Supergroup, *in* Geological Survey of Western Australia Annual Review 2002–03: Geological Survey of Western Australia, p. 53–59.

Martin, DM and Thorne, AM 2004, Tectonic setting and basin evolution of the Bangemall Supergroup in the northwestern Capricorn Orogen: Precambrian Research, v. 128, p. 385–409.

Martin, DM, Sheppard, S and Thorne, AM 2005, Geology of the Maroonah, Ullawarra, Capricorn, Mangaroon, Edmund, and Elliott Creek 1:100 000 sheets: Geological Survey of Western Australia, 1:100 000 Geological Series Explanatory Notes, 65p.

Martin, DM, Sircombe, KN, Thorne, AM, Cawood, PA and Nemchin, AA 2008, Provenance history of the Bangemall Supergroup and implications for the Mesoproterozoic paleogeography of the West Australian Craton, *in* Assembling Australia: Proterozoic building of a continent *edited by* PA Cawood and RJ Korsch: Precambrian Research v. 166, no. 1–4, p. 93–110.

Martin, DM and Thorne, AM 2000, Abracadabra! Another Jillawarra-style sub-basin in the Bangemall Supergroup, *in* GSWA 2000 extended abstracts: Geological data for WA explorers in the new millennium: Geological Survey of Western Australia, Record 2000/8, p. 9–10.

Martin, DM and Thorne, AM 2002, Revised lithostratigraphy of the Mesoproterozoic Bangemall Supergroup on the Edmund and Turee Creek 1:250 000 sheets, Western Australia: Geological Survey of Western Australia, Record 2002/15, 27p.

Martin, DM, Thorne, AM and Copp, IA 1999, A provisional revised stratigraphy for the Bangemall Group on the Edmund 1:250 000 sheet, *in* Geological Survey of Western Australia Annual Review 1998–99: Geological Survey of Western Australia, p. 51–55.

McCuaig, TC, Beresford, S and Hronsky, J 2010, Translating the mineral systems approach into an effective exploration targeting system: Ore Geology Reviews, v. 38, p. 128–138.

McCuaig, TC and Hronsky, JMA 2014, The mineral system concept: The key to exploration targeting, *in* Building Exploration Capability for the 21st Century *edited by* KD Kelly and HC Golden: Society of Economic Geologists, Inc., Special Publication No. 18, p. 153–175.

Montezuma Mining Company 2016, viewed June 2016, <www.montezumamining.com.au/projects/butcherbird_copper>.

Morris, PA and Pirajno, F 2005, Mesoproterozoic sill complexes in the Bangemall Supergroup, Western Australia: geology, geochemistry, and mineralization potential: Geological Survey of Western Australia, Report 99, 75p.

Muhling, PC and Brakel, AT 1985a, Geological map of the Bangemall Basin (1:1 000 000 scale), *in* Geology of the Bangemall Group: the evolution of a Proterozoic intracratonic sedimentary basin: Geological Survey of Western Australia, Bulletin 128, Plate 1.

Muhling, PC and Brakel, AT 1985b, Geology of the Bangemall Group: the evolution of a Proterozoic intracratonic sedimentary basin: Geological Survey of Western Australia, Bulletin 128, 266p.

Nelson, DR 2001, 169011: quartz dolerite, Strama Gap; Geochronology Record 150: Geological Survey of Western Australia, 5p.

Northern Star Resources 2015, viewed 7 April 2016, <www.nsrltd.com/our-assets>.

Paul, E, Flöttmann, T and Sandiford, M 1999, Structural geometry and controls on basement-involved deformation in the northern Flinders Ranges, Adelaide Fold Belt, South Australia: Australian Journal of Earth Sciences, v. 46, no. 3, p. 343–354.

Pearson, JM, Taylor, WR and Barley, ME 1996, Geology of the alkaline Gifford Creek Complex, Gascoyne Complex, Western Australia: Australian Journal of Earth Sciences, v. 43, no. 3, p. 299–309.

Pirajno, F and Gonzalez-Alvarez, I 2014, The ironstone veins of the Gifford Creek ferrocarbonatite complex, Gascoyne Province: Geological Survey of Western Australia, Record 2013/12, 19p.

Pirajno, F, Jones, JA, Hocking, RM and Halilovic, J 2004, Geology and tectonic evolution of Palaeoproterozoic basins of the eastern Capricorn Orogen, Western Australia: Precambrian Research, v. 128, no. 3–4, p. 315–342.

Pirajno, F, Thorne, AM, Mernagh, TP, Creaser, RA, Hell, A and Cutten, H 2010, The Abra deposit: a polymetallic mineral system in the Edmund Basin, Capricorn Orogen, Western Australia, *in* 13th Quadrennial IAGOD Symposium Proceedings *edited by* NJ Cook and others: International Association on Genesis of Ore Deposits (IAGOD); Giant Ore Deposits Down-Under, Adelaide, South Australia, 6 April 2010, p. 112–114.

Preiss, WV 2000, The Adelaide Geosyncline of South Australia and its significance in Neoproterozoic continental reconstruction: Precambrian Research, v. 100, p. 21–63.

Rahl, JM, Reiners, PW, Campbell, IH, Nicolescu, S and Allen, CM 2003, Combined single-grain (U-Th)/He and U/Pb dating of detrital zircons from the Navajo Sandstone, Utah: Geology, v. 31, no. 9, p. 761–764, doi:10.1130/G19653.1.

Rasmussen, B, Fletcher, IR, Muhling, JR, Thorne, AM, Cutten, HN, Pirajno, F and Hell, A 2010, In situ U–Pb monazite and xenotime geochronology of the Abra polymetallic deposit and associated sedimentary and volcanic rocks, Bangemall Supergroup, Western Australia: Geological Survey of Western Australia, Record 2010/12, 31p.

Sandfire Resources NL 2015, viewed 7 April 2015, <www.sandfire.com.au/operations/degrussa/mineral-resources-ore-reserves-and-mine-plan.html>.

Sandiford, M, Hand, M and McLaren, S 2001, Tectonic feedback, intraplate orogeny and the geochemical structure of the crust: a central Australian perspective, *in* Continental reactivation and reworking *edited by* JA Miller, IS Buick and M Hand: Geological Society, London, UK, Geological Society Special Publication 184, p. 195–218.

Scherer, E, Münker, C and Mezger, K 2001, Calibration of the lutetium–hafnium clock: Science, v. 293, p. 683–687.

Shaw, RD, Etheridge, MA and Lambeck, K 1991, Development of the Late Proterozoic to Mid-Paleozoic, intracratonic Amadeus Basin in central Australia: a key to understanding tectonic forces in plate interiors: Tectonics, v. 10, no. 4, p. 688–721, doi:10.1029/90TC02417.

Shaw, RD, Zeitler, PK, McDougall, I and Tingate, PR 1992, The Paleozoic history of an unusal intracratonic thrust belt in central Australia based on ^{40}Ar–^{39}Ar, K–Ar and fission track dating: Journal of the Geological Society, London, v. 149, no. 6, p. 937–954, doi:10.1144/gsjgs.149.6.0937.

Sheppard, S, Bodorkos, S, Johnson, SP, Wingate, MTD and Kirkland, CL 2010a, The Paleoproterozoic Capricorn Orogeny: intracontinental reworking not continent–continent collision: Geological Survey of Western Australia, Report 108, 33p.

Sheppard, S, Johnson, SP, Wingate, MTD, Kirkland, CL and Pirajno, F 2010b, Explanatory Notes for the Gascoyne Province: Geological Survey of Western Australia, Perth, Western Australia, 336p.

Sheppard, S, Occhipinti, SA and Nelson, DR 2005, Intracontinental reworking in the Capricorn Orogen, Western Australia: the 1680–1620 Ma Mangaroon Orogeny: Australian Journal of Earth Sciences, v. 52, p. 443–460.

Sheppard, S, Rasmussen, B, Muhling, JR, Farrell, TR and Fletcher, IR 2007, Grenvillian-aged orogenesis in the Palaeoproterozoic Gascoyne Complex, Western Australia: 1030–950 Ma reworking of the Proterozoic Capricorn Orogen: Journal of Metamorphic Geology, v. 25, p. 477–494.

Skilling, IP, White JDL and McPhie, J 2002, Peperite: a review of magma-sediment mingling: Journal of Volcanology and Geothermal Research, v. 114, no. 1–2, p. 1–17.

Stewart, JH 2013, Basin and range structure: a system of horsts and grabens produced by deep-seated extension: Geological Society of America Bulletin, v. 82, p. 1019–1044.

Takehara, M, Komure, M, Kiyokawa, S, Horie, K and Yokohama, K 2010, Detrital zircon SHRIMP U–Pb age of the 2.3 Ga diamictites of the Meteorite Bore Member in the South Pilbara, Western Australia, *in* Fifth International Archean Symposium Abstracts *edited by* IM Tyler and CM Knox-Robinson: Geological Survey of Western Australia; Fifth International Archean Symposium, Perth, Western Australia, September 2010; Record 2010/18, p. 223–224.

Teyssier, C 1985, A crustal thrust system in an intracratonic tectonic environment: Journal of Structural Geology, v. 7, p. 689–700.

Thorne, AM 2016h, Shingle Creek Group (P_-SK-xb-s): Geological Survey of Western Australia, WA Geology Online, Explanatory Notes extract, viewed 7 June 2016, <www.dmp.wa.gov.au/ens>.

Thorne, AM 2015a, Edmund Group (P_-ME-xs-k): Geological Survey of Western Australia, WA Geology Online, Explanatory Notes extract, viewed 24 March 2016, <www.dmp.wa.gov.au/ens>.

Thorne, AM 2015b, Edmund Group, Depositional Package 1 (P_-MEP1-kt): Geological Survey of Western Australia, WA Geology Online, Explanatory Notes extract, viewed 24 March 2016, <www.dmp.wa.gov.au/ens>.

Thorne, AM 2015c, Yilgatherra Formation (P_-MEy-st): Geological Survey of Western Australia, WA Geology Online, Explanatory Notes extract, viewed 24 March 2016, <www.dmp.wa.gov.au/ens>.

Thorne, AM 2015d, Irregully Formation (P_-MEi-kt): Geological Survey of Western Australia, WA Geology Online, Explanatory Notes extract, viewed 24 March 2016, <www.dmp.wa.gov.au/ens>.

Thorne, AM 2015e, Edmund Group, Depositional Package 2 (P_-MEP2-sk): Geological Survey of Western Australia, WA Geology Online, Explanatory Notes extract, viewed 24 March 2016, <www.dmp.wa.gov.au/ens>.

Thorne, AM 2015f, Gooragoora Formation (P_-MEg-ss): Geological Survey of Western Australia, WA Geology Online, Explanatory Notes extract, viewed 24 March 2016, <www.dmp.wa.gov.au/ens>.

Thorne, AM 2015g, Blue Billy Formation (P_-MEb-sl): Geological Survey of Western Australia, WA Geology Online, Explanatory Notes extract, viewed 24 March 2016, <www.dmp.wa.gov.au/ens>.

Thorne, AM 2015h, Cheyne Springs Formation (P_-MEp-kd): Geological Survey of Western Australia, WA Geology Online, Explanatory Notes extract, viewed 24 March 2016, <www.dmp.wa.gov.au/ens>.

Thorne, AM 2015i, Edmund Group, Depositional Package 3 (P_-MEP3-sk): Geological Survey of Western Australia, WA Geology Online, Explanatory Notes extract, viewed 24 March 2016, <www.dmp.wa.gov.au/ens>.

Thorne, AM 2015j, Kiangi Creek Formation (P_-MEk-sk): Geological Survey of Western Australia, WA Geology Online, Explanatory Notes extract, viewed 24 March 2016, <www.dmp.wa.gov.au/ens>.

Thorne, AM 2015k, Muntharra Formation (P_-MEm-kd): Geological Survey of Western Australia, WA Geology Online, Explanatory Notes extract, viewed 24 March 2016, <www.dmp.wa.gov.au/ens>.

Thorne, AM 2015l, Edmund Group, Depositional Package 4 (P_-MEP4-xs-k): Geological Survey of Western Australia, WA Geology Online, Explanatory Notes extract, viewed 24 March 2016, <www.dmp.wa.gov.au/ens>.

Thorne, AM 2015m, Discovery Formation (P_-MEd-cl): Geological Survey of Western Australia, WA Geology Online, Explanatory Notes extract, viewed 24 March 2016, <www.dmp.wa.gov.au/ens>.

Thorne, AM 2015n, Devil Creek Formation (P_-MEv-kd): Geological Survey of Western Australia, WA Geology Online, Explanatory Notes extract, viewed 24 March 2016, <www.dmp.wa.gov.au/ens>.

Thorne, AM 2015o, Ullawarra Formation (P_-MEl-sl): Geological Survey of Western Australia, WA Geology Online, Explanatory Notes extract, viewed 24 March 2016, <www.dmp.wa.gov.au/ens>.

Thorne, AM 2015p, Coodardoo Formation (P_-MEc-st): Geological Survey of Western Australia, WA Geology Online, Explanatory Notes extract, viewed 24 March 2016, <www.dmp.wa.gov.au/ens>.

Thorne, AM 2016a, Collier Group (P_-MC-s): Geological Survey of Western Australia, WA Geology Online, Explanatory Notes extract, viewed 24 March 2016, <www.dmp.wa.gov.au/ens>.

Thorne, AM 2016b, Collier Group, Depositional Package 5 (P_-MCP5-s): Geological Survey of Western Australia, WA Geology Online, Explanatory Notes extract, viewed 24 March 2016, <www.dmp.wa.gov.au/ens>.

Thorne, AM 2016c, Backdoor Formation (P_-MCb-sl): Geological Survey of Western Australia, WA Geology Online, Explanatory Notes extract, viewed 24 March 2016, <www.dmp.wa.gov.au/ens>.

Thorne, AM 2016d, Calyie Formation (P_-MCc-st): Geological Survey of Western Australia, WA Geology Online, Explanatory Notes extract, viewed 24 March 2016, <www.dmp.wa.gov.au/ens>.

Thorne, AM 2016e, Collier Group, Depositional Package 6 (P_-MCP6-s): Geological Survey of Western Australia, WA Geology Online, Explanatory Notes extract, viewed 24 March 2016, <www.dmp.wa.gov.au/ens>.

Thorne, AM 2016f, Ilgarari Formation (P_-MCi-sl): Geological Survey of Western Australia, WA Geology Online, Explanatory Notes extract, viewed 24 March 2016, <www.dmp.wa.gov.au/ens>.

Thorne, AM 2016g, Wyloo Group (P_-WY-s): Geological Survey of Western Australia, WA Geology Online, Explanatory Notes extract, viewed 19 April 2016, <www.dmp.wa.gov.au/ens>.

Thorne, AM and Cutten, HN 2010, Tangadee, WA Sheet 2649: Geological Survey of Western Australia, 1:100 000 Geological Series.

Thorne, AM and Cutten, HN 2011, Mulgul, WA Sheet 2548: Geological Survey of Western Australia, 1:100 000 Geological Series.

Thorne, AM and Seymour, DB 1991, Geology of the Ashburton Basin, Western Australia: Geological Survey of Western Australia, Bulletin 139, 141p.

Thorne, AM, Sheppard, S, Johnson, SP, Martin, DM, Korhonen, FJ and Wingate, MTD 2016, Edmundian Orogeny (CE): Geological Survey of Western Australia, WA Geology Online, Explanatory Notes extract, viewed 24 March 2016, <www.dmp.wa.gov.au/ens>.

Turner, A, Haines, P, Foster, D, Powell, R, Sandiford, M and Offler, R 2015, Did the Delamerian Orogeny start in the Neoproterozoic: The Journal of Geology, v. 117, p. 575–583.

Velasco, MS 2009, Eastern Basin and range crustal extension: a view from seismology and geodesy: The University of Arizona, US, PhD thesis (unpublished).

Ventor Resources Limited 2015, viewed 7 April 2016, <www.ventorresources.com.au/projects/thaduna-project.html>.

Vermeesch, P 2012, On the visualisation of detrital age distributions: Chemical Geology, v. 312–313, p. 190–194.

Walter, MR, Veevers, JJ, Calver, CR and Grey, K 1995, Neoproterozoic stratigraphy of the Centralian Superbasin, Australia: Precambrian Research, v. 73, no. 1–4, p. 173–195.

Wingate, MTD 2002, Age and palaeomagnetism of dolerite sills of the Bangemall Supergroup on the Edmund 1:250 000 sheet, Western Australia: Geological Survey of Western Australia, Record 2002/4, 48p.

Wingate, MTD and Bodorkos, S 2007, 156602: granophyric dolerite sill, No. 36 Well; Geochronology Record 695: Geological Survey of Western Australia, 5p.

Wingate, MTD and Giddings, JW 2000, Age and paleomagnetism of the Mundine Well dyke swarm, Western Australia: implications for an Australia–Laurentia connection at 755 Ma: Precambrian Research, v. 100, p. 335–357.

Wingate, MTD, Kirkland, CL and Thorne, AM 2010a, 149031: felsic volcaniclastic rock, Boundary Bore; Geochronology Record 871: Geological Survey of Western Australia, 6p.

Wingate, MTD, Kirkland, CL and Thorne, AM 2010b, 148994: quartz sandstone, Woolcott Well; Geochronology Record 874: Geological Survey of Western Australia, 5p.

Wingate, MTD, Kirkland, CL and Cutten, HN 2012a, 143440: felsic metavolcaniclastic rock, Nicken Bore; Geochronology Record 1029: Geological Survey of Western Australia, 6p.

Wingate, MTD, Kirkland, CL, Cutten, HN and Thorne, AM 2012b, 143445: dolerite sill, Waldburg Homestead; Geochronology Record 1077: Geological Survey of Western Australia, 4p.

Wingate, MTD, Kirkland, CL, Cutten, HN and Thorne, AM 2012c, 143450: dolerite sill, Top Camp Well; Geochronology Record 1079: Geological Survey of Western Australia, 4p.

Wingate, MTD, Kirkland, CL, Blay, OA and Johnson, SP 2013a, 207259: dolerite sill, Maranoo Well; Geochronology Record 1123: Geological Survey of Western Australia, 4p.

Wingate, MTD, Kirkland, CL and Johnson, SP 2013b, 195826: monzogranitic gneiss, McCarthy Well; Geochronology Record 1104: Geological Survey of Western Australia, 5p.

Wingate, MTD, Kirkland, CL and Cutten, HN 2013c, 189223: dolerite sill, Mount Arapiles; Geochronology Record 1118: Geological Survey of Western Australia, 4p.

Wingate, MTD, Kirkland, CL, Blay, OA and Johnson, SP 2015a, 206916: metadolerite sill, Swamp Well; Geochronology Record 1262: Geological Survey of Western Australia, 4p.

Wingate, MTD, Kirkland, CL, Blay, OA and Johnson, SP 2015b, 206991: metadolerite sill, Gap Well; Geochronology Record 1263: Geological Survey of Western Australia, 4p.

Wingate, MTD, Pirajno, F and Morris, PA 2004, Warakurna large igneous province: a new Mesoproterozoic large igneous province in west-central Australia: Geology, v. 32, no. 2, p. 105–108.

Woodhead, JD and Hergt, JM 2005, A preliminary appraisal of seven natural zircon reference materials for in situ Hf isotope determination: Geostandards and Geoanalytical Research, v. 29, p. 183–195.

Wright, C, Goleby, BR, Shaw, RD, Collins, CDN, Korsch, RJ, Barton, T, Greenhalgh, SA and Sugiharto, S 1991, Seismic reflection and refraction profiling in central Australia: implications for understanding the evolution of the Amadeus Basin, *in* Geological and Geophysical studies in the Amadeus Basin, central Australia *edited by* RJ Korsch and JM Kennard: Bureau of Mineral Resources, Australia, Bulletin 236, p. 41–57.

Wyborn, LAI, Heinrich, CA and Jaques, AL 1994, Australian Proterozoic mineral systems: essential ingredients and mappable criteria, *in* Australian mining looks north — the challenges and choices *edited by* PC Hallenstein: Australian Institute of Mining and Metallurgy; 1994 AusIMM Annual Conference, Darwin, Northern Territory, 5 August 1994, p. 109–115.

Yeates, AN, Gibson, DL, Towner, RR and Crowe, RWA 1984, Regional geology of the onshore Canning Basin, WA, *in* The Canning Basin, WA *edited by* PG Purcell: Geological Society of Australia and Petroleum Exploration Society of Australia; Canning Basin Symposium, Perth, Western Australia, Proceedings, p. 24–55.

Zhan, Y and Mory, AJ 2013, Structural interpretation of the northern Canning Basin, Western Australia, *in* The Sedimentary Basins of Western Australia IV *edited by* M Keep and SJ Moss: West Australian Basins Symposium, Perth, WA, 18 August 2013, 18p.

Zhao, JX, McCulloch, MT and Korsch, RJ 1994, Characterisation of a plume-related ~800 Ma magmatic event and its implications for basin formation in central–southern Australia: Earth and Planetary Science Letters, v. 121, no. 3–4, p. 349–367, doi:10.1016/0012-821X(94)90077-9.

Zi, JW, Rasmussen, B, Muhling, JR, Fletcher, IR, Thorne, AM, Johnson, SP, Cutten, HN, Dunkley, DJ and Korhonen, FJ 2015, In situ U–Pb geochronology of xenotime and monazite from the Abra polymetallic deposit in the Capricorn Orogen, Australia: Dating hydrothermal mineralization and fluid flow in a long-lived crustal structure: Precambrian Research, v. 260, p. 91–112.

Zwingmann, H, Cutten, HN, Wingate, MTD, Todd, AJ and Kirkland, CL 2012, 189218: siltstone fault-rock, Brumby Creek; Geochronology Record 1117: Geological Survey of Western Australia, 3p.

Appendix 1

Mineral occurrences in the Edmund and Collier Basins and underlying Paleoproterozoic basins

The distribution of major economic mineral deposits in the Edmund and Collier Basins and underlying older Proterozoic basins shows a clear spatial association with the major reactivated faults and an expected temporal relationship with their movement history, whether normal, reverse or transcurrent.

There is a history of productive mining in the Edmund and Collier Basins, and older underlying basins and basement rocks. Mined and projected estimated resource minerals include gold, copper and lead, and to a lesser extent silver, manganese, diamonds and rare earth elements. These include fault- and shear-related deposits but also supergene enrichment deposits and alluvial gold. Understanding the mineral prospectivity of the region, therefore, is improved by knowledge of the faulting and deformation history. The more significant deposits are briefly outlined here and include those in the older Bryah, Padbury and Yerrida Basins as well as the Edmund and Collier Basins. The Plutonic Mine in Archean rocks immediately east of the Collier Basin is also discussed as this deposit has a close association with nearby faults dissecting the Edmund and Collier Basins. Quoted reserves are for 'contained metal' rather than 'extracted metal', which is unlikely to be 100%. Historically, early mining was by hand excavation, followed progressively by more mechanized operations. Gold mineralization was the early focus of mining followed by added interest in copper. The Abra polymetallic deposit has been a focus of recent research and is described in more detail. Geochronology of minerals in the deposit has defined its mineralization history and additionally refined understanding of the depositional history of the Edmund Group.

Edmund Basin

Bangemall Mining Centre

The Bangemall Mining Centre (Fig. 21; Muhling and Brakel, 1985b) near Cobra Station, eastern Mount Phillips is hosted by the Edmund Group (1679–1452 Ma). Gold was discovered here in 1896. By 1899, 4.928 kg of gold had been recovered from quartz veins within the Kiangi Creek Formation and Narimbunna Dolerite in the Cobra Syclinorium bounded by the Lyons River and Edmund Faults.

Low Hill

Low Hill (Fig. 21), located on Mount Egerton is a deposit of cellular and massive gem-quality variscite, coloured turquoise to deep green, and containing finely disseminated gold (Hancock et al., 2009). The economic value of the deposit is the variscite rather than the gold content. Variscite is a hydrated aluminium phosphate mineral ($AlPO_4 \cdot 2H_2O$), and occurs at this locality as several thin seams in a zone about 0.5 m thick within Kiangi Creek Formation siltstone, as well as a single discordant vein 30–50 mm thick.

Abra

The Abra deposit (Fig. 21), located on Calyie, is the largest mineral deposit in the Edmund Basin, and was discovered in 1981 when diamond drilling intersected stratabound lead–copper–gold–silver mineralization as well as low-grade copper–barite mineralization at TC, Gnamma and Woodlands (Cooper et al., 1998). This followed earlier discoveries of base metals at Quartzite Well, Manganese Range, Copper Chert and Jeds in 1976 and the identification of anomalies by aeromagnetic surveys at Woodlands, Gnamma, Abra and Cadabra in 1976 and 1977. The strataform Abra deposit (Pirajno et al., 2010; Fig. 21) is hosted in the siliciclastic Irregully and Gooragoora Formations and is characterized by a lower funnel-shaped Brecciated Zone, interpreted as a feeder pipe, overlain by stratabound mineralization in a Black Zone and a higher exhalative SEDEX Red Zone. The feeder pipe consists of a stockwork of Fe-carbonate quartz, barite, pyrite, magnetite and chalcopyrite veins. The Black Zone consists of banded Pb, Zn and minor Cu sulfides, laminated or brecciated hematite, magnetite, Fe-rich carbonate, barite and schelite, and the overlying Red Zone consists of banded jaspilite, hematite, galena, pyrite, barite, siderite and quartz. Mineralization has been dated at 1610–1590 Ma (Zi et al., 2015) from xenotime associated with magnetite from the Black Zone. Later mineral remobilization has been dated at c.1284 Ma (pyrite Re–Os; Pirajno et al., 2010). Xenotime interpreted as metamorphic, from the nearby Tangadee Rhyolite (Kiangi Creek Formation), has been dated at c.1235 and 1030 Ma (Rasmussen et al., 2010). These may correlate with hydrothermal solutions that extend into the Kiangi Creek Formation metasedimentary rocks overlying the Abra mineralization. The deposit contains an Indicated and Inferred Resource of 93 Mt at 4.0% Pb and 10 g/t Ag (2.5% Pb cutoff), and the lower, copper-gold enriched stockwork domain contains an Indicated and Inferred Resource of 14 Mt grading 0.62% Cu and 0.49 g/t Au (0.4% Cu cutoff) (Abra Mining Limited website, viewed 2014). Mineralization occurs within the Quartzite Well Fault Zone, which is an eastern continuation of the Lyons River Fault. This fault system has been imaged on the Capricorn Orogen deep crustal seismic survey (Johnson et al., 2013) located 250 km west of Abra, extending down to, and offsetting, the Moho, suggesting this mantle-tapping structure acted as a conduit for heated magmatic fluids. These magmatic fluids are interpreted to have mixed with meteoric fluids enriched with base-metal minerals leached from the Edmund Group sediments (Pirajno et al., 2010).

Collier Basin

Ilgarari and Kumarina Mining Centres

The Ilgarari and Kumarina Mining Centres (Fig. 21), on Ilgarari and Wonyulgunna, were discovered in 1913 and are hosted in the Collier Group (1171–1069 Ma). A total of 1369 t of copper ore was mined between 1913 and 1970, with an average grade of 25% copper. Mineralization occurs in a series of northeast-striking faults and shears, including the Ilgarari and Kumarina Faults, along contacts of Narimbunna Dolerite and Ilgarari Formation siltstone. Nearby Butcher Bird mine produced 8.46 t grading 30% copper between 1916 and 1918 (Montezuma Mining Company, 2016). Mineralization is associated with the regional northeast-trending Butcherbird Shear Zone.

Padbury Basin

Egerton Mining Centre

The Egerton Mining Centre (Fig. 21), located in the Padbury Basin (1983–1811 Ma), Egerton Inlier, on Mount Egerton was first mined in 1910 (Cooper et al., 1998). The main deposits are Hibernian and Gaffneys Find. A recent evaluation by Egerton Gold NL (1993), stated a Preliminary Inferred and Indicated Resource of 170 000 t at 5.5 g/t gold. The gold occurs along the sheared contact of a gabbro body and metamorphosed sandstone and siltstone of the Labouchere Formation, Padbury Group. Hibernian is located on the northeast-trending Hiburnian Fault and Gaffneys Find close to similar northeast-trending faults.

Nathans and Labouchere Mines

Opencut mines Nathans and Labouchere (Fig. 21) are also in Padbury Group sediments, and are located 5 and 11 km west and northwest, respectively, of Fortnum Mine on Milgun. Nathans Mine is located on a north–south-trending fault, 2 km south of the Mount Clere Fault. Labouchere is located on the Labouchere Fault.

Bryah Basin

Fortnum Mine

The Fortnum Mine (Fig. 21) is located on Milgun and within the Bryah Basin (2014–1920 Ma). The Fortnum Mine produced 540 000 oz of gold between 1994 and 2001, when the mine was closed. Mineralization is associated with pyritic quartz-hematite jasperoid in the upper part of the Narracoota Formation volcanics, overlain by volcaniclastics of the Thaduna Formation of the Bryah Group, and is found in the Fortnum – Mount Clere Fault zone and D34 Shear Zone (Fortnam Gold Mine, 2015).

DeGrussa Mine

The copper–gold DeGrussa deposit (Fig. 21) was discovered by Sandfire Resources in 2009 on Doolgunna. Openpit extraction and underground mining commenced in 2011. The deposit has a Positive Definite Feasibility of 14.33 Mt, grading 4.6% copper and 1.6 g/t gold for 652 000 t of contained copper and 742 000 oz of contained gold (Sandfire Resources NL, 2015). Mineralization is in basalt, mafic and ultramafic schist and volcaniclastic sediments of the Naracoota Formation, Bryah Group, and lies within the northeast-trending Jenkin Fault Zone.

Horseshoe Lights Mine

The Horseshoe Lights deposit (Fig. 21) on Jamindi was discovered in 1946 and by the time the mine closed in 1994 had produced 300 000 oz of gold and 45 000 t of copper. Mineralization is in the Narracoota Formation of the Bryah Group and 1 km south of the Horseshoe Lights Fault. Horseshoe Lights has a Measured, Indicated and Inferred Mineral Resource of 12.85 million t at 1% copper and 0.1 g/t gold, containing 128 600 t of copper metal and 36 000 oz of gold, using a 0.5% Cu cutoff grade (Horseshoe Lights Mine, 2015).

Peak Hill Goldfields

Gold was first discovered in the Peak Hill Goldfields (Fig. 21) on Bryah in 1892 with a township established in 1897. By 1913, at Peak Hill 270 000 oz of gold had been produced. Renewed activity in the 1980s produced a further 650 000 oz of gold. Nearby Harmony on Bryah was discovered in 1991 and mined between 1995 and 1997, producing 661 000 oz of gold.

Yerrida Basin

Thaduna, Green Dragon and Enigma

Copper was discovered in 1941 at the Thaduna prospect (Fig. 21) on Thaduna and the nearby Green Dragon prospect on Marymia, in mineralized fault zones within wacke of the Thaduna Formation, Yerrida Group (2200–1800 Ma) in the Proterozoic Yerrida Basin. Historic mining at Green Dragon ceased in 1971 having produced 9100 t at 5.1% copper. From the Thaduna Mine, 30 290 t at 8.7% copper were produced (Ventor Resources Limited, 2015). The Enigma deposit on Marymia, also nearby, has recorded copper grades generally below 3% but as high as 7.6%. Mineralization occurs in the Paleoproterozoic Johnson Cairn Formation, Winplain Group of the Yerrida Basin. This is a secondary copper–carbonate deposit in an anticlinal structure adjacent to an interpreted northeast-trending fault.

Archean rocks

Plutonic Mine

Gold was discovered at the site of the present Plutonic Mine (Fig. 21) on Three Rivers, in 1988 by Great Central Mines and operated as an openpit from 1990. Underground mining commenced in 1995. Historically, 5.3 million oz were produced with 2.5 million oz of gold from the openpit and 2.8 million oz from underground sources (Northern Star Resources Ltd, 2015). Mineralization occurs in Archean rocks of the Marymia Inler. Amphibolite lenses associated with komatitic basalt and metasedimentary rocks are overthrust by Archean metagranite. These mineralized host rocks were named the Plutonic Well Greenstone Belt by Gazley et al. (2012). The mine is adjacent to the MMR Fault and the immediate area is heavily faulted.

Post Edmund Group intrusives

Gifford Creek

The Gifford Creek Ferrocarbonatite Suite (Fig. 21; Pearson et al., 1996) in southeast Edmund contains rare earth elements (REE). The suite comprises 1300–1200 Ma (Johnson, 2013) high-level alkaline sills, ironstone dykes and veins intruding monzogranite of the Pimbyana Granite and Yangibana Granite of the Durlacher Supersuite, and metasedimentary rocks of the Pooranoo Metamorphics as well as the overlying basal sediments of the Edmund Group (Pirajno and Gonzalez-Alvarez, 2014). The deposit is local to the Lyons River Fault, which is considered to have channelled the alkaline mantle-derived melts into the upper crust. In the process, these melts interacted with metasomatized, subcontinental mantle, and extracted REE from upper crustal granites. The REE were then concentrated in monazites within the ironstones. Subsequent hydrothermal activity, possibly during the Edmundian Orogeny, is also thought to have upgraded the REE content.

Alluvial gold

The potential for alluvial gold in the region of the Edmund and Collier Basins has also been recognized. Ivanhoe Mining's evaluation of the Bangemall Mining Centre (Fig. 21) on Mount Phillips in the 1980s highlighted the main potential to be alluvial gold in the immediate area of the workings known as Prospectors Gully. At present, the mining centre is being worked with metal detectors and by dryblowing, producing small quantities of gold nuggets. Hancock et al. (2009) compared the mineralogy and geochemistry of alluvial gold and nearby lode deposits at the Egerton Mining Centre on Mount Egerton, the Bangemall Mining Centre on Mount Phillips, Low Hill on Mount Egerton and also the Star of Mangaroon mine on Mangaroon. They identified that alluvial gold from Hiburnian in the Egerton Mining Centre was derived from several sources but is similar to bedrock-hosted gold from the nearby Gaffneys Find deposit. Alluvial gold from McCarthys Patch in the Bangemall Mining Centre was derived from a single source similar to bedrock-hosted gold from the nearby Cobra deposit. The authors suggest there have been at least two periods of hydrothermal gold mineralization during the Proterozoic and at least one period of secondary gold formation during the Phanerozoic.

Diamonds

Diamonds (Fig. 21) were recovered from stream sediment samples and from kimberlitic rocks in the early 1980s. A kimberlite dyke located 7 km southwest of Mount Palgrave on Maroonah intrudes the Devil Creek Formation and possibly the Discovery Formation over a strike length of 2 km (Duncan, 1993; Cooper et al., 1998). One small diamond (0.000017 metric carats) was recovered from a 135 kg sample of kimberlite. Diamonds were also recovered from stream sediment samples taken 17 km southwest of Ullawarra Station in the area of the Eerstelling Lamproites (Rohde, 1993); however, none from a lamproite outcrop.

Manganese

Manganese occurs in Edmund and Collier Group units with strong silicification and is often apparent as prominent lateritic surface enrichment, giving the rocks a deep blue–black appearance. Cooper (1998) listed a number of manganese occurrences. In the Collier Group, surface enrichment in Ilgarari Formation siltstone occurs close to the Ilgarari and Butcher Bird Mines. In the Edmund Group, in Irregully Formation, manganese is found close to the Manganese Range prospect and to the Quartzite Well Fault, and in Ullawarra Formation at a number of localities on the southwest limb of the Wanna Syncline (Fig. 21). None of these appear to be economically viable. Pirajno et al. (2004) discussed supergene manganese occurrence in the Mount Fraser, Mount Padbury, Ravelstone (Peak Hill) and Horseshoe areas of the Bryah and Padbury Groups.

Appendix 2

Comparisons with other depositional basins

Canning Basin

The intracratonic Paleozoic Canning Basin covers an area of 640 000 km^2, separating the Kimberley and Pilbara Cratons, and contains up to 15-km thickness of Ordovician to Cretaceous sediments. The Canning Basin is subdivided into many structural elements, including the Fitzroy Trough between the Lennard Shelf and Broome Platform. As one of the main depocentres of the Canning Basin, study of the Fitzroy Trough demonstrates the tectonic history of the area. The northwest–southeast-oriented trough initiated as an early Paleozoic rift and was later subjected to mid-Devonian–Carboniferous extension, mid-Carboniferous compression, and an Early Permian thermal sag (Yeates et al., 1984; Kennard et al., 1994; Zhan and Mory, 2013). The early northeast–southwest extension produced a half-graben structure resulting largely from normal movement on the Fenton Fault system along the southwestern margin of the Fitzroy Trough. Across the current 100-km width of the Fitzroy Trough, total extension during the Carboniferous was estimated to have averaged about 10 km (Zhan and Mory, 2013). Subsequent transcurrent fault movements within the trough have modified the normal faults on which this estimate is based, but these modifications appear to have been minor (Zhan and Mory, 2013). Calculated from restoration of folding, total shortening across the Fitzroy Trough, largely during the Triassic to Mid-Jurassic Fitzroy Transpression, was estimated as much as 3% (Zhan and Mory, 2013).

Amadeus Basin

Similar to the Edmund and Collier Basins, the Amadeus Basin appears to have been formed between two basement blocks and later subjected to north–south shortening by reactivation of older basement faults (Maidment et al., 2013). But the basin's tectonic history is more complicated. The Amadeus is a remnant of the larger Centralian Superbasin (Walter et al., 1995) that formed in the late Proterozoic following a plume-related c. 800 Ma magmatic event (Zhao et al., 1994). This intracratonic superbasin was then disrupted internally by the 570–530 Ma Petermann Orogeny (Sandiford et al., 2001) with central uplift and thrusting, subdividing the superbasin into the individual Amadeus, Georgina, Ngalia and Officer Basins (Walter et al., 1995; Sandiford et al., 2001), with later deformation during the 430–300 Ma Alice Springs Orogeny (Sandiford et al., 2001). These individual basins, which include significant Paleozoic sediments older than mid-Carboniferous, are effectively those parts of the Centralian Superbasin that underwent little or no basement-involved deformation during the Petermann and Alice Springs Orogenies (Hand and Sandiford, 1999). Prior to the Petermann Orogeny, sediment thickness increased towards the presently exposed Musgrave Province, and the Officer and Amadeus Basins were connected by a continuous sedimentary blanket to a thickness of 4 km, thinning towards the central Amadeus Basin to less than 2 km (Hand and Sandiford, 1999). Prior to the Alice Springs Orogeny, the depocentre had moved beyond the northern margin of the Amadeus Basin, with 8 km of sediment south of the southern Georgina Basin. A similar pattern is noted with a trough between the Amadeus and Ngalia Basins containing in excess of 7 km of sediment. Hand and Sandiford (1999) determined the importance of regional thermal controls on fault reactivation. They found a correlation between greater sediment thickness in different parts of the Amadeus Basin and reactivation of basement faults, suggesting that sediment thermal blanketing was a controlling factor resulting in long-term lithospheric weakening. Thus, uplift of the Arunta Orogen and Musgrave Province took place where sediment thickness was greatest and the remnant basins represent areas where sediment thickness was the least. However, Comacho et al. (2002) refuted this model identifying that detrital zircon populations of all the sediments in the Amadeus Basin were derived from the Musgrave Complex, which was emergent rather than covered by sediments as required by the model. It may just be that the reverse faults that were most active during the Peterman and Alice Springs Orogenies, uplifting the basement blocks, were also the most active during the formation of the Centralian Superbasin, that is, normal movement and graben formation. Basin inversion took place by reactivation on original favoured deep crustal faults.

Flöttmann and Hand (1999) discuss basement-cored, downward-facing antiformal synclines at the northern margin of the Amadeus Basin that formed during the Alice Springs Orogeny and had been interpreted as fold nappes involving large horizontal thin-skinned crustal shortening >70 km (>50%) (Teyssier, 1985). However, deep seismic reflection profiles (Goleby et al., 1989, 1990; Wright et al., 1991) indicate that an uncomplicated homoclinal structure involving much less shortening could be modelled. Thick-skinned deformation required maximum crustal shortening of 32 km over a width of about 110 km or about 22% (Shaw et al., 1991, 1992). Flöttmann and Hand (1999) calculated from cross-section balancing over this area a shortening of about 30%, much less than suggested by Teyssier (1985).

Adelaide Rift Complex

The Adelaide Rift Complex comprises largely marine metasedimentary rocks deposited during at least five major successive rift cycles (Preiss, 2000) between the mid-Neoproterozoic and mid-Cambrian. These metasedimentary rocks are as much as 18 km thick (Preiss, 2000), forming an arc-shaped belt some 1000 km long and several hundred kilometres wide, and comprise many sequences separated by breaks in sedimentation. The complex of rifts and sags of the Adelaide Rift Complex are interpreted as an intracontinental rift, evolving to passive margin after the breakup of Rodinia. Subsequent

deformation began as early as 545 Ma (Turner et al., 2015) leading up to the Delamerian Orogeny (514–495 Ma; Foden et al., 2006), which produced folding and faulting of the strata, the eroded remnants of which are the Flinders and Mount Lofty Ranges. This deformation resulted from the northwest–southeast compression between the Gawler Craton and the Curnamona Province and was accompanied by intrusion of granites. Delamerian deformation was least in the Central Flinders Zone, where shortening was generally less than 10% (Paul et al., 1999) and greatest, as much as 50%, in the Fleurieu Arc (Flöttmann et al., 1997). Although there is an overlap in time, the Adelaide Rift Complex developed independently of the Centralian Superbasin, which was a product of continental sag (Preiss, 2000). In the Fleurieu Arc of the Mount Lofty Ranges and Kangaroo Island to the south, there are early northwest-directed thrusts and to the north these are overprinted by north–south folds and sinistral transpressive faults of the Nackara Arc. The Central Flinders Zone to the north of the Nackara Arc has a shallower basement and less deformation than the fold arcs. The eastern limit of the fold arcs is marked by intruded I-type and some S-type granites dated 515–505 Ma and possibly produced by west-dipping subduction beneath the orogen (Preiss, 2000). Metamorphic grade in the cover rocks of the Delamerian Orogen ranges from unmetamorphosed to upper amphibolite facies. Post-Delamerian, east–west compression uplifted the Delamerian mountain range by reactivation of Delamerian faults as a series of thrust faults dipping west and east beneath the uplifted regions. Preiss (2000) suggested that the causes of plate convergence may have involved collision of a microcontinent originating from farther south in the Neoproterozoic proto-Pacific Ocean or a Cambrian island against the southeastern promontory in the margin of the Australian continent.

Basin and Range Province

The Basin and Range Province covers much of western US and extends south into northwestern Mexico. The province is characterized by parallel north–south-trending mountain ranges separated by wide, flat bottom valleys, recognized as a series of tilted half-graben blocks, 24–32 km wide. The elevation difference between peak summit and valley floor is as much as 3000 m and the amount of extension, which commenced about 12–17 Ma to produce this, has been variously calculated (Colgan et al., 2006). Stewart (2013) interpreted the graben underlying valleys as complex collapse zones over narrow zones of extension at depth and that these zones are related to fragmentation of a crustal slab above a plastically extended substratum. Stewart (2013) estimated extension of 2.4 km across a 24–48 km width of each zone of extension beneath the graben, effectively 7–10%. Colgan et al. (2006) determined extension of about 23 km across a 220 km-wide region between Santa Rose and Warner Ranges in northwestern Nevada. Reported as 12%, this extension took place on a single generation of high-angle normal faults since c. 12 Ma. Colgan (2006) noted that in other parts of the Basin and Range Province, crust that had been thickened to 45–50 km by Cretaceous thrusting, was subsequently thinned to 30 km by large magnitude (>50%) extension. Velasco (2009) quotes a figure of 200% extension since the late Oligocene on listric normal faults, which sole on a detachment surface at 10 km depth, interpreted to be a reactivated thrust. The Basin and Range Province is still being uplifted, in part a response to subduction of the East Pacific Rise and initiation of the San Andreas Fault. The western US is a region of high heat flow, which lowers the density of the lithosphere and stimulates isostatic uplift. It is suggested that outward plastic flow at depth has resulted in gravitational collapse in the upper crust.

Comparison of extension and shortening in other basins

In order to evaluate the estimated extension and shortening in the Edmund and Collier Basins, comparisons are made with other depositional basins. These include the Canning and Amadeus Basins and Adelaide Rift Complex in Australia, and also with the Basin and Range Province in the US. Although the tectonic setting and age of each of these basins is different to the Edmund and Collier Basins, the comparisons give some indication as to whether the figures calculated here are reasonable. Detail is given in Appendix 1. In the Fitzroy Trough of the Canning Basin, with 15 km of sediments, extension is estimated at 10%, and subsequent shortening 3% (Zhan and Mory, 2013). The Amadeus Basin is a remnant of the larger Centralian Superbasin (Walter et al., 1995). The amount of extension does not appear to have been calculated, but estimates of shortening range from 22% (Shaw et al., 1991, 1992) to 30% (Flöttmann and Hand, 1999) to >50% (Teyssier, 1985). In the Adelaide Rift Complex, extension has not been calculated. Shortening has been estimated at generally less than 10% (Paul et al., 1999; Preiss, 2000) and greatest in the Fleurieu Arc, as much as 50% (Flöttmann et al., 1997). In the Basin and Range Province in the US, extension has been calculated at 7–12% (Colgan et al., 2006; Stewart, 2013) or more extreme values of 50–200% (Colgan et al., 2006; Velasco, 2009). Extension of 7.2% in the Edmund Basin, shortening of 4.7 – 17% of the Edmund Basin (due to the Mutherbukin Tectonic Event) and shortening of 3.8 – 17.5% of the Edmund and Collier Basin (due to the Edmundian Orogeny) compare favourably with these other deformed depositional basins.

Appendix 3

Lu–Hf isotope analyses

Hafnium isotope analyses were conducted on previously dated zircons using a New Wave/Merchantek LUV213 laser-ablation microprobe, attached to a Nu Plasma multi-collector inductively coupled plasma mass spectrometer (LA-MC-ICPMS). The analyses employed a beam diameter of about 40 μm and a 5 Hz repetition rate, and energies of 0.6–1.3 mJ per pulse, which resulted in ablation pits typically 40–60 μm deep during a 30–120 s analysis. The ablated sample material was transported from the laser cell to the ICP-MS torch by a helium carrier gas. The measurement of accurate $^{176}Hf/^{177}Hf$ ratios in zircon requires correction of the isobaric interferences of ^{176}Lu and ^{176}Yb on ^{176}Hf. Interference of ^{176}Lu on ^{176}Hf was corrected by measurement of interference-free ^{175}Lu, and using the invariant $^{176}Lu/^{175}Lu$ correction factor of 0.02669 (DeBievre and Taylor, 1993). The interference of ^{176}Yb on ^{176}Hf was corrected by measuring the interference-free ^{172}Yb isotope and using the $^{176}Yb/^{172}Yb$ ratio to calculate the intensity of ^{176}Yb. The appropriate value of $^{176}Yb/^{172}Yb$ (0.5865) was determined by successively doping a JMC475 Hf standard (100 ppb solution) with various amounts of Yb, and determining the value of $^{176}Yb/^{172}Yb$ required to yield the value of $^{176}Hf/^{177}Hf$ in the undoped solution.

Standard zircons (Mud Tank and Temora II), along with samples, were analysed. Samples were run over the course of several years and during the course of this study the mean Mud Tank $^{176}Hf/^{177}Hf$ value was 0.282528 ± 0.000026 and the mean Temora $^{176}Hf/^{177}Hf$ value was 0.282686 ± 0.000034. The mean Mud Tank values of each individual batch and the long-term average are within two standard deviations of the recommended value (0.282522 ± 0.000042 2σ; Griffin et al., 2007). Temora II zircon has an average $^{176}Yb/^{177}Hf$ ratio of 0.037, which is similar to the average $^{176}Yb/^{177}Hf$ ratio of Gascoyne Province magmatic zircon of 0.042. The average $^{176}Hf/^{177}Hf$ ratio for Temora II during batches is consistent with the published values of 0.282686 ± 8 (solution ICPMS; Woodhead and Hergt, 2005) and 0.282687 ± 24 (LA-ICPMS, Hawkesworth and Kemp, 2006).

Calculation of initial $^{176}Hf/^{177}Hf$ is based on the ^{176}Lu decay constant of Scherer et al. (2001) (1.867 x10-11 yr^{-1}). Since $^{176}Hf/^{177}Hf$ departures from the CHUR evolution line are very small, the epsilon notation is used whereby one epsilon unit represents a one part per 10 000 deviation from the CHUR composition. Calculation of εHf values employs the decay constant of Scherer et al. (2001) and the CHUR values of Blichert-Toft and Albarède (1997).

Measured isotope compositions are referred to modelled bulk-Earth Hf reservoirs, including Depleted Mantle (DM; Griffin et al., 2000, 2004) and Chondritic Uniform Reservoir (CHUR; Blichert-Toft and Albarède, 1997). Model ages, (T_{DM}), which are calculated using the measured $^{176}Lu/^{177}Hf$ of the zircon, provide only a minimum age for the source material of the magma from which the zircon crystallized, because the $^{176}Lu/^{177}Hf$ ratio of zircon is much lower than the $^{176}Lu/^{177}Hf$ ratio of all reasonable reservoirs for Hf. Therefore, we have calculated two-stage model ages (T_{DM}^2), which assumes that the parental magma was produced from an average continental crust ($^{176}Lu/^{177}Hf$ = 0.015) that originally was derived from a depleted-mantle source with $(^{176}Hf/^{177}Hf)_i$ = 0.279718 at 4.56 Ga and $^{176}Lu/^{177}Hf$ = 0.0384 (Griffin et al., 2004).

Appendix 4

Detrital zircon analyses, Edmund and Collier Groups

Analysis no.	$^{207}Pb/^{206}Pb$ date (Ma)	$^{176}Hf/^{177}Hf$ measured	$^{176}Lu/^{177}Hf$ measured	$^{176}Yb/^{177}Hf$ measured	$^{176}Hf/^{177}Hf$ initial	$\varepsilon Hf_{(i)}$	T_{DM2} (Ga)
EDMUND GROUP							
Depositional Package 1							
Yilgatherra Formation							
GSWA 152956: metasandstone							
1	1791 ± 13	0.281558	0.001152	0.052426	0.281519 ± 0.000012	-4.5 ± 0.4	2.8
2	2130 ± 11	0.281335	0.000988	0.044145	0.281295 ± 0.000022	-4.7 ± 0.8	3.0
4	1789 ± 20	0.281579	0.001373	0.064342	0.281532 ± 0.000015	-4.0 ± 0.5	2.7
5	1804 ± 21	0.281542	0.002389	0.080634	0.281460 ± 0.000023	-6.2 ± 0.8	2.9
6	1981 ± 7	0.281469	0.000758	0.035838	0.281440 ± 0.000019	-2.9 ± 0.7	2.8
8	2693 ± 10	0.281136	0.000689	0.028206	0.281101 ± 0.000014	1.4 ± 0.5	3.1
9	1781 ± 37	0.281478	0.002805	0.087426	0.281383 ± 0.000049	-9.5 ± 1.7	3.1
11	1844 ± 15	0.281541	0.000845	0.037075	0.281511 ± 0.000012	-3.5 ± 0.4	2.7
13	1794 ± 16	0.281525	0.001859	0.073273	0.281462 ± 0.000017	-6.4 ± 0.6	2.9
14	1778 ± 16	0.281669	0.001233	0.062698	0.281627 ± 0.000023	-0.9 ± 0.8	2.5
16	1801 ± 26	0.281537	0.000875	0.032605	0.281507 ± 0.000011	-4.6 ± 0.4	2.8
18	1755 ± 33	0.281511	0.000506	0.023837	0.281494 ± 0.000018	-6.1 ± 0.6	2.8
20	1797 ± 9	0.281506	0.000707	0.035866	0.281482 ± 0.000014	-5.6 ± 0.5	2.8
22	1811 ± 18	0.281517	0.001510	0.075220	0.281465 ± 0.000013	-5.9 ± 0.5	2.9
24	1819 ± 18	0.281492	0.001256	0.059424	0.281449 ± 0.000014	-6.3 ± 0.5	2.9
25	1849 ± 18	0.281559	0.001519	0.067759	0.281506 ± 0.000019	-3.6 ± 0.7	2.8
27	1819 ± 12	0.281552	0.000755	0.034591	0.281526 ± 0.000022	-3.6 ± 0.8	2.7
28	2291 ± 6	0.281249	0.000548	0.026889	0.281225 ± 0.000014	-3.5 ± 0.5	3.1
30	2274 ± 15	0.281243	0.000644	0.031876	0.281215 ± 0.000011	-4.2 ± 0.4	3.1
32	2298 ± 10	0.281226	0.000222	0.010450	0.281216 ± 0.000012	-3.6 ± 0.4	3.1
GSWA 169093: sandstone							
1	1804 ± 25	0.281535	0.001855	0.084646	0.281472 ± 0.000011	-5.8 ± 0.4	2.9
2	2013 ± 16	0.281478	0.001075	0.044973	0.281437 ± 0.000012	-2.3 ± 0.4	2.8
4	2194 ± 12	0.281257	0.001867	0.065640	0.281179 ± 0.000015	-7.3 ± 0.5	3.3
5	1837 ± 27	0.281582	0.001480	0.065686	0.281530 ± 0.000034	-3.0 ± 1.2	2.7
9	1813 ± 36	0.281546	0.001335	0.043381	0.281500 ± 0.000011	-4.6 ± 0.4	2.8
11	1692 ± 16	0.281582	0.000521	0.018983	0.281565 ± 0.000014	-5.1 ± 0.5	2.7
13	1786 ± 29	0.281624	0.000923	0.038461	0.281593 ± 0.000016	-1.9 ± 0.6	2.6
15	1983 ± 23	0.281540	0.000815	0.032468	0.281509 ± 0.000017	-0.4 ± 0.6	2.7
16	1830 ± 21	0.281510	0.000851	0.034917	0.281480 ± 0.000011	-4.9 ± 0.4	2.8
17	1767 ± 20	0.281492	0.002001	0.072655	0.281425 ± 0.000013	-8.3 ± 0.5	3.0
18	1687 ± 16	0.281527	0.002581	0.087661	0.281445 ± 0.000019	-9.5 ± 0.7	3.0
19	2262 ± 9	0.281295	0.000389	0.010805	0.281278 ± 0.000015	-2.2 ± 0.5	3.0
21	1845 ± 39	0.281517	0.000827	0.025221	0.281488 ± 0.000015	-4.3 ± 0.5	2.8
24	1749 ± 38	0.281497	0.001288	0.056674	0.281454 ± 0.000009	-7.7 ± 0.3	2.9
25	1819 ± 20	0.281443	0.000934	0.031527	0.281411 ± 0.000011	-7.7 ± 0.4	3.0
26	1787 ± 22	0.281518	0.001312	0.044854	0.281474 ± 0.000019	-6.2 ± 0.7	2.9
28	1786 ± 22	0.281600	0.001179	0.042776	0.281560 ± 0.000014	-3.1 ± 0.5	2.7
29	1966 ± 16	0.281411	0.000240	0.010679	0.281402 ± 0.000012	-4.6 ± 0.4	2.9
31	1795 ± 46	0.281675	0.002638	0.081842	0.281585 ± 0.000018	-2.0 ± 0.6	2.6

Analysis no.	$^{207}Pb/^{206}Pb$ date (Ma)	$^{176}Hf/^{177}Hf$ measured	$^{176}Lu/^{177}Hf$ measured	$^{176}Yb/^{177}Hf$ measured	$^{176}Hf/^{177}Hf$ initial	$\varepsilon Hf_{(i)}$	T_{DM2} (Ga)
Irregully Formation							
GSWA 148969: dolomitic quartz sandstone							
1	2428 ± 5	0.281163	0.001076	0.065248	0.281113 ± 0.000009	-4.3 ± 0.3	3.2
8	1763 ± 8	0.281543	0.001450	0.081252	0.281495 ± 0.000012	-6.0 ± 0.4	2.8
13	1809 ± 15	0.281666	0.001428	0.073204	0.281617 ± 0.000009	-0.6 ± 0.3	2.5
16	2383 ± 8	0.281219	0.000588	0.029458	0.281192 ± 0.000009	-2.5 ± 0.3	3.1
18	1941 ± 9	0.281428	0.001136	0.057476	0.281386 ± 0.000010	-5.8 ± 0.3	3.0
24	1784 ± 27	0.281479	0.001328	0.069356	0.281435 ± 0.000012	-8.3 ± 0.4	3.0
26	1802 ± 10	0.281531	0.001163	0.062628	0.281491 ± 0.000008	-5.2 ± 0.3	2.8
35	1799 ± 9	0.281485	0.001008	0.051809	0.281451 ± 0.000011	-6.7 ± 0.4	2.9
38	2037 ± 8	0.281216	0.001411	0.066342	0.281161 ± 0.000009	-11.5 ± 0.3	3.4
44	2954 ± 3	0.281054	0.002405	0.134198	0.280918 ± 0.000015	0.9 ± 0.5	3.3
45	2449 ± 5	0.281174	0.001274	0.067562	0.281114 ± 0.000011	-3.8 ± 0.4	3.2
49	2161 ± 15	0.281165	0.000461	0.023856	0.281146 ± 0.000008	-9.3 ± 0.3	3.4
52	1822 ± 8	0.281766	0.001963	0.113674	0.281698 ± 0.000013	2.6 ± 0.5	2.3
55	2630 ± 11	0.280988	0.000719	0.036107	0.280952 ± 0.000012	-5.4 ± 0.4	3.5
70	2468 ± 6	0.281208	0.000366	0.015865	0.281191 ± 0.000012	-0.6 ± 0.4	3.0
73	2307 ± 4	0.281237	0.001027	0.055095	0.281192 ± 0.000012	-4.3 ± 0.4	3.2
74	2090 ± 5	0.281235	0.000594	0.032804	0.281211 ± 0.000010	-8.6 ± 0.3	3.3
83	2237 ± 14	0.281322	0.000363	0.019916	0.281307 ± 0.000012	-1.8 ± 0.4	2.9
91	1761 ± 5	0.281398	0.001369	0.075812	0.281352 ± 0.000016	-11.0 ± 0.6	3.2
101	2926 ± 7	0.280991	0.001968	0.106280	0.280881 ± 0.000017	-1.0 ± 0.6	3.4
GSWA 152954: dolomitic sandstone							
2	2752 ± 7	0.281074	0.000912	0.031459	0.281026 ± 0.000013	0.1 ± 0.5	3.2
5	1763 ± 28	0.281564	0.000505	0.022598	0.281547 ± 0.000017	-4.1 ± 0.6	2.7
11	1796 ± 14	0.281584	0.000804	0.038761	0.281557 ± 0.000017	-3.0 ± 0.6	2.7
13	2816 ± 5	0.281084	0.000979	0.048725	0.281031 ± 0.000012	1.8 ± 0.4	3.2
20	2675 ± 8	0.280905	0.001244	0.060710	0.280841 ± 0.000019	-8.3 ± 0.7	3.7
31	2438 ± 13	0.281225	0.001187	0.061580	0.281170 ± 0.000013	-2.1 ± 0.5	3.1
38	1812 ± 8	0.281436	0.002444	0.076599	0.281352 ± 0.000022	-9.9 ± 0.8	3.1
40	1828 ± 8	0.281446	0.001452	0.075401	0.281396 ± 0.000017	-8.0 ± 0.6	3.0
46	1776 ± 9	0.281444	0.000652	0.026410	0.281422 ± 0.000014	-8.2 ± 0.5	3.0
48	1800 ± 7	0.281554	0.001621	0.073345	0.281499 ± 0.000022	-5.0 ± 0.8	2.8
49	1769 ± 13	0.281626	0.000864	0.038359	0.281597 ± 0.000009	-2.2 ± 0.3	2.6
54	2743 ± 4	0.281070	0.001449	0.048486	0.280994 ± 0.000020	-1.3 ± 0.7	3.3
57	2518 ± 7	0.281208	0.000524	0.028017	0.281183 ± 0.000017	0.3 ± 0.6	3.0
58	3376 ± 6	0.280616	0.000402	0.019398	0.280590 ± 0.000017	-0.9 ± 0.6	3.8
59	2182 ± 4	0.281295	0.001146	0.063116	0.281247 ± 0.000011	-5.2 ± 0.4	3.1
60	1781 ± 7	0.281622	0.000943	0.053302	0.281590 ± 0.000016	-2.2 ± 0.6	2.6
61	1982 ± 10	0.281568	0.001304	0.057693	0.281519 ± 0.000017	-0.1 ± 0.6	2.6
64	1787 ± 7	0.281590	0.000710	0.038257	0.281566 ± 0.000017	-2.9 ± 0.6	2.7
66	1778 ± 15	0.281377	0.002707	0.084216	0.281286 ± 0.000030	-13.0 ± 1.1	3.3
68	2449 ± 6	0.281135	0.002173	0.071939	0.281033 ± 0.000023	-6.7 ± 0.8	3.4

Analysis no.	$^{207}Pb/^{206}Pb$ date (Ma)	$^{176}Hf/^{177}Hf$ measured	$^{176}Lu/^{177}Hf$ measured	$^{176}Yb/^{177}Hf$ measured	$^{176}Hf/^{177}Hf$ initial	$\varepsilon Hf_{(i)}$	T_{DM2} (Ga)
Depositional Package 2							
Gooragoora Formation							
GSWA 148970: quartz sandstone							
1	1824 ± 16	0.281562	0.000525	0.026417	0.281544 ± 0.000012	-2.8 ± 0.4	2.7
3	1722 ± 30	0.281662	0.000775	0.035061	0.281637 ± 0.000009	-1.8 ± 0.3	2.5
5	1790 ± 11	0.281539	0.000733	0.036836	0.281514 ± 0.000010	-4.6 ± 0.4	2.8
12	2477 ± 8	0.281209	0.000622	0.032197	0.281180 ± 0.000013	-0.8 ± 0.5	3.1
13	1724 ± 11	0.281620	0.003052	0.164138	0.281520 ± 0.000015	-5.9 ± 0.5	2.8
15	1779 ± 8	0.281542	0.000779	0.041607	0.281516 ± 0.000010	-4.8 ± 0.4	2.8
16	1768 ± 10	0.281525	0.001097	0.048385	0.281488 ± 0.000013	-6.1 ± 0.5	2.8
19	1761 ± 18	0.281610	0.000539	0.028907	0.281592 ± 0.000016	-2.5 ± 0.6	2.6
20	2558 ± 9	0.280995	0.001213	0.043356	0.280936 ± 0.000018	-7.6 ± 0.6	3.6
21	1795 ± 11	0.281516	0.000958	0.030763	0.281483 ± 0.000036	-5.6 ± 1.3	2.8
24	1664 ± 71	0.281373	0.000667	0.036607	0.281352 ± 0.000015	-13.3 ± 0.5	3.2
25	1750 ± 17	0.281544	0.000775	0.041961	0.281518 ± 0.000013	-5.4 ± 0.5	2.8
28	1747 ± 25	0.281641	0.000686	0.035779	0.281618 ± 0.000010	-1.9 ± 0.3	2.6
34	1800 ± 15	0.281520	0.000675	0.036481	0.281497 ± 0.000010	-5.0 ± 0.3	2.8
35	2634 ± 9	0.281177	0.000627	0.029724	0.281145 ± 0.000009	1.6 ± 0.3	3.0
38	1794 ± 10	0.281499	0.000776	0.040900	0.281473 ± 0.000012	-6.0 ± 0.4	2.9
44	1757 ± 17	0.281668	0.000684	0.033242	0.281645 ± 0.000012	-0.7 ± 0.4	2.5
46	1990 ± 10	0.281567	0.000850	0.043071	0.281535 ± 0.000017	0.6 ± 0.6	2.6
49	1806 ± 18	0.281659	0.001295	0.071301	0.281615 ± 0.000016	-0.7 ± 0.6	2.5
51	2626 ± 9	0.281101	0.000544	0.029679	0.281074 ± 0.000022	-1.1 ± 0.8	3.2
52	1820 ± 10	0.281578	0.001549	0.090337	0.281525 ± 0.000020	-3.6 ± 0.7	2.7
53	1825 ± 9	0.281436	0.002104	0.108875	0.281363 ± 0.000020	-9.2 ± 0.7	3.1
Depositional Package 3							
Kiangi Creek Formation							
GSWA 156614: quartz sandstone							
3	1848 ± 7	0.281758	0.001411	0.063174	0.281709 ± 0.000019	3.6 ± 0.7	2.3
4	2738 ± 7	0.280958	0.000502	0.022147	0.280932 ± 0.000022	-3.6 ± 0.8	3.4
6	1723 ± 31	0.281586	0.000540	0.020438	0.281568 ± 0.000019	-4.2 ± 0.7	2.7
8	1752 ± 9	0.281624	0.000309	0.011200	0.281614 ± 0.000014	-2.0 ± 0.5	2.6
10	2272 ± 11	0.281202	0.000077	0.004275	0.281199 ± 0.000011	-4.8 ± 0.4	3.2
16	1794 ± 13	0.281457	0.000413	0.018084	0.281443 ± 0.000014	-7.1 ± 0.5	2.9
22	1770 ± 13	0.281558	0.001995	0.095453	0.281491 ± 0.000020	-5.9 ± 0.7	2.8
23	1780 ± 10	0.281571	0.000848	0.038942	0.281542 ± 0.000013	-3.9 ± 0.5	2.7
26	1745 ± 13	0.281627	0.000707	0.033069	0.281604 ± 0.000013	-2.5 ± 0.5	2.6
33	1767 ± 9	0.281652	0.000823	0.025120	0.281624 ± 0.000018	-1.3 ± 0.6	2.5
34	1786 ± 10	0.281585	0.000750	0.026653	0.281560 ± 0.000016	-3.1 ± 0.6	2.7
44	1761 ± 15	0.281723	0.001216	0.050659	0.281682 ± 0.000020	0.7 ± 0.7	2.4
45	1756 ± 9	0.281641	0.001071	0.038906	0.281605 ± 0.000017	-2.2 ± 0.6	2.6
47	1742 ± 15	0.281644	0.000910	0.030756	0.281614 ± 0.000016	-2.2 ± 0.6	2.6
48	2530 ± 13	0.281163	0.000361	0.017076	0.281146 ± 0.000018	-0.8 ± 0.6	3.1
49	1734 ± 12	0.281675	0.000749	0.036875	0.281650 ± 0.000023	-1.1 ± 0.8	2.5
52	1770 ± 14	0.281651	0.000590	0.025774	0.281631 ± 0.000020	-0.9 ± 0.7	2.5
59	2724 ± 8	0.281144	0.000984	0.039117	0.281093 ± 0.000019	1.8 ± 0.7	3.1
61	1787 ± 16	0.281647	0.000502	0.023988	0.281630 ± 0.000015	-0.6 ± 0.5	2.5
62	1773 ± 10	0.281611	0.000969	0.046841	0.281578 ± 0.000017	-2.7 ± 0.6	2.6

Analysis no.	$^{207}Pb/^{206}Pb$ date (Ma)	$^{176}Hf/^{177}Hf$ measured	$^{176}Lu/^{177}Hf$ measured	$^{176}Yb/^{177}Hf$ measured	$^{176}Hf/^{177}Hf$ initial	$\varepsilon Hf_{(i)}$	T_{DM2} (Ga)
GSWA 169061: lithic quartz sanstone							
1	1799 ± 27	0.281584	0.000551	0.023880	0.281565 ± 0.000011	-2.6 ± 0.4	2.7
2	1803 ± 26	0.281557	0.000791	0.027258	0.281530 ± 0.000020	-3.8 ± 0.7	2.7
4	1811 ± 30	0.281507	0.000746	0.033747	0.281481 ± 0.000014	-5.3 ± 0.5	2.8
6	1778 ± 25	0.281529	0.001396	0.042894	0.281482 ± 0.000024	-6.1 ± 0.8	2.9
8	1797 ± 35	0.281513	0.000826	0.026840	0.281485 ± 0.000015	-5.5 ± 0.5	2.8
10	1810 ± 29	0.281520	0.001443	0.044759	0.281470 ± 0.000082	-5.7 ± 2.9	2.9
11	1783 ± 31	0.281515	0.001038	0.038215	0.281480 ± 0.000026	-6.0 ± 0.9	2.9
13	2002 ± 24	0.281594	0.000535	0.021936	0.281574 ± 0.000017	2.3 ± 0.6	2.5
15	1810 ± 19	0.281531	0.000645	0.029890	0.281509 ± 0.000016	-4.4 ± 0.6	2.8
16	1777 ± 27	0.281517	0.000776	0.028711	0.281491 ± 0.000018	-5.8 ± 0.6	2.8
19	1837 ± 20	0.281540	0.000517	0.022808	0.281522 ± 0.000016	-3.3 ± 0.6	2.7
21	1769 ± 76	0.281496	0.000481	0.021026	0.281480 ± 0.000015	-6.3 ± 0.5	2.9
22	1752 ± 30	0.281493	0.000659	0.028528	0.281471 ± 0.000015	-7.0 ± 0.5	2.9
25	1919 ± 40	0.281658	0.000622	0.022316	0.281635 ± 0.000033	2.6 ± 1.2	2.4
26	2289 ± 30	0.281243	0.000570	0.025678	0.281218 ± 0.000016	-3.8 ± 0.6	3.1
28	1762 ± 20	0.281501	0.000980	0.034771	0.281468 ± 0.000020	-6.9 ± 0.7	2.9
29	1812 ± 18	0.281551	0.000773	0.033127	0.281524 ± 0.000010	-3.8 ± 0.4	2.7
30	1836 ± 20	0.281514	0.001346	0.052187	0.281467 ± 0.000023	-5.3 ± 0.8	2.8
31	2033 ± 49	0.281663	0.000480	0.018802	0.281644 ± 0.000014	5.5 ± 0.5	2.3
33	2270 ± 17	0.281241	0.000800	0.030172	0.281206 ± 0.000013	-4.6 ± 0.5	3.1
GSWA 148973: silicified quartz sandstone							
1	1776 ± 6	0.281484	0.001852	0.101593	0.281422 ± 0.000017	-8.2 ± 0.6	3.0
2	1678 ± 11	0.281538	0.000792	0.039550	0.281513 ± 0.000017	-7.2 ± 0.6	2.9
39	2949 ± 10	0.281035	0.001306	0.069664	0.280961 ± 0.000016	2.4 ± 0.6	3.2
19	2719 ± 4	0.280930	0.001759	0.074307	0.280839 ± 0.000032	-7.3 ± 1.1	3.7
21	1875 ± 21	0.281489	0.001956	0.073442	0.281419 ± 0.000029	-6.1 ± 1.0	2.9
24	1787 ± 7	0.281522	0.000846	0.030734	0.281493 ± 0.000016	-5.5 ± 0.6	2.8
27	2518 ± 5	0.281224	0.001063	0.040779	0.281173 ± 0.000016	-0.1 ± 0.6	3.0
32	1796 ± 9	0.281445	0.000874	0.045583	0.281415 ± 0.000015	-8.0 ± 0.5	3.0
34	1782 ± 6	0.281249	0.003253	0.114974	0.281139 ± 0.000016	-18.1 ± 0.6	3.6
44	1783 ± 12	0.281559	0.000847	0.044919	0.281530 ± 0.000014	-4.2 ± 0.5	2.7
45	1811 ± 9	0.281450	0.000986	0.035962	0.281416 ± 0.000014	-7.6 ± 0.5	3.0
47	1701 ± 46	0.281570	0.001774	0.092108	0.281513 ± 0.000019	-6.7 ± 0.7	2.8
50	1809 ± 6	0.281431	0.001307	0.064504	0.281386 ± 0.000012	-8.8 ± 0.4	3.0
64	1690 ± 22	0.281611	0.001888	0.073447	0.281551 ± 0.000012	-5.6 ± 0.4	2.8
77	1980 ± 8	0.281552	0.001228	0.039464	0.281506 ± 0.000019	-0.6 ± 0.7	2.7
78	2288 ± 15	0.281204	0.000736	0.041986	0.281172 ± 0.000013	-5.4 ± 0.5	3.2
80	1759 ± 8	0.281586	0.001835	0.099218	0.281525 ± 0.000011	-5.0 ± 0.4	2.8
85	1789 ± 7	0.281512	0.001344	0.054746	0.281466 ± 0.000018	-6.4 ± 0.6	2.9
90	1774 ± 8	0.281465	0.001733	0.090223	0.281407 ± 0.000010	-8.8 ± 0.4	3.0
92	2657 ± 4	0.280879	0.000679	0.034458	0.280844 ± 0.000011	-8.6 ± 0.4	3.7

Analysis no.	$^{207}Pb/^{206}Pb$ date (Ma)	$^{176}Hf/^{177}Hf$ measured	$^{176}Lu/^{177}Hf$ measured	$^{176}Yb/^{177}Hf$ measured	$^{176}Hf/^{177}Hf$ initial	$\varepsilon Hf_{(i)}$	T_{DM2} (Ga)
Depositional Package 4							
Ullawarra Formation, Curran Member							
GSWA 148974: lithic sandstone							
3	1998 ± 9	0.281640	0.001896	0.091707	0.281568 ± 0.000012	2.0 ± 0.4	2.5
4	2321 ± 6	0.281433	0.000781	0.043066	0.281398 ± 0.000017	3.4 ± 0.6	2.7
9	1798 ± 6	0.281503	0.000947	0.051844	0.281471 ± 0.000015	-6.0 ± 0.5	2.9
11	2447 ± 8	0.281198	0.000816	0.042522	0.281160 ± 0.000014	-2.2 ± 0.5	3.1
12	1789 ± 9	0.281515	0.000457	0.024643	0.281500 ± 0.000013	-5.2 ± 0.5	2.8
19	2460 ± 3	0.281046	0.000739	0.037884	0.281011 ± 0.000013	-7.2 ± 0.5	3.5
20	2713 ± 7	0.281193	0.000599	0.023658	0.281162 ± 0.000009	4.0 ± 0.3	2.9
21	2528 ± 6	0.281065	0.001004	0.050979	0.281017 ± 0.000009	-5.4 ± 0.3	3.4
22.1	1585 ± 57	0.282087	0.001881	0.076064	0.282031 ± 0.000012	9.0 ± 0.4	1.7
22.2	1628 ± 30	0.282021	0.002752	0.078325	0.281936 ± 0.000021	6.7 ± 0.7	1.9
42	1815 ± 13	0.281552	0.000943	0.046591	0.281520 ± 0.000010	-3.9 ± 0.4	2.7
45	2707 ± 6	0.281120	0.000793	0.034749	0.281079 ± 0.000008	0.9 ± 0.3	3.1
55	1792 ± 12	0.281527	0.000569	0.024869	0.281508 ± 0.000012	-4.8 ± 0.4	2.8
58	2565 ± 6	0.281276	0.000850	0.034671	0.281234 ± 0.000017	3.2 ± 0.6	2.9
64	2685 ± 6	0.281185	0.000544	0.021386	0.281157 ± 0.000021	3.2 ± 0.7	3.0
67	2491 ± 7	0.281381	0.001471	0.044381	0.281311 ± 0.000013	4.2 ± 0.5	2.8
77	2521 ± 7	0.281294	0.001331	0.063711	0.281230 ± 0.000012	2.0 ± 0.4	2.9
83	2718 ± 12	0.281107	0.000373	0.015893	0.281088 ± 0.000012	1.5 ± 0.4	3.1
87	1677 ± 9	0.281712	0.001285	0.061108	0.281671 ± 0.000011	-1.6 ± 0.4	2.5
COLLIER GROUP							
Depositional Package 5							
Backdoor Formation							
GSWA 148976: quartz sandstone							
1	2410 ± 5	0.281319	0.001039	0.049014	0.281271 ± 0.000020	0.9 ± 0.7	2.9
5	2726 ± 14	0.281107	0.000444	0.023304	0.281084 ± 0.000016	1.5 ± 0.6	3.1
7	2605 ± 7	0.281289	0.000554	0.029377	0.281261 ± 0.000021	5.1 ± 0.7	2.8
10	2501 ± 8	0.281166	0.001057	0.058250	0.281116 ± 0.000015	-2.5 ± 0.5	3.2
12	2514 ± 6	0.281189	0.001332	0.057180	0.281125 ± 0.000017	-1.9 ± 0.6	3.2
13	1765 ± 10	0.281248	0.000938	0.055464	0.281217 ± 0.000019	-15.8 ± 0.7	3.5
20	1813 ± 9	0.281465	0.000832	0.046138	0.281436 ± 0.000018	-6.9 ± 0.6	2.9
23	2519 ± 13	0.281291	0.001039	0.055108	0.281241 ± 0.000020	2.3 ± 0.7	2.9
25	2651 ± 4	0.281123	0.001493	0.073730	0.281047 ± 0.000013	-1.5 ± 0.5	3.2
26	1787 ± 9	0.281572	0.000733	0.033601	0.281547 ± 0.000017	-3.5 ± 0.6	2.7
27	2504 ± 6	0.281465	0.001478	0.078539	0.281394 ± 0.000017	7.5 ± 0.6	2.6
29	1640 ± 9	0.281584	0.001621	0.084950	0.281534 ± 0.000016	-7.4 ± 0.6	2.8
44	2720 ± 6	0.281085	0.000948	0.038061	0.281036 ± 0.000022	-0.3 ± 0.8	3.2
45	2637 ± 5	0.281183	0.000442	0.019831	0.281161 ± 0.000015	2.2 ± 0.5	3.0
50	2526 ± 4	0.281135	0.000381	0.020660	0.281117 ± 0.000016	-1.9 ± 0.6	3.2
52	2553 ± 6	0.281250	0.000885	0.051519	0.281207 ± 0.000017	1.9 ± 0.6	2.9
53	1802 ± 10	0.281169	0.001213	0.040051	0.281128 ± 0.000029	-18.1 ± 1.0	3.6
57	2454 ± 5	0.281190	0.001424	0.072556	0.281123 ± 0.000024	-3.3 ± 0.8	3.2
58	1694 ± 9	0.281715	0.001327	0.076834	0.281672 ± 0.000021	-1.2 ± 0.7	2.5
60	3280 ± 4	0.280633	0.000809	0.047692	0.280582 ± 0.000015	-3.4 ± 0.5	3.8

Analysis no.	$^{207}Pb/^{206}Pb$ date (Ma)	$^{176}Hf/^{177}Hf$ measured	$^{176}Lu/^{177}Hf$ measured	$^{176}Yb/^{177}Hf$ measured	$^{176}Hf/^{177}Hf$ initial	$\varepsilon Hf_{(i)}$	T_{DM2} (Ga)
GSWA 148977: quartz sandstone							
6	1771 ± 10	0.281610	0.000497	0.022159	0.281593 ± 0.000016	-2.3 ± 0.6	2.6
7	1781 ± 6	0.281599	0.000648	0.025358	0.281577 ± 0.000017	-2.6 ± 0.6	2.6
11	1801 ± 14	0.281535	0.000959	0.045781	0.281502 ± 0.000014	-4.8 ± 0.5	2.8
12	1773 ± 12	0.281541	0.000953	0.044954	0.281509 ± 0.000012	-5.2 ± 0.4	2.8
13	2016 ± 8	0.281600	0.001059	0.052659	0.281559 ± 0.000018	2.1 ± 0.6	2.5
15	1769 ± 17	0.281579	0.001328	0.065450	0.281534 ± 0.000017	-4.4 ± 0.6	2.7
23	2960 ± 12	0.280993	0.001143	0.054154	0.280928 ± 0.000019	1.4 ± 0.7	3.3
25	2253 ± 11	0.281215	0.000380	0.019140	0.281199 ± 0.000020	-5.3 ± 0.7	3.2
39	2290 ± 6	0.281224	0.000710	0.035519	0.281193 ± 0.000014	-4.6 ± 0.5	3.2
42	1840 ± 15	0.281451	0.000885	0.040020	0.281420 ± 0.000019	-6.8 ± 0.7	3.0
43	1821 ± 13	0.281612	0.000436	0.019396	0.281597 ± 0.000022	-1.0 ± 0.8	2.6
45	3517 ± 5	0.280537	0.000820	0.037786	0.280481 ± 0.000013	-1.4 ± 0.5	3.9
50	1956 ± 7	0.281597	0.000466	0.023033	0.281580 ± 0.000014	1.5 ± 0.5	2.5
55	2000 ± 6	0.281575	0.000429	0.019770	0.281559 ± 0.000011	1.7 ± 0.4	2.5
58	1800 ± 9	0.281564	0.000519	0.025622	0.281546 ± 0.000020	-3.3 ± 0.7	2.7
61	1790 ± 9	0.281568	0.001087	0.054708	0.281531 ± 0.000019	-4.0 ± 0.7	2.7
62	3509 ± 5	0.280527	0.000509	0.024096	0.280493 ± 0.000016	-1.2 ± 0.6	3.9
63	2460 ± 6	0.281198	0.001132	0.041748	0.281145 ± 0.000018	-2.4 ± 0.6	3.2
70	2454 ± 5	0.281156	0.001305	0.072867	0.281095 ± 0.000024	-4.4 ± 0.8	3.3
71	2825 ± 4	0.280945	0.001628	0.086013	0.280857 ± 0.000020	-4.2 ± 0.7	3.5
74	1785 ± 10	0.281608	0.000419	0.020644	0.281594 ± 0.000015	-1.9 ± 0.5	2.6
GSWA 156541: quartz sandstone							
3	1788 ± 14	0.281401	0.000638	0.022553	0.281379 ± 0.000015	-9.5 ± 0.5	3.1
5	1621 ± 10	0.281430	0.001377	0.049129	0.281388 ± 0.000021	-13.0 ± 0.7	3.2
13	1603 ± 23	0.281959	0.003458	0.101471	0.281854 ± 0.000033	3.2 ± 1.2	2.1
14	1662 ± 12	0.281646	0.001468	0.047388	0.281600 ± 0.000020	-4.5 ± 0.7	2.7
25	3149 ± 9	0.280788	0.001095	0.045828	0.280722 ± 0.000019	-1.5 ± 0.7	3.6
30	2710 ± 8	0.281078	0.001611	0.058372	0.280994 ± 0.000020	-2.0 ± 0.7	3.3
43	2713 ± 8	0.281143	0.001847	0.068532	0.281047 ± 0.000027	-0.1 ± 0.9	3.2
47	2977 ± 9	0.280942	0.001248	0.039680	0.280871 ± 0.000026	-0.2 ± 0.9	3.4
51	2815 ± 7	0.281115	0.000651	0.026619	0.281080 ± 0.000027	3.5 ± 0.9	3.0
52	2501 ± 10	0.281396	0.000349	0.015033	0.281379 ± 0.000028	6.8 ± 1.0	2.6
58	2530 ± 8	0.281199	0.001402	0.051832	0.281131 ± 0.000032	-1.3 ± 1.1	3.1
59	2727 ± 9	0.281096	0.000543	0.016771	0.281068 ± 0.000029	1.0 ± 1.0	3.1
62	2812 ± 9	0.281063	0.001307	0.050883	0.280993 ± 0.000040	0.3 ± 1.4	3.2
80	3315 ± 8	0.280901	0.002383	0.087288	0.280749 ± 0.000039	3.4 ± 1.4	3.4
81	2490 ± 11	0.281355	0.001110	0.039822	0.281302 ± 0.000035	3.9 ± 1.2	2.8
90	2570 ± 5	0.281265	0.000854	0.027617	0.281223 ± 0.000032	2.9 ± 1.1	2.9
99	2446 ± 7	0.281167	0.000925	0.043158	0.281124 ± 0.000042	-3.5 ± 1.5	3.2
101	2698 ± 12	0.280755	0.001225	0.038886	0.280692 ± 0.000040	-13.1 ± 1.4	4.0
102	2610 ± 7	0.281163	0.001730	0.064547	0.281077 ± 0.000037	-1.4 ± 1.3	3.2
106	2933 ± 9	0.280760	0.000776	0.027534	0.280716 ± 0.000036	-6.7 ± 1.3	3.8

Appendix 5

Detrital zircon analyses, potential source regions

Analysis no.	$^{207}Pb/^{206}Pb$ date (Ma)	$^{176}Hf/^{177}Hf$ measured	$^{176}Lu/^{177}Hf$ measured	$^{176}Yb/^{177}Hf$ measured	$^{176}Hf/^{177}Hf$ initial	$\varepsilon Hf_{(i)}$	T_{DM2} (Ga)
GASCOYNE PROVINCE							
2555–2430 Ma Halfway Gneiss							
GSWA 164309: foliated porphyritic biotite granodiorite							
1.1	2560 ± 3	0.281246	0.002086	0.058487	0.281144 ± 0.000026	-0.2 ± 0.9	3.1
2.1	2563 ± 5	0.281243	0.001233	0.033703	0.281183 ± 0.000034	1.3 ± 1.2	3.0
3.1	2534 ± 5	0.281185	0.001103	0.037499	0.281132 ± 0.000028	-1.2 ± 1.0	3.1
5.1	2553 ± 9	0.281180	0.000687	0.023413	0.281146 ± 0.000013	-0.2 ± 0.5	3.1
6.1	2553 ± 6	0.281179	0.000867	0.031802	0.281137 ± 0.000022	-0.6 ± 0.8	3.1
13.1	2566 ± 10	0.281194	0.001107	0.039080	0.281140 ± 0.000019	-0.2 ± 0.7	3.1
15.1	2517 ± 8	0.281197	0.000704	0.024175	0.281163 ± 0.000016	-0.5 ± 0.6	3.1
17.1	2537 ± 4	0.281186	0.000628	0.021058	0.281156 ± 0.000013	-0.3 ± 0.5	3.1
19.1	2605 ± 10	0.281236	0.000622	0.019315	0.281205 ± 0.000016	3.1 ± 0.6	2.9
21.1	2562 ± 9	0.281134	0.000862	0.027096	0.281092 ± 0.000018	-2.0 ± 0.6	3.2
24.1	2546 ± 7	0.281220	0.000896	0.028355	0.281176 ± 0.000012	0.7 ± 0.4	3.0
25.1	2673 ± 6	0.281027	0.000232	0.007264	0.281015 ± 0.000022	-2.1 ± 0.8	3.3
26.1	2576 ± 8	0.281088	0.000766	0.024275	0.281050 ± 0.000015	-3.1 ± 0.5	3.3
28.1	2546 ± 6	0.281205	0.001333	0.038111	0.281140 ± 0.000017	-0.6 ± 0.6	3.1
29.1	2539 ± 10	0.281248	0.000662	0.019819	0.281216 ± 0.000018	1.9 ± 0.6	2.9
GSWA 168950: pegmatite-banded tonalite gneiss							
1.1	2506 ± 2	0.281121	0.000625	0.032041	0.281091 ± 0.000006	-3.3 ± 0.2	3.2
2.1	2471 ± 2	0.281100	0.001780	0.088567	0.281016 ± 0.000008	-6.8 ± 0.3	3.4
3.1	2518 ± 1	0.281152	0.000601	0.036244	0.281123 ± 0.000009	-1.9 ± 0.3	3.2
5.1	2456 ± 6	0.281127	0.000227	0.013264	0.281116 ± 0.000012	-3.5 ± 0.4	3.2
6.1	2635 ± 7	0.281092	0.000702	0.036276	0.281057 ± 0.000011	-1.5 ± 0.4	3.2
8.1	2519 ± 4	0.281105	0.000479	0.020540	0.281082 ± 0.000007	-3.3 ± 0.3	3.3
9.1	2507 ± 3	0.281117	0.000690	0.041587	0.281084 ± 0.000013	-3.5 ± 0.5	3.3
10.1	2564 ± 12	0.281152	0.000447	0.025597	0.281130 ± 0.000447	-0.6 ± 0.3	3.1
11.1	2478 ± 2	0.281187	0.000560	0.032601	0.281161 ± 0.000011	-1.5 ± 0.4	3.1
12.1	2449 ± 4	0.281109	0.000303	0.018000	0.281095 ± 0.000012	-4.5 ± 0.4	3.3
13.1	2701 ± 4	0.281010	0.001260	0.067265	0.280945 ± 0.000014	-4.0 ± 0.5	3.4
14.1	2730 ± 6	0.281073	0.001540	0.081686	0.280993 ± 0.000012	-1.6 ± 0.4	3.3
15.1	2619 ± 9	0.281154	0.000823	0.040745	0.281113 ± 0.000013	0.1 ± 0.5	3.1
15.2	2534 ± 2	0.281190	0.000565	0.031019	0.281163 ± 0.000013	-0.1 ± 0.5	3.1
16.1	2519 ± 3	0.281132	0.000842	0.043136	0.281092 ± 0.000842	-3.0 ± 0.4	3.2
17.1	2466 ± 11	0.281194	0.000075	0.004954	0.281190 ± 0.000012	-0.7 ± 0.4	3.0
20.2	2506 ± 8	0.281160	0.000197	0.010743	0.281151 ± 0.000012	-1.2 ± 0.4	3.1
21.1	2472 ± 2	0.281134	0.000708	0.042113	0.281101 ± 0.000708	-3.7 ± 0.3	3.2
22.1	2507 ± 2	0.281119	0.000565	0.033149	0.281092 ± 0.000009	-3.2 ± 0.3	3.2
23.1	2515 ± 5	0.281126	0.000189	0.010377	0.281117 ± 0.000011	-2.2 ± 0.4	3.2
GSWA 142988: biotite tonalite							
1.1	2806 ± 9	0.280852	0.001060	0.047229	0.280795 ± 0.000015	-6.9 ± 0.5	3.7
3.1	2558 ± 6	0.281176	0.001172	0.045702	0.281119 ± 0.000014	-1.1 ± 0.5	3.1
5.1	2701 ± 8	0.281122	0.001286	0.056760	0.281056 ± 0.000011	0.0 ± 0.4	3.2
6.1	3253 ± 5	0.280774	0.000902	0.037836	0.280718 ± 0.000013	0.8 ± 0.5	3.6

Analysis no.	$^{207}Pb/^{206}Pb$ date (Ma)	$^{176}Hf/^{177}Hf$ measured	$^{176}Lu/^{177}Hf$ measured	$^{176}Yb/^{177}Hf$ measured	$^{176}Hf/^{177}Hf$ initial	$\varepsilon Hf_{(i)}$	T_{DM2} (Ga)
7.1	2666 ± 11	0.281206	0.000618	0.022574	0.281174 ± 0.000010	3.4 ± 0.4	2.9
8.1	2667 ± 5	0.281101	0.001318	0.056934	0.281034 ± 0.000014	-1.6 ± 0.5	3.3
9.1	2704 ± 5	0.281142	0.001009	0.042690	0.281090 ± 0.000010	1.2 ± 0.4	3.1
15.1	2655 ± 5	0.281108	0.000716	0.030861	0.281072 ± 0.000008	-0.5 ± 0.3	3.2
16.1	2711 ± 4	0.281081	0.001551	0.065746	0.281001 ± 0.000011	-1.8 ± 0.4	3.3
17.1	2801 ± 5	0.280827	0.000729	0.030728	0.280788 ± 0.000009	-7.2 ± 0.3	3.7
20.1	3040 ± 5	0.280808	0.000899	0.036580	0.280756 ± 0.000009	-2.8 ± 0.3	3.6
21.1	2689 ± 6	0.281033	0.000743	0.031856	0.280995 ± 0.000010	-2.5 ± 0.4	3.3
23.1	2683 ± 5	0.280999	0.000734	0.031839	0.280961 ± 0.000007	-3.8 ± 0.2	3.4
24.1	3274 ± 4	0.280701	0.000915	0.036772	0.280643 ± 0.000007	-1.4 ± 0.2	3.7
26.1	2667 ± 5	0.281068	0.001270	0.060972	0.281003 ± 0.000013	-2.7 ± 0.5	3.3
28.1	2716 ± 6	0.280964	0.000795	0.037581	0.280923 ± 0.000011	-4.4 ± 0.4	3.5
GSWA 188973: metagranodiorite							
2.1	2419 ± 6	0.281214	0.000976	0.047891	0.281169 ± 0.000013	-2.5 ± 0.5	3.1
7.1	2457 ± 8	0.281196	0.001177	0.043967	0.281141 ± 0.000012	-2.6 ± 0.4	3.2
8.1	2669 ± 5	0.281082	0.001117	0.050152	0.281025 ± 0.000016	-1.9 ± 0.6	3.3
10.1	2421 ± 6	0.281234	0.000633	0.029098	0.281205 ± 0.000011	-1.2 ± 0.4	3.0
11.1	2387 ± 43	0.281240	0.000782	0.035950	0.281204 ± 0.000782	-2.0 ± 0.5	3.1
12.1	2466 ± 11	0.281167	0.000926	0.041717	0.281123 ± 0.000015	-3.1 ± 0.5	3.2
13.1	2432 ± 6	0.281229	0.000843	0.036155	0.281190 ± 0.000010	-1.5 ± 0.4	3.1
14.1	2401 ± 6	0.281241	0.001417	0.060308	0.281176 ± 0.000011	-2.7 ± 0.4	3.1
15.1	2541 ± 4	0.281082	0.000846	0.033418	0.281041 ± 0.000009	-4.3 ± 0.3	3.3
16.1	2445 ± 6	0.281229	0.001115	0.048109	0.281177 ± 0.000007	-1.6 ± 0.2	3.1
17.1	2501 ± 10	0.281336	0.000898	0.035960	0.281293 ± 0.000007	3.8 ± 0.3	2.8
22.1	2429 ± 7	0.281202	0.000630	0.028830	0.281173 ± 0.000011	-2.1 ± 0.4	3.1
24.1	2428 ± 5	0.281205	0.001207	0.054466	0.281149 ± 0.000013	-3.0 ± 0.5	3.2
2005–1975 Ma Dalgaringa Supersuite							
GSWA 142925: biotite monzogranite							
2.1	2000 ± 8	0.281467	0.001199	0.049017	0.281421 ± 0.000020	-3.2 ± 0.7	2.8
3.1	1981 ± 12	0.281415	0.000694	0.031617	0.281389 ± 0.000021	-4.7 ± 0.7	2.9
4.1	2002 ± 8	0.281418	0.000800	0.036650	0.281388 ± 0.000018	-4.3 ± 0.6	2.9
5.1	1993 ± 10	0.281486	0.000610	0.022389	0.281463 ± 0.000020	-1.8 ± 0.7	2.8
6.1	1995 ± 8	0.281474	0.000680	0.031599	0.281448 ± 0.000018	-2.3 ± 0.6	2.8
7.1	1990 ± 8	0.281451	0.001126	0.037746	0.281408 ± 0.000015	-3.8 ± 0.5	2.9
13.1	2011 ± 10	0.281459	0.000515	0.024000	0.281439 ± 0.000024	-2.3 ± 0.8	2.8
14.1	2001 ± 7	0.281452	0.000711	0.033514	0.281425 ± 0.000017	-3.0 ± 0.6	2.8
15.1	2024 ± 13	0.281436	0.000555	0.025213	0.281415 ± 0.000021	-2.8 ± 0.7	2.8
16.1	1998 ± 13	0.281354	0.000360	0.015640	0.281340 ± 0.000015	-6.1 ± 0.5	3.0
17.1	2008 ± 9	0.281426	0.000658	0.029441	0.281401 ± 0.000015	-3.7 ± 0.5	2.9
18.1	2006 ± 8	0.281440	0.000645	0.029568	0.281415 ± 0.000023	-3.2 ± 0.8	2.9
19.1	2012 ± 8	0.281422	0.000575	0.026089	0.281400 ± 0.000017	-3.6 ± 0.6	2.9
20.1	2004 ± 7	0.281441	0.000702	0.031566	0.281414 ± 0.000016	-3.3 ± 0.6	2.9
21.1	2008 ± 10	0.281470	0.000453	0.019845	0.281453 ± 0.000016	-1.9 ± 0.6	2.8
22.1	2001 ± 8	0.281437	0.000644	0.025985	0.281413 ± 0.000019	-3.4 ± 0.7	2.9

Analysis no.	$^{207}Pb/^{206}Pb$ date (Ma)	$^{176}Hf/^{177}Hf$ measured	$^{176}Lu/^{177}Hf$ measured	$^{176}Yb/^{177}Hf$ measured	$^{176}Hf/^{177}Hf$ initial	$\varepsilon Hf_{(i)}$	T_{DM2} (Ga)
GSWA 142926: foliated biotite tonalite							
1.1	2009 ± 3	0.281512	0.000833	0.025598	0.281480 ± 0.000037	-0.9 ± 1.3	2.7
2.1	2006 ± 3	0.281476	0.000644	0.023064	0.281451 ± 0.000022	-2.0 ± 0.8	2.8
3.1	1979 ± 4	0.281428	0.000985	0.035840	0.281391 ± 0.000014	-4.7 ± 0.5	2.9
4.1	2010 ± 11	0.281396	0.000639	0.027461	0.281372 ± 0.000019	-4.7 ± 0.7	2.9
5.1	1999 ± 3	0.281431	0.001248	0.040596	0.281384 ± 0.000022	-4.5 ± 0.8	2.9
7.1	2007 ± 4	0.281470	0.000787	0.033070	0.281440 ± 0.000022	-2.3 ± 0.8	2.8
8.1	1990 ± 3	0.281411	0.000756	0.029728	0.281382 ± 0.000018	-4.8 ± 0.6	2.9
10.1	2002 ± 2	0.281453	0.001004	0.036004	0.281415 ± 0.000014	-3.3 ± 0.5	2.9
11.1	2001 ± 3	0.281453	0.001028	0.035521	0.281414 ± 0.000013	-3.4 ± 0.5	2.9
12.1	2039 ± 3	0.281396	0.000876	0.034916	0.281362 ± 0.000015	-4.4 ± 0.5	2.9
13.1	2000 ± 5	0.281471	0.001259	0.053768	0.281423 ± 0.000018	-3.1 ± 0.6	2.8
14.1	1992 ± 4	0.281372	0.000847	0.032607	0.281340 ± 0.000016	-6.2 ± 0.6	3.0
15.1	2005 ± 7	0.281545	0.001187	0.052465	0.281500 ± 0.000021	-0.3 ± 0.7	2.7
19.1	2002 ± 3	0.281457	0.000870	0.033766	0.281424 ± 0.000022	-3.0 ± 0.8	2.8
20.1	2006 ± 3	0.281376	0.000889	0.035588	0.281342 ± 0.000013	-5.8 ± 0.5	3.0
GSWA 142933: biotite-hypersthene-clinopyroxene mafic granulite							
1.1	1981 ± 8	0.281797	0.001674	0.062209	0.281734 ± 0.000048	7.5 ± 1.7	2.1
2.1	1986 ± 9	0.281517	0.000422	0.012576	0.281501 ± 0.000021	-0.6 ± 0.7	2.7
3.1	1997 ± 6	0.281519	0.001079	0.043744	0.281478 ± 0.000021	-1.2 ± 0.7	2.7
4.1	2004 ± 4	0.281455	0.000865	0.031283	0.281422 ± 0.000016	-3.0 ± 0.6	2.8
5.1	1977 ± 5	0.281514	0.001135	0.042475	0.281471 ± 0.000017	-1.9 ± 0.6	2.7
6.1	1972 ± 12	0.281523	0.000700	0.024642	0.281497 ± 0.000019	-1.1 ± 0.7	2.7
7.1	1975 ± 16	0.281528	0.000347	0.012779	0.281515 ± 0.000020	-0.4 ± 0.7	2.6
8.1	1975 ± 19	0.281583	0.000422	0.012241	0.281567 ± 0.000035	1.5 ± 1.2	2.5
9.1	2002 ± 6	0.281528	0.001047	0.035807	0.281488 ± 0.000022	-0.7 ± 0.8	2.7
10.1	1985 ± 9	0.281494	0.000787	0.029854	0.281464 ± 0.000024	-2.0 ± 0.8	2.8
13.1	1986 ± 9	0.281602	0.001756	0.074352	0.281536 ± 0.000013	0.6 ± 0.5	2.6
14.1	1981 ± 4	0.281519	0.000365	0.011449	0.281505 ± 0.000021	-0.6 ± 0.7	2.7
17.1	1986 ± 7	0.281508	0.000870	0.033555	0.281475 ± 0.000012	-1.6 ± 0.4	2.7
22.1	1985 ± 7	0.281568	0.001336	0.051700	0.281518 ± 0.000020	-0.1 ± 0.7	2.6
23.1	1989 ± 6	0.281452	0.000611	0.025529	0.281429 ± 0.000023	-3.1 ± 0.8	2.8
GSWA 168952: biotite-hornblende tonalite							
1.1	2000 ± 10	0.281411	0.001138	0.055926	0.281368 ± 0.000013	-5.1 ± 0.5	3.0
2.1	1995 ± 10	0.281365	0.000802	0.030620	0.281335 ± 0.000011	-6.4 ± 0.4	3.0
4.1	2014 ± 8	0.281387	0.001330	0.055124	0.281336 ± 0.000016	-5.9 ± 0.6	3.0
5.1	2003 ± 9	0.281372	0.000687	0.035743	0.281346 ± 0.000012	-5.8 ± 0.4	3.0
7.1	1982 ± 12	0.281401	0.000677	0.032098	0.281375 ± 0.000010	-5.2 ± 0.4	3.0
8.1	2012 ± 10	0.281394	0.000911	0.039635	0.281359 ± 0.000015	-5.1 ± 0.5	3.0
10.1	1997 ± 11	0.281384	0.000927	0.041949	0.281349 ± 0.000010	-5.8 ± 0.4	3.0
11.1	2023 ± 9	0.281368	0.000854	0.037465	0.281335 ± 0.000010	-5.7 ± 0.3	3.0
13.1	2005 ± 8	0.281374	0.001049	0.047583	0.281334 ± 0.000011	-6.1 ± 0.4	3.0
14.1	1986 ± 8	0.281319	0.000440	0.019629	0.281302 ± 0.000010	-7.7 ± 0.3	3.1
16.1	1986 ± 8	0.281340	0.000890	0.039526	0.281306 ± 0.000011	-7.6 ± 0.4	3.1
17.1	2002 ± 8	0.281256	0.000722	0.032056	0.281229 ± 0.000009	-10.0 ± 0.3	3.3
19.1	2013 ± 8	0.281274	0.000599	0.025807	0.281251 ± 0.000010	-8.9 ± 0.3	3.2
20.1	2008 ± 6	0.281255	0.000925	0.043668	0.281220 ± 0.000012	-10.1 ± 0.4	3.3
21.1	2016 ± 11	0.281202	0.000566	0.025563	0.281180 ± 0.000015	-11.4 ± 0.5	3.4

Analysis no.	$^{207}Pb/^{206}Pb$ date (Ma)	$^{176}Hf/^{177}Hf$ measured	$^{176}Lu/^{177}Hf$ measured	$^{176}Yb/^{177}Hf$ measured	$^{176}Hf/^{177}Hf$ initial	$\varepsilon Hf_{(i)}$	T_{DM2} (Ga)
GSWA 142928: Nardoo Granite, biotite tonalite							
1.1	1975 ± 9	0.281444	0.000850	0.036242	0.281412 ± 0.000025	-4.1 ± 0.9	2.9
2.1	1977 ± 14	0.281440	0.000714	0.030371	0.281413 ± 0.000017	-4.0 ± 0.6	2.9
3.1	1955 ± 27	0.281474	0.000853	0.029275	0.281442 ± 0.000017	-3.4 ± 0.6	2.8
4.1	1968 ± 8	0.281481	0.000637	0.018172	0.281457 ± 0.000031	-2.6 ± 1.1	2.8
5.1	1962 ± 12	0.281422	0.000873	0.031028	0.281389 ± 0.000023	-5.2 ± 0.8	2.9
6.1	1956 ± 11	0.281378	0.000713	0.027123	0.281352 ± 0.000022	-6.6 ± 0.8	3.0
9.1	1979 ± 11	0.281428	0.001086	0.042271	0.281387 ± 0.000016	-4.9 ± 0.6	2.9
13.1	1959 ± 7	0.281491	0.001011	0.033066	0.281453 ± 0.000016	-3.0 ± 0.6	2.8
14.1	1968 ± 8	0.281440	0.000992	0.040495	0.281403 ± 0.000022	-4.5 ± 0.8	2.9
16.1	1976 ± 5	0.281449	0.000766	0.028071	0.281420 ± 0.000016	-3.7 ± 0.6	2.9
17.1	1967 ± 13	0.281470	0.000982	0.036103	0.281433 ± 0.000015	-3.5 ± 0.5	2.8
18.1	1984 ± 17	0.281556	0.000810	0.028790	0.281525 ± 0.000015	0.2 ± 0.5	2.6
20.1	1982 ± 20	0.281416	0.000444	0.015876	0.281399 ± 0.000016	-4.4 ± 0.6	2.9
21.1	1972 ± 11	0.281484	0.001346	0.048587	0.281434 ± 0.000022	-3.4 ± 0.8	2.8
22.1	1981 ± 10	0.281455	0.000263	0.010104	0.281445 ± 0.000013	-2.7 ± 0.5	2.8
GSWA 142932: Nardoo Granite, porphyritic granodiorite							
1.1	1978 ± 9	0.281403	0.000734	0.023684	0.281375 ± 0.000021	-5.3 ± 0.7	3.0
2.1	1972 ± 6	0.281351	0.000603	0.018878	0.281328 ± 0.000028	-7.1 ± 1.0	3.1
3.1	1999 ± 9	0.281351	0.000783	0.024848	0.281321 ± 0.000026	-6.7 ± 0.9	3.1
4.1	2024 ± 16	0.281452	0.000753	0.023779	0.281423 ± 0.000020	-2.6 ± 0.7	2.8
5.1	1965 ± 8	0.281421	0.000974	0.030150	0.281385 ± 0.000025	-5.3 ± 0.9	2.9
6.1	1975 ± 7	0.281284	0.000495	0.017553	0.281265 ± 0.000031	-9.3 ± 1.1	3.2
7.1	1991 ± 7	0.281414	0.000615	0.023221	0.281391 ± 0.000020	-4.5 ± 0.7	2.9
8.1	1966 ± 9	0.281510	0.001061	0.039033	0.281470 ± 0.000023	-2.2 ± 0.8	2.8
11.1	1979 ± 19	0.281500	0.001728	0.065560	0.281435 ± 0.000032	-3.2 ± 1.1	2.8
12.1	1974 ± 9	0.281460	0.000715	0.023423	0.281433 ± 0.000022	-3.3 ± 0.8	2.8
13.1	1973 ± 7	0.281472	0.000808	0.029155	0.281442 ± 0.000013	-3.1 ± 0.5	2.8
16.1	2026 ± 16	0.281390	0.000481	0.014119	0.281371 ± 0.000021	-4.3 ± 0.7	2.9
17.1	1985 ± 7	0.281488	0.000794	0.024936	0.281458 ± 0.000023	-2.2 ± 0.8	2.8
22.1	1977 ± 8	0.281474	0.000864	0.029107	0.281442 ± 0.000017	-3.0 ± 0.6	2.8
23.1	1978 ± 7	0.281437	0.001222	0.039320	0.281391 ± 0.000019	-4.7 ± 0.7	2.9
1820–1775 Ma Moorarie Supersuite							
GSWA 142849: foliated coarse-grained monzogranite							
4.1	1829 ± 16	0.281554	0.001885	0.087914	0.281489 ± 0.000023	-4.7 ± 0.8	2.8
5.1	1835 ± 12	0.281520	0.000619	0.025722	0.281498 ± 0.000016	-4.2 ± 0.6	2.8
18.1	1797 ± 11	0.281388	0.000476	0.019413	0.281372 ± 0.000012	-9.5 ± 0.4	3.1
22.1	1783 ± 17	0.281455	0.000613	0.026226	0.281434 ± 0.000018	-7.6 ± 0.6	3.0
25.1	1823 ± 17	0.281398	0.000778	0.020889	0.281371 ± 0.000013	-9.0 ± 0.5	3.1
GSWA 159996: Scrubber Granite, biotite monzogranite							
1.1	1811 ± 14	0.281458	0.000401	0.014407	0.281444 ± 0.000027	-6.7 ± 0.9	2.9
5.1	1749 ± 27	0.281606	0.000733	0.025950	0.281582 ± 0.000020	-3.2 ± 0.7	2.6
8.1	1805 ± 13	0.281462	0.000576	0.020170	0.281442 ± 0.000015	-6.9 ± 0.5	2.9
9.1	1798 ± 9	0.281467	0.000519	0.017984	0.281449 ± 0.000018	-6.8 ± 0.6	2.9
10.1	2127 ± 18	0.281279	0.000755	0.027891	0.281248 ± 0.000012	-6.4 ± 0.4	3.1
13.1	2282 ± 8	0.281360	0.000972	0.036369	0.281318 ± 0.000010	-0.4 ± 0.3	2.9
19.1	2263 ± 8	0.281325	0.000706	0.023638	0.281295 ± 0.000016	-1.6 ± 0.6	2.9

Analysis no.	$^{207}Pb/^{206}Pb$ date (Ma)	$^{176}Hf/^{177}Hf$ measured	$^{176}Lu/^{177}Hf$ measured	$^{176}Yb/^{177}Hf$ measured	$^{176}Hf/^{177}Hf$ initial	$\varepsilon Hf_{(i)}$	T_{DM2} (Ga)
20.1	2297 ± 8	0.281343	0.000668	0.021058	0.281314 ± 0.000016	-0.2 ± 0.6	2.9
21.1	1792 ± 8	0.281514	0.000586	0.020616	0.281494 ± 0.000014	-5.3 ± 0.5	2.8
22.1	1805 ± 10	0.281604	0.000743	0.024528	0.281579 ± 0.000015	-2.0 ± 0.5	2.6
25.1	1788 ± 8	0.281510	0.000731	0.024090	0.281485 ± 0.000023	-5.7 ± 0.8	2.8
26.1	1791 ± 13	0.281578	0.001110	0.036746	0.281540 ± 0.000036	-3.7 ± 1.3	2.7
GSWA 159987: Dumbie Granodiorite, foliated porphyritic biotite granodiorite							
1.1	1816 ± 18	0.281554	0.000264	0.011033	0.281545 ± 0.000023	-3.0 ± 0.8	2.7
4.1	2107 ± 16	0.281397	0.000445	0.021538	0.281379 ± 0.000012	-2.2 ± 0.4	2.9
5.1	2125 ± 10	0.281381	0.000577	0.026301	0.281358 ± 0.000012	-2.6 ± 0.4	2.9
6.1	2390 ± 27	0.281279	0.000646	0.026304	0.281250 ± 0.000012	-0.3 ± 0.4	3.0
8.1	2120 ± 12	0.281391	0.000943	0.035174	0.281353 ± 0.000016	-2.8 ± 0.6	2.9
9.1	1793 ± 19	0.281404	0.000431	0.019959	0.281389 ± 0.000012	-9.0 ± 0.4	3.1
10.1	2105 ± 10	0.281387	0.001018	0.038127	0.281346 ± 0.000011	-3.4 ± 0.4	2.9
12.1	2419 ± 9	0.281196	0.000978	0.047829	0.281151 ± 0.000014	-3.2 ± 0.5	3.2
13.1	1812 ± 7	0.281389	0.000313	0.014486	0.281378 ± 0.000015	-9.0 ± 0.5	3.1
14.1	1813 ± 6	0.281352	0.000555	0.025523	0.281333 ± 0.000011	-10.6 ± 0.4	3.2
15.1	2112 ± 10	0.281335	0.001465	0.071180	0.281276 ± 0.000012	-5.8 ± 0.4	3.1
16.1	1806 ± 9	0.281434	0.000290	0.012142	0.281424 ± 0.000012	-7.5 ± 0.4	3.0
17.1	2100 ± 8	0.281372	0.000775	0.034389	0.281341 ± 0.000010	-3.7 ± 0.3	3.0
18.1	2427 ± 7	0.281252	0.000653	0.030317	0.281222 ± 0.000013	-0.5 ± 0.5	3.0
19.1	2442 ± 8	0.281232	0.000546	0.023337	0.281207 ± 0.000013	-0.7 ± 0.5	3.0
22.1	2308 ± 6	0.281286	0.000636	0.033596	0.281258 ± 0.000009	-1.9 ± 0.3	3.0
23.1	2304 ± 5	0.281242	0.000166	0.007681	0.281235 ± 0.000013	-2.8 ± 0.5	3.1
26.1	2435 ± 6	0.281247	0.000291	0.011957	0.281233 ± 0.000008	0.1 ± 0.3	3.0
27.1	2424 ± 9	0.281226	0.001012	0.046061	0.281179 ± 0.000012	-2.0 ± 0.4	3.1
GSWA 188975: Dumbie Granodiorite, metatonalite							
1.1	1803 ± 6	0.281361	0.001092	0.032081	0.281324 ± 0.000012	-11.1 ± 0.4	3.2
2.1	1792 ± 6	0.281500	0.000876	0.039489	0.281470 ± 0.000013	-6.2 ± 0.5	2.9
3.1	1789 ± 8	0.281375	0.000340	0.014568	0.281363 ± 0.000008	-10.0 ± 0.3	3.1
4.1	1798 ± 8	0.281335	0.001453	0.072369	0.281285 ± 0.000013	-12.6 ± 0.5	3.3
5.1	2307 ± 5	0.281197	0.000441	0.016556	0.281178 ± 0.000011	-4.8 ± 0.4	3.2
6.1	2113 ± 9	0.281286	0.000718	0.029987	0.281257 ± 0.000009	-6.4 ± 0.3	3.1
7.1	1791 ± 9	0.281335	0.000014	0.000694	0.281335 ± 0.000007	-11.0 ± 0.2	3.2
8.1	2202 ± 119	0.281243	0.000276	0.009638	0.281231 ± 0.000007	-5.3 ± 0.2	3.1
10.1	1800 ± 8	0.281327	0.000341	0.014597	0.281315 ± 0.000008	-11.5 ± 0.3	3.2
11.1	1807 ± 6	0.281321	0.000672	0.023893	0.281298 ± 0.000009	-11.9 ± 0.3	3.2
12.1	2288 ± 8	0.281250	0.000427	0.017717	0.281231 ± 0.000012	-3.3 ± 0.4	3.1
14.1	2326 ± 6	0.281243	0.000135	0.005472	0.281237 ± 0.000010	-2.2 ± 0.4	3.0
15.2	2304 ± 41	0.281235	0.000565	0.021789	0.281210 ± 0.000005	-3.7 ± 0.2	3.1
16.1	1813 ± 8	0.281342	0.000999	0.038351	0.281308 ± 0.000007	-11.5 ± 0.2	3.2
18.1	1914 ± 6	0.281390	0.000537	0.014758	0.281370 ± 0.000009	-6.9 ± 0.3	3.0
19.1	1812 ± 7	0.281393	0.000876	0.030319	0.281363 ± 0.000010	-9.5 ± 0.3	3.1
20.1	2200 ± 10	0.281218	0.000276	0.011130	0.281206 ± 0.000008	-6.2 ± 0.3	3.2
21.1	1803 ± 6	0.281332	0.000954	0.037148	0.281299 ± 0.000010	-12.0 ± 0.4	3.2
22.1	1812 ± 9	0.281396	0.000298	0.012007	0.281386 ± 0.000006	-8.7 ± 0.2	3.0
23.1	2122 ± 8	0.281324	0.000494	0.018354	0.281304 ± 0.000010	-4.5 ± 0.3	3.0

Analysis no.	$^{207}Pb/^{206}Pb$ date (Ma)	$^{176}Hf/^{177}Hf$ measured	$^{176}Lu/^{177}Hf$ measured	$^{176}Yb/^{177}Hf$ measured	$^{176}Hf/^{177}Hf$ initial	$\varepsilon Hf_{(i)}$	T_{DM2} (Ga)
GSWA 88412: foliated porphyritic monzogranite							
4.1	1792 ± 12	0.281669	0.001359	0.057430	0.281623 ± 0.000016	-0.7 ± 0.6	2.5
5.1	1781 ± 12	0.281627	0.001221	0.056695	0.281586 ± 0.000013	-2.3 ± 0.5	2.6
7.1	1787 ± 12	0.281644	0.001325	0.058780	0.281599 ± 0.000018	-1.7 ± 0.6	2.6
9.1	1806 ± 10	0.281656	0.001392	0.057692	0.281608 ± 0.000018	-0.9 ± 0.6	2.6
10.1	1781 ± 17	0.281614	0.000831	0.035342	0.281586 ± 0.000015	-2.3 ± 0.5	2.6
19.1	1786 ± 13	0.281601	0.001286	0.057640	0.281557 ± 0.000015	-3.2 ± 0.5	2.7
22.1	1799 ± 10	0.281668	0.001218	0.056469	0.281626 ± 0.000011	-0.5 ± 0.4	2.5
23.1	1794 ± 10	0.281597	0.000702	0.031921	0.281573 ± 0.000014	-2.5 ± 0.5	2.6
GSWA 88405: biotite granodiorite							
3.1	1803 ± 17	0.281642	0.000779	0.034881	0.281615 ± 0.000019	-0.7 ± 0.7	2.5
9.1	1785 ± 14	0.281610	0.001640	0.072339	0.281554 ± 0.000032	-3.3 ± 1.1	2.7
14.1	1814 ± 16	0.281654	0.000955	0.043694	0.281621 ± 0.000017	-0.3 ± 0.6	2.5
15.1	1781 ± 18	0.281550	0.000673	0.023296	0.281527 ± 0.000023	-4.4 ± 0.8	2.7
19.1	1785 ± 13	0.281722	0.001089	0.049292	0.281685 ± 0.000026	1.3 ± 0.9	2.4
23.1	1794 ± 16	0.281582	0.001139	0.046635	0.281543 ± 0.000013	-3.5 ± 0.5	2.7
29.1	1794 ± 14	0.281576	0.000719	0.029815	0.281552 ± 0.000011	-3.2 ± 0.4	2.7
37.1	1796 ± 10	0.281632	0.000812	0.033936	0.281604 ± 0.000007	-1.3 ± 0.3	2.6
GSWA 88419: porphyritic monzogranite							
1.1	1764 ± 13	0.281612	0.001123	0.042077	0.281574 ± 0.000009	-3.1 ± 0.3	2.7
3.1	1796 ± 13	0.281720	0.001254	0.057002	0.281677 ± 0.000031	1.3 ± 1.1	2.4
5.1	1798 ± 17	0.281481	0.000587	0.024940	0.281461 ± 0.000009	-6.4 ± 0.3	2.9
8.1	1777 ± 17	0.281653	0.000843	0.023640	0.281625 ± 0.000014	-1.0 ± 0.5	2.5
12.1	1774 ± 11	0.281635	0.001429	0.057489	0.281587 ± 0.000027	-2.4 ± 0.9	2.6
19.1	1790 ± 11	0.281656	0.000941	0.040871	0.281624 ± 0.000015	-0.7 ± 0.5	2.5
22.1	1783 ± 12	0.281641	0.001191	0.049983	0.281601 ± 0.000010	-1.7 ± 0.4	2.6
36.2	1785 ± 17	0.281651	0.000432	0.015004	0.281636 ± 0.000014	-0.4 ± 0.5	2.5
GSWA 191995: foliated monzogranite							
1.1	1799 ± 8	0.281608	0.000842	0.034424	0.281579 ± 0.000032	-2.1 ± 1.1	2.6
4.1	1825 ± 10	0.281593	0.001496	0.060581	0.281541 ± 0.000024	-2.9 ± 0.8	2.7
5.1	1790 ± 18	0.281698	0.000985	0.045937	0.281665 ± 0.000044	0.7 ± 1.5	2.4
7.1	1778 ± 8	0.281295	0.001103	0.040932	0.281258 ± 0.000030	-14.0 ± 1.1	3.4
15.1	1792 ± 8	0.281141	0.000639	0.028734	0.281119 ± 0.000026	-18.6 ± 0.9	3.7
18.1	1788 ± 7	0.281553	0.000704	0.026126	0.281529 ± 0.000014	-4.2 ± 0.5	2.7
19.1	1808 ± 12	0.281645	0.001040	0.042244	0.281609 ± 0.000019	-0.9 ± 0.7	2.5
21.1	1884 ± 7	0.281569	0.000704	0.028496	0.281544 ± 0.000018	-1.5 ± 0.6	2.6
22.1	1803 ± 16	0.281363	0.000385	0.018436	0.281350 ± 0.000024	-10.2 ± 0.8	3.1
23.1	1840 ± 11	0.281718	0.001321	0.058784	0.281672 ± 0.000011	2.1 ± 0.4	2.4
24.1	1797 ± 7	0.281370	0.000703	0.030045	0.281346 ± 0.000068	-10.5 ± 2.4	3.1
25.1	2409 ± 6	0.281048	0.001203	0.047716	0.280993 ± 0.000012	-9.0 ± 0.4	3.5
GSWA 180938: equigranular biotite monzogranite							
4.1	1774 ± 8	0.281686	0.001670	0.065476	0.281630 ± 0.000017	-0.9 ± 0.6	2.5
5.1	2037 ± 7	0.281338	0.000622	0.024189	0.281314 ± 0.000008	-6.1 ± 0.3	3.1
9.1	2187 ± 4	0.281416	0.001000	0.040246	0.281374 ± 0.000016	-0.6 ± 0.6	2.8
10.1	1823 ± 30	0.281535	0.000619	0.026267	0.281514 ± 0.000016	-3.9 ± 0.6	2.8
13.1	1785 ± 7	0.281567	0.002510	0.082501	0.281482 ± 0.000019	-5.9 ± 0.7	2.8
14.1	1767 ± 7	0.281648	0.001590	0.060128	0.281595 ± 0.000230	-2.3 ± 8.1	2.6

Analysis no.	$^{207}Pb/^{206}Pb$ date (Ma)			$^{176}Hf/^{177}Hf$ measured	$^{176}Lu/^{177}Hf$ measured	$^{176}Yb/^{177}Hf$ measured	$^{176}Hf/^{177}Hf$ initial			$\varepsilon Hf_{(i)}$			T_{DM2} (Ga)
16.1	1788	±	14	0.281506	0.000223	0.009793	0.281498	±	0.000010	-5.2	±	0.3	2.8
17.1	1747	±	36	0.281624	0.001293	0.046924	0.281581	±	0.000013	-3.2	±	0.5	2.7
19.1	1800	±	6	0.281600	0.001774	0.069553	0.281539	±	0.000013	-3.5	±	0.5	2.7
26.1	1778	±	19	0.281583	0.002151	0.071666	0.281510	±	0.000013	-5.0	±	0.5	2.8
GSWA 190660: metamonzogranite													
1.1	1787	±	10	0.281573	0.000563	0.020453	0.281554	±	0.000016	-3.3	±	0.6	2.7
2.1	1933	±	9	0.281531	0.001386	0.058868	0.281480	±	0.000017	-2.6	±	0.6	2.8
3.1	1806	±	9	0.281443	0.000613	0.022423	0.281422	±	0.000021	-7.5	±	0.7	3.0
4.1	1796	±	5	0.281583	0.001406	0.046908	0.281535	±	0.000012	-3.8	±	0.4	2.7
5.1	1791	±	4	0.281567	0.001608	0.058240	0.281512	±	0.000013	-4.7	±	0.5	2.8
6.1	1792	±	5	0.281620	0.000893	0.031164	0.281590	±	0.000015	-1.9	±	0.5	2.6
7.1	1787	±	6	0.281551	0.001039	0.039342	0.281516	±	0.000009	-4.7	±	0.3	2.8
8.1	1796	±	4	0.281582	0.001283	0.045827	0.281538	±	0.000009	-3.7	±	0.3	2.7
9.1	1794	±	14	0.281568	0.001110	0.038556	0.281530	±	0.000009	-4.0	±	0.3	2.7
10.1	1792	±	6	0.281571	0.001508	0.054549	0.281520	±	0.000013	-4.4	±	0.5	2.8
11.1	1786	±	8	0.281554	0.000816	0.026048	0.281526	±	0.000011	-4.3	±	0.4	2.7
12.1	1794	±	7	0.281548	0.001489	0.057237	0.281497	±	0.000014	-5.1	±	0.5	2.8
13.1	1802	±	10	0.281541	0.001424	0.041926	0.281492	±	0.000023	-5.1	±	0.8	2.8
14.1	1781	±	5	0.281572	0.001122	0.039477	0.281534	±	0.000013	-4.1	±	0.5	2.7
15.1	1776	±	9	0.281618	0.002537	0.086659	0.281533	±	0.000012	-4.3	±	0.4	2.7
16.1	1789	±	10	0.281559	0.001768	0.059768	0.281499	±	0.000015	-5.2	±	0.5	2.8
17.1	1784	±	7	0.281568	0.001855	0.055791	0.281505	±	0.000012	-5.1	±	0.4	2.8
GSWA 190662: Middle Spring Granite, gneissic metamonzogranite													
1.1	1797	±	21	0.281606	0.000642	0.023993	0.281584	±	0.000024	-2.0	±	0.8	2.6
2.1	1762	±	22	0.281616	0.000845	0.023373	0.281588	±	0.000030	-2.7	±	1.1	2.6
3.1	1773	±	21	0.281375	0.000668	0.024868	0.281353	±	0.000024	-10.8	±	0.8	3.1
4.1	1848	±	10	0.281589	0.001622	0.059680	0.281532	±	0.000048	-2.7	±	1.7	2.7
6.1	1784	±	18	0.281768	0.000232	0.010157	0.281760	±	0.000044	4.0	±	1.5	2.2
7.1	1841	±	66	0.281541	0.000513	0.018838	0.281523	±	0.000029	-3.2	±	1.0	2.7
10.1	2703	±	6	0.281252	0.000981	0.035289	0.281201	±	0.000061	5.2	±	2.1	2.9
11.1	1819	±	35	0.281622	0.001775	0.051287	0.281561	±	0.000049	-2.3	±	1.7	2.6
14.1	1795	±	13	0.281694	0.000816	0.028890	0.281666	±	0.000028	0.9	±	1.0	2.4
19.1	1770	±	16	0.281566	0.000336	0.014567	0.281555	±	0.000016	-3.7	±	0.6	2.7
22.1	1789	±	26	0.281573	0.000549	0.016969	0.281554	±	0.000025	-3.2	±	0.9	2.7
25.1	1788	±	26	0.281499	0.000576	0.020303	0.281479	±	0.000012	-5.9	±	0.4	2.9
GSWA 190661: metatonalite													
1.1	1794	±	10	0.281356	0.000882	0.035771	0.281326	±	0.000020	-11.2	±	0.7	3.2
2.1	1804	±	8	0.281592	0.001206	0.044968	0.281551	±	0.000011	-3.0	±	0.4	2.7
3.1	1810	±	10	0.281591	0.001137	0.043512	0.281552	±	0.000009	-2.8	±	0.3	2.7
4.1	1795	±	9	0.281581	0.001431	0.059084	0.281532	±	0.000010	-3.9	±	0.4	2.7
5.1	1789	±	5	0.281633	0.000527	0.019338	0.281615	±	0.000011	-1.1	±	0.4	2.5
7.1	1803	±	7	0.281568	0.001180	0.038610	0.281528	±	0.000011	-3.9	±	0.4	2.7
9.1	1805	±	7	0.281598	0.002016	0.068636	0.281529	±	0.000010	-3.8	±	0.4	2.7
10.1	1802	±	8	0.281601	0.001241	0.048822	0.281559	±	0.000008	-2.8	±	0.3	2.7
12.1	1807	±	7	0.281628	0.000971	0.035553	0.281595	±	0.000016	-1.4	±	0.6	2.6

Analysis no.	$^{207}Pb/^{206}Pb$ date (Ma)	$^{176}Hf/^{177}Hf$ measured	$^{176}Lu/^{177}Hf$ measured	$^{176}Yb/^{177}Hf$ measured	$^{176}Hf/^{177}Hf$ initial	$\varepsilon Hf_{(i)}$	T_{DM2} (Ga)
GSWA 178024: biotite granodiorite							
1.1	1784 ± 14	0.281831	0.001687	0.041817	0.281774 ± 0.000083	4.4 ± 2.9	2.2
2.1	1770 ± 10	0.281645	0.001372	0.048062	0.281599 ± 0.000037	-2.1 ± 1.3	2.6
3.1	1787 ± 12	0.281666	0.002011	0.061158	0.281598 ± 0.000063	-1.7 ± 2.2	2.6
4.1	1779 ± 10	0.281665	0.001234	0.042637	0.281623 ± 0.000024	-1.0 ± 0.8	2.5
5.1	1763 ± 12	0.281625	0.001173	0.050380	0.281586 ± 0.000035	-2.7 ± 1.2	2.6
20.1	1800 ± 12	0.281582	0.002642	0.077277	0.281492 ± 0.000037	-5.2 ± 1.3	2.8
21.1	1802 ± 21	0.281547	0.000418	0.014322	0.281533 ± 0.000011	-3.7 ± 0.4	2.7
22.1	1794 ± 14	0.281602	0.001092	0.041762	0.281565 ± 0.000017	-2.8 ± 0.6	2.7
24.1	1792 ± 14	0.281688	0.000951	0.036268	0.281656 ± 0.000023	0.4 ± 0.8	2.5
25.1	1789 ± 15	0.281608	0.000577	0.021884	0.281588 ± 0.000016	-2.0 ± 0.6	2.6
26.1	1766 ± 21	0.281591	0.000808	0.028878	0.281564 ± 0.000013	-3.4 ± 0.5	2.7
27.1	1761 ± 22	0.281627	0.000885	0.034781	0.281597 ± 0.000034	-2.3 ± 1.2	2.6
GSWA 169058: Gooche Gneiss, augen orthogneiss							
3.1	1771 ± 10	0.281653	0.001397	0.061344	0.281606 ± 0.000024	-1.8 ± 0.8	2.6
4.1	1777 ± 20	0.281571	0.000875	0.035105	0.281542 ± 0.000026	-4.0 ± 0.9	2.7
6.1	1771 ± 21	0.281642	0.001506	0.067601	0.281591 ± 0.000029	-2.3 ± 1.0	2.6
17.1	1778 ± 10	0.281654	0.001222	0.050825	0.281613 ± 0.000012	-1.4 ± 0.4	2.6
19.1	1793 ± 11	0.281563	0.000927	0.037795	0.281531 ± 0.000020	-4.0 ± 0.7	2.7
GSWA 169089: granophyric syenogranite							
2.1	1739 ± 48	0.281389	0.002407	0.070594	0.281310 ± 0.000045	-13.1 ± 1.6	3.3
3.2	1776 ± 27	0.281578	0.002351	0.078067	0.281499 ± 0.000031	-5.5 ± 1.1	2.8
4.1	1790 ± 19	0.281536	0.000847	0.035048	0.281507 ± 0.000036	-4.9 ± 1.3	2.8
4.3	1797 ± 18	0.281530	0.000743	0.023971	0.281505 ± 0.000022	-4.8 ± 0.8	2.8
5.1	1805 ± 35	0.281521	0.001306	0.044182	0.281476 ± 0.000020	-5.6 ± 0.7	2.8
5.2	1774 ± 48	0.281537	0.000932	0.036791	0.281506 ± 0.000018	-5.3 ± 0.6	2.8
6.1	1983 ± 10	0.281439	0.001253	0.040513	0.281392 ± 0.000012	-4.6 ± 0.4	2.9
7.1	2755 ± 10	0.280950	0.001736	0.059065	0.280858 ± 0.000019	-5.8 ± 0.7	3.6
8.1	1784 ± 19	0.281533	0.001485	0.048779	0.281483 ± 0.000032	-5.9 ± 1.1	2.8
8.2	1772 ± 16	0.281503	0.001122	0.050778	0.281465 ± 0.000020	-6.8 ± 0.7	2.9
10.1	1782 ± 14	0.281540	0.000762	0.024760	0.281514 ± 0.000016	-4.8 ± 0.6	2.8
10.2	1766 ± 16	0.281588	0.001667	0.050291	0.281532 ± 0.000040	-4.5 ± 1.4	2.7
GSWA 169088: foliated biotite monzogranite							
3.1	2622 ± 6	0.281152	0.000787	0.027604	0.281113 ± 0.000010	0.2 ± 0.3	3.1
4.1	1794 ± 11	0.281560	0.000313	0.013031	0.281549 ± 0.000011	-3.3 ± 0.4	2.7
5.1	1796 ± 9	0.281533	0.000867	0.033762	0.281503 ± 0.000009	-4.9 ± 0.3	2.8
7.1	1810 ± 11	0.281620	0.001042	0.044395	0.281584 ± 0.000009	-1.7 ± 0.3	2.6
9.1	1886 ± 16	0.281582	0.000337	0.014703	0.281570 ± 0.000013	-0.5 ± 0.5	2.6
10.1	1803 ± 30	0.281630	0.000801	0.032322	0.281603 ± 0.000017	-1.2 ± 0.6	2.6
14.1	1801 ± 40	0.281519	0.001039	0.045700	0.281484 ± 0.000017	-5.5 ± 0.6	2.8
16.1	1747 ± 42	0.281532	0.001223	0.052396	0.281492 ± 0.000017	-6.4 ± 0.6	2.9
17.1	1949 ± 14	0.281559	0.000538	0.021805	0.281539 ± 0.000012	-0.1 ± 0.4	2.6
22.1	1815 ± 21	0.281515	0.000792	0.031862	0.281488 ± 0.000014	-5.0 ± 0.5	2.8
23.1	1824 ± 19	0.281501	0.001549	0.060776	0.281447 ± 0.000015	-6.2 ± 0.5	2.9

Analysis no.	$^{207}Pb/^{206}Pb$ date (Ma)	$^{176}Hf/^{177}Hf$ measured	$^{176}Lu/^{177}Hf$ measured	$^{176}Yb/^{177}Hf$ measured	$^{176}Hf/^{177}Hf$ initial	$\varepsilon Hf_{(i)}$	T_{DM2} (Ga)
GSWA 169087: foliated biotite granodiorite							
1.1	1981 ± 20	0.281474	0.000478	0.017059	0.281456 ± 0.000010	-2.4 ± 0.3	2.8
3.1	1754 ± 20	0.281588	0.000641	0.023614	0.281567 ± 0.000012	-3.6 ± 0.4	2.7
5.1	1808 ± 9	0.281529	0.001199	0.049622	0.281488 ± 0.000012	-5.2 ± 0.4	2.8
7.1	1787 ± 24	0.281612	0.001490	0.051722	0.281562 ± 0.000022	-3.0 ± 0.8	2.7
8.1	1792 ± 27	0.281660	0.001707	0.059492	0.281602 ± 0.000018	-1.5 ± 0.6	2.6
9.1	1808 ± 22	0.281518	0.000621	0.024383	0.281497 ± 0.000012	-4.9 ± 0.4	2.8
10.1	1853 ± 19	0.281454	0.000587	0.023698	0.281433 ± 0.000009	-6.1 ± 0.3	2.9
12.1	1802 ± 15	0.281668	0.001988	0.074797	0.281600 ± 0.000017	-1.3 ± 0.6	2.6
13.1	2284 ± 8	0.281303	0.001545	0.064802	0.281236 ± 0.000011	-3.3 ± 0.4	3.1
15.1	1783 ± 12	0.281577	0.000819	0.035060	0.281549 ± 0.000024	-3.6 ± 0.8	2.7
16.1	1919 ± 9	0.281582	0.001829	0.065367	0.281515 ± 0.000026	-1.7 ± 0.9	2.7
18.1	1811 ± 9	0.281354	0.001424	0.064324	0.281305 ± 0.000014	-11.6 ± 0.5	3.2
20.1	1803 ± 16	0.281645	0.001284	0.046984	0.281601 ± 0.000017	-1.3 ± 0.6	2.6
21.1	1768 ± 15	0.281551	0.000989	0.037057	0.281518 ± 0.000016	-5.0 ± 0.6	2.8
24.1	1763 ± 5	0.281791	0.002087	0.086717	0.281721 ± 0.000045	2.1 ± 1.6	2.3
1680–1620 Ma Durlacher Supersuite							
GSWA 142855: Discretion Granite, porphyritic monzogranite							
2.1	1619 ± 42	0.281434	0.000734	0.028678	0.281412 ± 0.000013	-12.2 ± 0.5	3.1
3.1	1591 ± 36	0.281484	0.001490	0.052390	0.281439 ± 0.000010	-11.8 ± 0.4	3.1
4.1	1634 ± 31	0.281515	0.001635	0.068110	0.281464 ± 0.000021	-9.9 ± 0.7	3.0
5.1	1561 ± 45	0.281433	0.000823	0.031433	0.281409 ± 0.000017	-13.6 ± 0.6	3.2
7.1	1625 ± 172	0.281437	0.000639	0.024201	0.281417 ± 0.000015	-11.8 ± 0.5	3.1
8.1	1639 ± 31	0.281553	0.001456	0.057383	0.281508 ± 0.000019	-8.3 ± 0.7	2.9
10.1	1682 ± 63	0.281429	0.000735	0.027279	0.281406 ± 0.000018	-10.9 ± 0.6	3.1
14.1	1597 ± 42	0.281508	0.000994	0.038911	0.281478 ± 0.000016	-10.3 ± 0.6	3.0
17.1	1623 ± 43	0.281485	0.000689	0.027376	0.281464 ± 0.000025	-10.2 ± 0.9	3.0
20.1	1629 ± 25	0.281400	0.001366	0.052132	0.281358 ± 0.000016	-13.8 ± 0.6	3.2
24.1	1629 ± 50	0.281430	0.000793	0.029649	0.281406 ± 0.000018	-12.2 ± 0.6	3.1
25.1	1664 ± 46	0.281476	0.000814	0.031949	0.281450 ± 0.000016	-9.8 ± 0.6	3.0
GSWA 183215: Davey Well Granite, coarse-grained porphyritic biotite monzogranite							
1.1	1671 ± 5	0.281526	0.000705	0.022900	0.281504 ± 0.000013	-7.7 ± 0.5	2.9
4.1	1655 ± 41	0.281506	0.000462	0.017290	0.281492 ± 0.000016	-8.5 ± 0.6	2.9
6.1	1674 ± 7	0.281523	0.000719	0.026862	0.281500 ± 0.000019	-7.8 ± 0.7	2.9
8.1	1661 ± 23	0.281542	0.000495	0.019105	0.281526 ± 0.000012	-7.1 ± 0.4	2.8
11.1	1641 ± 43	0.281565	0.000454	0.018174	0.281551 ± 0.000013	-6.7 ± 0.5	2.8
13.1	1673 ± 16	0.281536	0.000552	0.021061	0.281519 ± 0.000022	-7.1 ± 0.8	2.8
16.1	1698 ± 14	0.281551	0.000569	0.021834	0.281533 ± 0.000019	-6.1 ± 0.7	2.8
18.2	1670 ± 5	0.281560	0.000726	0.029913	0.281537 ± 0.000018	-6.6 ± 0.6	2.8
23.1	1642 ± 14	0.281515	0.000817	0.033271	0.281490 ± 0.000024	-8.9 ± 0.8	2.9
23.2	1658 ± 9	0.281559	0.000726	0.029516	0.281536 ± 0.000017	-6.9 ± 0.6	2.8
25.1	1668 ± 16	0.281516	0.000536	0.021006	0.281499 ± 0.000009	-7.9 ± 0.3	2.9
26.1	1663 ± 7	0.281528	0.000696	0.026351	0.281506 ± 0.000007	-7.8 ± 0.2	2.9
27.1	1649 ± 12	0.281548	0.000608	0.023200	0.281529 ± 0.000010	-7.3 ± 0.3	2.8
28.1	1677 ± 13	0.281530	0.000613	0.020439	0.281511 ± 0.000007	-7.3 ± 0.2	2.9
30.1	1647 ± 14	0.281543	0.000718	0.024128	0.281521 ± 0.000007	-7.7 ± 0.2	2.9

Analysis no.	$^{207}Pb/^{206}Pb$ date (Ma)	$^{176}Hf/^{177}Hf$ measured	$^{176}Lu/^{177}Hf$ measured	$^{176}Yb/^{177}Hf$ measured	$^{176}Hf/^{177}Hf$ initial	$\varepsilon Hf_{(i)}$	T_{DM2} (Ga)
GSWA 183207: Tetlow Granite, meta-tonalite/quartz diorite							
4.1	1659 ± 26	0.281535	0.000597	0.020787	0.281516 ± 0.000008	-7.5 ± 0.3	2.9
7.1	1707 ± 20	0.281546	0.000540	0.019497	0.281529 ± 0.000009	-6.0 ± 0.3	2.8
8.1	2453 ± 6	0.281213	0.000878	0.031816	0.281172 ± 0.000009	-1.6 ± 0.3	3.1
9.1	1687 ± 18	0.281526	0.000554	0.020035	0.281508 ± 0.000008	-7.2 ± 0.3	2.9
10.1	1698 ± 21	0.281540	0.000711	0.021247	0.281517 ± 0.000007	-6.6 ± 0.2	2.8
12.1	1665 ± 12	0.281544	0.000692	0.022252	0.281522 ± 0.000007	-7.2 ± 0.2	2.8
15.1	1649 ± 17	0.281575	0.000550	0.020270	0.281558 ± 0.000010	-6.3 ± 0.4	2.8
16.1	1656 ± 7	0.281562	0.000500	0.017996	0.281546 ± 0.000012	-6.5 ± 0.4	2.8
17.1	1664 ± 12	0.281565	0.000452	0.017467	0.281551 ± 0.000013	-6.2 ± 0.5	2.8
20.1	1659 ± 12	0.281552	0.000802	0.025936	0.281527 ± 0.000009	-7.2 ± 0.3	2.8
21.1	1653 ± 19	0.281557	0.000410	0.016139	0.281544 ± 0.000009	-6.7 ± 0.3	2.8
22.1	1654 ± 11	0.281544	0.000580	0.023676	0.281526 ± 0.000010	-7.3 ± 0.3	2.8
25.1	1662 ± 4	0.281564	0.000930	0.032569	0.281535 ± 0.000007	-6.8 ± 0.3	2.8
GSWA 185944: Davey Well Granite, porphyritic monzogranite							
2.1	1591 ± 33	0.281480	0.000506	0.018040	0.281465 ± 0.000014	-10.9 ± 0.5	3.0
5.1	2116 ± 10	0.281503	0.000680	0.024626	0.281476 ± 0.000020	1.4 ± 0.7	2.6
9.1	2125 ± 15	0.281155	0.000075	0.002723	0.281152 ± 0.000008	-9.9 ± 0.3	3.4
12.1	1681 ± 22	0.281519	0.000660	0.018882	0.281498 ± 0.000012	-7.7 ± 0.4	2.9
18.1	1610 ± 32	0.281494	0.000952	0.026806	0.281465 ± 0.000009	-10.5 ± 0.3	3.0
21.1	1652 ± 24	0.281530	0.000651	0.021579	0.281510 ± 0.000041	-7.9 ± 1.4	2.9
22.1	1653 ± 61	0.281553	0.000692	0.023427	0.281531 ± 0.000026	-7.1 ± 0.9	2.8
24.1	1633 ± 18	0.281669	0.000865	0.029687	0.281642 ± 0.000039	-3.7 ± 1.4	2.6
27.1	1667 ± 17	0.281458	0.001654	0.054282	0.281406 ± 0.000025	-11.3 ± 0.9	3.1
28.1	1673 ± 17	0.281520	0.000343	0.010977	0.281509 ± 0.000014	-7.5 ± 0.5	2.9
29.1	1649 ± 46	0.281525	0.000663	0.022561	0.281504 ± 0.000013	-8.2 ± 0.5	2.9
32.1	1586 ± 29	0.281440	0.000507	0.017385	0.281425 ± 0.000015	-12.4 ± 0.5	3.1
GSWA 169053: biotite-muscovite monzogranite							
2.1	1728 ± 9	0.281473	0.001284	0.06776	0.281431 ± 0.000011	-9.0 ± 0.4	3.0
3.1	2222 ± 7	0.281130	0.000146	0.00743	0.281124 ± 0.000008	-8.7 ± 0.3	3.4
4.1	1938 ± 17	0.281284	0.001403	0.04933	0.281232 ± 0.000012	-11.3 ± 0.4	3.3
5.1	1940 ± 9	0.281295	0.000467	0.02306	0.281278 ± 0.000006	-9.6 ± 0.2	3.2
6.1	1706 ± 9	0.281476	0.003026	0.09873	0.281378 ± 0.000022	-11.4 ± 0.8	3.1
7.1	1790 ± 6	0.281576	0.001903	0.09198	0.281511 ± 0.000018	-4.7 ± 0.6	2.8
8.1	2115 ± 12	0.281297	0.001019	0.05217	0.281256 ± 0.000013	-6.4 ± 0.5	3.1
9.1	1682 ± 9	0.281618	0.001546	0.06642	0.281569 ± 0.000012	-5.2 ± 0.4	2.7
10.1	1783 ± 30	0.281532	0.000962	0.03593	0.281499 ± 0.000014	-5.3 ± 0.5	2.8
11.1	2048 ± 19	0.281343	0.000391	0.01629	0.281328 ± 0.000006	-5.4 ± 0.2	3.0
12.1	1801 ± 6	0.281848	0.001734	0.07010	0.281789 ± 0.000011	5.4 ± 0.4	2.1
13.1	1713 ± 9	0.281538	0.001321	0.05597	0.281495 ± 0.000011	-7.1 ± 0.4	2.9
14.1	1824 ± 9	0.281714	0.001490	0.06606	0.281662 ± 0.000018	1.4 ± 0.6	2.4
15.1	2046 ± 7	0.281295	0.000629	0.03047	0.281271 ± 0.000010	-7.5 ± 0.3	3.2
15.2	1683 ± 8	0.281588	0.001643	0.06950	0.281536 ± 0.000011	-6.3 ± 0.4	2.8
16.1	1770 ± 10	0.281495	0.002705	0.09545	0.281404 ± 0.000026	-9.0 ± 0.9	3.0
17.1	1797 ± 9	0.281540	0.000888	0.04354	0.281510 ± 0.000015	-4.6 ± 0.5	2.8
18.1	1679 ± 9	0.281474	0.002259	0.07741	0.281402 ± 0.000029	-11.1 ± 1.0	3.1
19.1	1667 ± 9	0.281537	0.002857	0.10174	0.281447 ± 0.000028	-9.8 ± 1.0	3.0

Analysis no.	$^{207}Pb/^{206}Pb$ date (Ma)			$^{176}Hf/^{177}Hf$ measured	$^{176}Lu/^{177}Hf$ measured	$^{176}Yb/^{177}Hf$ measured	$^{176}Hf/^{177}Hf$ initial			$\varepsilon Hf_{(i)}$			T_{DM2} (Ga)
20.1	1676	±	9	0.281580	0.001686	0.07137	0.281526	±	0.000011	-6.8	±	0.4	2.8
20.2	2201	±	11	0.281278	0.000513	0.02512	0.281256	±	0.000011	-4.4	±	0.4	3.1
21.1	1682	±	8	0.281556	0.001916	0.07104	0.281495	±	0.000025	-7.8	±	0.9	2.9
22.1	1680	±	9	0.281523	0.001396	0.06008	0.281479	±	0.000012	-8.4	±	0.4	2.9
23.1	1669	±	8	0.281559	0.001466	0.05906	0.281513	±	0.000010	-7.4	±	0.3	2.9
23.2	2392	±	7	0.281242	0.001359	0.06045	0.281180	±	0.000010	-2.8	±	0.3	3.1
24.1	1621	±	9	0.281534	0.002193	0.07869	0.281467	±	0.000035	-10.2	±	1.2	3.0
25.1	1630	±	9	0.281482	0.001270	0.05542	0.281443	±	0.000016	-10.8	±	0.6	3.0
26.1	1645	±	8	0.281556	0.001668	0.06752	0.281504	±	0.000012	-8.3	±	0.4	2.9
26.2	1818	±	16	0.281774	0.001514	0.06716	0.281722	±	0.000008	3.4	±	0.3	2.3
27.1	1645	±	8	0.281612	0.001800	0.08118	0.281556	±	0.000012	-6.5	±	0.4	2.8
28.1	2373	±	10	0.281220	0.001095	0.05070	0.281170	±	0.000012	-3.5	±	0.4	3.2
28.2	1673	±	13	0.281565	0.001430	0.05978	0.281520	±	0.000011	-7.1	±	0.4	2.8
GSWA 169062: Dingo Creek Granite, porphyritic syenogranite													
2.1	1660	±	17	0.281650	0.000404	0.01763	0.281637	±	0.000035	-3.2	±	1.2	2.6
3.1	1632	±	30	0.281500	0.000018	0.00101	0.281499	±	0.000011	-8.8	±	0.4	2.9
4.1	1687	±	7	0.281596	0.000712	0.03358	0.281573	±	0.000029	-4.9	±	1.0	2.7
11.1	1779	±	22	0.281528	0.001396	0.06150	0.281481	±	0.000023	-6.1	±	0.8	2.9
13.1	1767	±	24	0.281520	0.001147	0.05259	0.281482	±	0.000006	-6.3	±	0.2	2.9
14.1	1693	±	11	0.281581	0.000728	0.02768	0.281558	±	0.000013	-5.3	±	0.5	2.7
15.1	1659	±	14	0.281623	0.000071	0.00270	0.281621	±	0.000009	-3.8	±	0.3	2.6
16.1	1660	±	42	0.281484	0.000021	0.00120	0.281483	±	0.000012	-8.7	±	0.4	2.9
17.1	1783	±	19	0.281451	0.001336	0.06034	0.281406	±	0.000015	-8.7	±	0.5	3.0
18.1	1680	±	11	0.281558	0.000582	0.02604	0.281539	±	0.000010	-6.2	±	0.3	2.8
19.1	1669	±	12	0.281594	0.000505	0.02318	0.281578	±	0.000013	-5.1	±	0.5	2.7
21.1	1656	±	24	0.281462	0.000010	0.00103	0.281462	±	0.000008	-9.5	±	0.3	3.0
22.1	1686	±	14	0.281447	0.000015	0.00098	0.281447	±	0.000006	-9.4	±	0.2	3.0
23.1	1686	±	22	0.281436	0.000023	0.00120	0.281435	±	0.000014	-9.8	±	0.5	3.0
25.1	1679	±	5	0.281547	0.000927	0.04029	0.281518	±	0.000011	-7.0	±	0.4	2.8
26.1	1679	±	8	0.281561	0.000119	0.00613	0.281557	±	0.000006	-5.6	±	0.2	2.8
27.1	1781	±	16	0.281500	0.000949	0.04338	0.281468	±	0.000013	-6.5	±	0.5	2.9
GSWA 169055: Yangibana Granite, biotite-muscovite monzogranite													
2.1	2616	±	8	0.281083	0.000626	0.02332	0.281052	±	0.000010	-2.1	±	0.3	3.3
3.1	1665	±	20	0.281632	0.000364	0.01471	0.281621	±	0.000008	-3.7	±	0.3	2.6
4.1	1678	±	21	0.281739	0.000980	0.04689	0.281708	±	0.000014	-0.3	±	0.5	2.4
5.1	1845	±	25	0.281584	0.001089	0.04385	0.281546	±	0.000011	-2.3	±	0.4	2.7
8.1	1657	±	15	0.281588	0.000276	0.01139	0.281579	±	0.000013	-5.3	±	0.5	2.7
9.1	1650	±	12	0.281572	0.000235	0.01254	0.281565	±	0.000010	-6.0	±	0.3	2.8
10.1	1667	±	18	0.281535	0.001239	0.04777	0.281496	±	0.000015	-8.1	±	0.5	2.9
11.1	1677	±	13	0.281587	0.000753	0.03124	0.281563	±	0.000025	-5.5	±	0.9	2.7
13.1	1669	±	18	0.281643	0.000154	0.00689	0.281638	±	0.000011	-3.0	±	0.4	2.6
14.1	2683	±	11	0.281657	0.000199	0.01066	0.281647	±	0.000010	20.6	±	0.3	1.8
17.1	1673	±	29	0.281551	0.000597	0.02308	0.281532	±	0.000018	-6.7	±	0.6	2.8
18.1	2427	±	6	0.281568	0.000170	0.00918	0.281560	±	0.000008	11.6	±	0.3	2.2

Analysis no.	$^{207}Pb/^{206}Pb$ date (Ma)	$^{176}Hf/^{177}Hf$ measured	$^{176}Lu/^{177}Hf$ measured	$^{176}Yb/^{177}Hf$ measured	$^{176}Hf/^{177}Hf$ initial	$\varepsilon Hf_{(i)}$	T_{DM2} (Ga)
GSWA 178029: Pimbyana Granite, biotite monzogranite							
1.1	1689 ± 27	0.281558	0.001108	0.05184	0.281523 ± 0.000010	-6.6 ± 0.3	2.8
3.1	1664 ± 17	0.281560	0.001055	0.04820	0.281527 ± 0.000010	-7.1 ± 0.3	2.8
4.1	1653 ± 28	0.281498	0.001348	0.04415	0.281456 ± 0.000016	-9.8 ± 0.6	3.0
5.1	1709 ± 32	0.281501	0.002066	0.08058	0.281434 ± 0.000022	-9.3 ± 0.8	3.0
7.1	1704 ± 28	0.281606	0.001123	0.03925	0.281570 ± 0.000010	-4.6 ± 0.3	2.7
8.1	1701 ± 27	0.281559	0.001653	0.06136	0.281506 ± 0.000014	-7.0 ± 0.5	2.9
9.1	1694 ± 21	0.281599	0.000967	0.05184	0.281568 ± 0.000010	-4.9 ± 0.3	2.7
11.1	1696 ± 16	0.281585	0.001379	0.06753	0.281541 ± 0.000010	-5.8 ± 0.4	2.8
12.1	1674 ± 20	0.281573	0.000992	0.04848	0.281542 ± 0.000010	-6.3 ± 0.3	2.8
13.1	1696 ± 18	0.281524	0.000438	0.01454	0.281510 ± 0.000012	-6.9 ± 0.4	2.8
14.1	1711 ± 33	0.281497	0.001468	0.05406	0.281449 ± 0.000018	-8.7 ± 0.6	3.0
15.1	1650 ± 20	0.281516	0.001752	0.06794	0.281461 ± 0.000019	-9.7 ± 0.7	3.0
16.1	1667 ± 21	0.281633	0.001325	0.05144	0.281591 ± 0.000017	-4.7 ± 0.6	2.7
17.1	1717 ± 47	0.281687	0.000709	0.03214	0.281664 ± 0.000005	-1.0 ± 0.2	2.5
19.1	1753 ± 17	0.281662	0.001392	0.06542	0.281616 ± 0.000009	-1.9 ± 0.3	2.6
20.1	1677 ± 25	0.281769	0.001280	0.06623	0.281728 ± 0.000012	0.4 ± 0.4	2.4
21.1	1661 ± 19	0.281734	0.000798	0.03985	0.281709 ± 0.000024	-0.7 ± 0.8	2.4
23.1	1684 ± 52	0.281596	0.000813	0.03864	0.281570 ± 0.000009	-5.1 ± 0.3	2.7
24.1	1653 ± 17	0.281570	0.001163	0.05730	0.281534 ± 0.000008	-7.1 ± 0.3	2.8
25.1	1742 ± 45	0.281595	0.002143	0.09633	0.281524 ± 0.000012	-5.4 ± 0.4	2.8
NORTHERN CAPRICORN BASINS							
>2008 Ma Shingle Creek Group							
Beasley River Quartzite							
GSWA 169084: ferruginous sandstone							
2	2557 ± 23	0.281245	0.000632	0.018310	0.281214 ± 0.000015	2.3 ± 0.5	2.9
3	2846 ± 25	0.281063	0.000720	0.019128	0.281024 ± 0.000008	2.2 ± 0.3	3.2
4	3097 ± 11	0.280953	0.001297	0.041141	0.280876 ± 0.000012	2.8 ± 0.4	3.3
6	2552 ± 13	0.281133	0.001311	0.037991	0.281069 ± 0.000021	-3.0 ± 0.7	3.3
9	3003 ± 21	0.280997	0.000976	0.033987	0.280941 ± 0.000012	2.9 ± 0.4	3.2
10	3005 ± 15	0.281063	0.001229	0.040192	0.280992 ± 0.000011	4.8 ± 0.4	3.1
11	2448 ± 16	0.281262	0.000866	0.024889	0.281222 ± 0.000026	0.0 ± 0.9	3.0
12	3212 ± 12	0.280904	0.001066	0.029432	0.280838 ± 0.000020	4.1 ± 0.7	3.3
14	2442 ± 18	0.281314	0.001149	0.033303	0.281260 ± 0.000035	1.3 ± 1.2	2.9
16	2420 ± 18	0.281258	0.000805	0.026810	0.281221 ± 0.000012	-0.7 ± 0.4	3.0
18	2464 ± 19	0.281268	0.001174	0.036059	0.281213 ± 0.000016	0.1 ± 0.6	3.0
19	3530 ± 17	0.280456	0.000686	0.021902	0.280409 ± 0.000010	-3.7 ± 0.4	4.1
20	2422 ± 18	0.281259	0.001044	0.040217	0.281211 ± 0.000013	-1.0 ± 0.5	3.0
21	2461 ± 16	0.281339	0.001033	0.040129	0.281290 ± 0.000015	2.8 ± 0.5	2.8
24	2436 ± 16	0.281203	0.000776	0.027707	0.281167 ± 0.000011	-2.2 ± 0.4	3.1
25	2440 ± 16	0.281231	0.001142	0.036504	0.281178 ± 0.000020	-1.7 ± 0.7	3.1
26	2524 ± 25	0.281080	0.000730	0.022581	0.281045 ± 0.000015	-4.5 ± 0.5	3.3
27	2538 ± 16	0.281127	0.001114	0.034176	0.281073 ± 0.000019	-3.2 ± 0.7	3.3
29	2525 ± 16	0.281174	0.001335	0.041798	0.281110 ± 0.000016	-2.2 ± 0.6	3.2

Analysis no.	$^{207}Pb/^{206}Pb$ date (Ma)	$^{176}Hf/^{177}Hf$ measured	$^{176}Lu/^{177}Hf$ measured	$^{176}Yb/^{177}Hf$ measured	$^{176}Hf/^{177}Hf$ initial	$\varepsilon Hf_{(i)}$	T_{DM2} (Ga)
2008–1804 Ma Wyloo Group							
Mt McGrath Formation							
GSWA 143474: sandstone							
1	2695 ± 10	0.281085	0.000923	0.035929	0.281037 ± 0.000013	-0.8 ± 0.5	3.2
3	2436 ± 8	0.281253	0.001060	0.041167	0.281204 ± 0.000015	-0.9 ± 0.5	3.0
6	2676 ± 8	0.281086	0.001514	0.051310	0.281009 ± 0.000013	-2.3 ± 0.5	3.3
9	2712 ± 12	0.281009	0.000738	0.025280	0.280971 ± 0.000015	-2.8 ± 0.5	3.4
11	2719 ± 11	0.281143	0.000583	0.020795	0.281113 ± 0.000013	2.4 ± 0.5	3.0
13	2702 ± 8	0.281214	0.000680	0.025582	0.281179 ± 0.000010	4.4 ± 0.4	2.9
15	2564 ± 10	0.281287	0.000769	0.024994	0.281249 ± 0.000024	3.7 ± 0.8	2.8
17	2444 ± 8	0.281271	0.000831	0.029081	0.281232 ± 0.000019	0.3 ± 0.7	3.0
19	2432 ± 11	0.281123	0.000764	0.024903	0.281088 ± 0.000018	-5.1 ± 0.6	3.3
22	2680 ± 11	0.281036	0.000813	0.033722	0.280994 ± 0.000016	-2.7 ± 0.6	3.3
25	2600 ± 9	0.281160	0.000897	0.036697	0.281115 ± 0.000011	-0.3 ± 0.4	3.1
28	2664 ± 13	0.281158	0.000513	0.012656	0.281132 ± 0.000016	1.8 ± 0.6	3.0
31	2442 ± 7	0.281145	0.001585	0.053216	0.281071 ± 0.000027	-5.5 ± 0.9	3.3
34	2707 ± 12	0.281263	0.001313	0.048856	0.281195 ± 0.000042	5.1 ± 1.5	2.9
37	2879 ± 10	0.281109	0.000283	0.009871	0.281093 ± 0.000031	5.4 ± 1.1	3.0
39	2529 ± 8	0.281192	0.000374	0.015199	0.281174 ± 0.000017	0.2 ± 0.6	3.0
41	2455 ± 10	0.281268	0.000570	0.023748	0.281241 ± 0.000014	0.9 ± 0.5	2.9
44	2719 ± 11	0.281104	0.000689	0.031474	0.281068 ± 0.000022	0.8 ± 0.8	3.1
46	2523 ± 8	0.281127	0.001610	0.054962	0.281049 ± 0.000023	-4.4 ± 0.8	3.3
48	2515 ± 12	0.281184	0.000150	0.005612	0.281177 ± 0.000015	0.0 ± 0.5	3.0
50	2678 ± 7	0.281212	0.002516	0.085820	0.281083 ± 0.000024	0.4 ± 0.8	3.1
52	3259 ± 7	0.280737	0.001815	0.076094	0.280623 ± 0.000016	-2.4 ± 0.6	3.8
55	2718 ± 9	0.281028	0.000861	0.028983	0.280983 ± 0.000031	-2.2 ± 1.1	3.3
57	2669 ± 11	0.281246	0.000845	0.025397	0.281203 ± 0.000024	4.5 ± 0.8	2.9
59	2683 ± 7	0.281235	0.001029	0.055385	0.281182 ± 0.000013	4.1 ± 0.5	2.9
61	2461 ± 7	0.281282	0.000665	0.028237	0.281251 ± 0.000013	1.4 ± 0.5	2.9
63	2807 ± 10	0.280841	0.002573	0.093645	0.280703 ± 0.000034	-10.1 ± 1.2	3.9
65	3030 ± 10	0.280798	0.001162	0.050243	0.280730 ± 0.000012	-4.0 ± 0.4	3.7
67	3021 ± 8	0.280748	0.001018	0.043260	0.280689 ± 0.000015	-5.7 ± 0.5	3.8
70	2819 ± 7	0.281010	0.002235	0.086748	0.280889 ± 0.000030	-3.2 ± 1.1	3.5
72	2526 ± 8	0.281252	0.000975	0.035087	0.281205 ± 0.000022	1.2 ± 0.8	3.0
74	2732 ± 9	0.281206	0.000458	0.013939	0.281182 ± 0.000018	5.2 ± 0.6	2.9
76	2928 ± 10	0.280799	0.000837	0.035800	0.280752 ± 0.000011	-5.6 ± 0.4	3.7
78	2702 ± 13	0.281199	0.000504	0.018692	0.281173 ± 0.000027	4.1 ± 0.9	2.9
80	2447 ± 7	0.281155	0.000602	0.024702	0.281127 ± 0.000024	-3.4 ± 0.8	3.2
83	3565 ± 57	0.280451	0.000747	0.027009	0.280400 ± 0.000038	-3.2 ± 1.3	4.0
85	2722 ± 9	0.281223	0.000659	0.024480	0.281189 ± 0.000016	5.2 ± 0.6	2.9
87	2644 ± 10	0.281354	0.000575	0.017973	0.281325 ± 0.000032	8.2 ± 1.1	2.6
90	2670 ± 13	0.281215	0.000705	0.028197	0.281179 ± 0.000019	3.6 ± 0.7	2.9

Analysis no.	$^{207}Pb/^{206}Pb$ date (Ma)	$^{176}Hf/^{177}Hf$ measured	$^{176}Lu/^{177}Hf$ measured	$^{176}Yb/^{177}Hf$ measured	$^{176}Hf/^{177}Hf$ initial	$\varepsilon Hf_{(i)}$	T_{DM2} (Ga)
GSWA 169081: pebbly sandstone							
1	2476 ± 16	0.281305	0.000838	0.028772	0.281265 ± 0.000011	2.2 ± 0.4	2.9
2	2602 ± 19	0.281121	0.000259	0.009353	0.281108 ± 0.000008	-0.5 ± 0.3	3.1
4	2691 ± 7	0.281140	0.000713	0.024529	0.281103 ± 0.000010	1.4 ± 0.3	3.1
6	2553 ± 12	0.281281	0.000676	0.021886	0.281248 ± 0.000011	3.4 ± 0.4	2.9
8	2680 ± 8	0.281339	0.003040	0.115686	0.281183 ± 0.000013	4.0 ± 0.5	2.9
9	2710 ± 14	0.281146	0.000215	0.007839	0.281135 ± 0.000010	3.0 ± 0.4	3.0
10	2722 ± 29	0.281178	0.001370	0.043435	0.281107 ± 0.000012	2.3 ± 0.4	3.1
11	2735 ± 13	0.281158	0.000818	0.026044	0.281115 ± 0.000012	2.9 ± 0.4	3.0
13	2843 ± 12	0.281080	0.000757	0.022251	0.281039 ± 0.000009	2.7 ± 0.3	3.1
14	2811 ± 7	0.281103	0.001770	0.061996	0.281008 ± 0.000010	0.8 ± 0.4	3.2
16	2688 ± 13	0.281182	0.000272	0.009229	0.281168 ± 0.000008	3.7 ± 0.3	2.9
17	2719 ± 11	0.281144	0.000223	0.008826	0.281132 ± 0.000014	3.1 ± 0.5	3.0
18	2820 ± 6	0.280832	0.000515	0.014269	0.280804 ± 0.000008	-6.2 ± 0.3	3.7
21	2644 ± 14	0.281100	0.000017	0.000957	0.281099 ± 0.000005	0.2 ± 0.2	3.1
23	2695 ± 11	0.281177	0.000535	0.017332	0.281149 ± 0.000010	3.2 ± 0.3	3.0
24	2449 ± 9	0.281210	0.000330	0.011055	0.281195 ± 0.000012	-0.9 ± 0.4	3.0
27	3290 ± 9	0.280612	0.000537	0.018538	0.280578 ± 0.000009	-3.3 ± 0.3	3.8
28	2693 ± 14	0.281161	0.000453	0.014493	0.281138 ± 0.000008	2.7 ± 0.3	3.0
29	2674 ± 14	0.281147	0.000397	0.013084	0.281127 ± 0.000008	1.9 ± 0.3	3.0
30	2739 ± 14	0.281207	0.000560	0.018816	0.281178 ± 0.000008	5.2 ± 0.3	2.9
32	2743 ± 6	0.280990	0.000616	0.022727	0.280958 ± 0.000007	-2.6 ± 0.3	3.4
33	2732 ± 16	0.281146	0.000637	0.022379	0.281113 ± 0.000008	2.7 ± 0.3	3.0
34	2791 ± 8	0.281156	0.001122	0.039425	0.281096 ± 0.000015	3.5 ± 0.5	3.0
GSWA 169082: sandstone							
2	3061 ± 33	0.280897	0.000880	0.034248	0.280845 ± 0.000010	0.8 ± 0.3	3.4
3	2460 ± 16	0.281179	0.001169	0.048285	0.281124 ± 0.000012	-3.2 ± 0.4	3.2
5	2589 ± 33	0.281112	0.000202	0.005839	0.281102 ± 0.000008	-1.0 ± 0.3	3.2
6	2670 ± 34	0.281183	0.000602	0.018078	0.281152 ± 0.000010	2.7 ± 0.4	3.0
9	3185 ± 40	0.280887	0.000518	0.020734	0.280855 ± 0.000009	4.1 ± 0.3	3.3
10	2431 ± 48	0.281271	0.000919	0.042710	0.281228 ± 0.000010	-0.1 ± 0.3	3.0
12	2574 ± 26	0.281333	0.000365	0.015275	0.281315 ± 0.000012	6.2 ± 0.4	2.7
13	2949 ± 50	0.280898	0.000892	0.032955	0.280848 ± 0.000015	-1.7 ± 0.5	3.5
14	2864 ± 13	0.280929	0.000880	0.040022	0.280881 ± 0.000011	-2.5 ± 0.4	3.5
15	2455 ± 25	0.281238	0.000641	0.025702	0.281208 ± 0.000009	-0.3 ± 0.3	3.0
17	2727 ± 18	0.281165	0.000472	0.018112	0.281140 ± 0.000008	3.6 ± 0.3	3.0
19	2441 ± 26	0.281247	0.000634	0.023618	0.281217 ± 0.000010	-0.3 ± 0.3	3.0
20	2689 ± 22	0.281140	0.000671	0.021270	0.281105 ± 0.000012	1.5 ± 0.4	3.1
22	2699 ± 27	0.281150	0.000822	0.031073	0.281108 ± 0.000008	1.8 ± 0.3	3.1
23	2982 ± 31	0.280796	0.000644	0.024378	0.280759 ± 0.000010	-4.1 ± 0.4	3.7
24	2599 ± 24	0.281274	0.001570	0.061911	0.281196 ± 0.000010	2.6 ± 0.3	2.9
26	2512 ± 23	0.281217	0.000921	0.038927	0.281173 ± 0.000013	-0.2 ± 0.5	3.1
29	2713 ± 16	0.281178	0.000220	0.008399	0.281167 ± 0.000008	4.2 ± 0.3	2.9
30	3077 ± 48	0.280785	0.000394	0.015247	0.280762 ± 0.000012	-1.8 ± 0.4	3.6
31	2618 ± 19	0.281239	0.000428	0.016383	0.281218 ± 0.000007	3.8 ± 0.3	2.9
32	2817 ± 56	0.281126	0.001064	0.039654	0.281069 ± 0.000012	3.1 ± 0.4	3.1

Analysis no.	$^{207}Pb/^{206}Pb$ date (Ma)	$^{176}Hf/^{177}Hf$ measured	$^{176}Lu/^{177}Hf$ measured	$^{176}Yb/^{177}Hf$ measured	$^{176}Hf/^{177}Hf$ initial	$\varepsilon Hf_{(i)}$	T_{DM2} (Ga)
Ashburton Formation							
GSWA 148922: crystal–vitric tuff							
5	1816 ± 32	0.281365	0.001057	0.032853	0.281329 ± 0.000020	-10.6 ± 0.7	3.2
6	1782 ± 28	0.281446	0.000947	0.044934	0.281414 ± 0.000017	-8.4 ± 0.6	3.0
7	1800 ± 17	0.281440	0.000687	0.029533	0.281417 ± 0.000012	-7.9 ± 0.4	3.0
9	1796 ± 23	0.281419	0.001326	0.042820	0.281374 ± 0.000013	-9.5 ± 0.5	3.1
11	1792 ± 21	0.281353	0.002173	0.064732	0.281279 ± 0.000039	-12.9 ± 1.4	3.3
16	1801 ± 28	0.281413	0.000886	0.030494	0.281383 ± 0.000015	-9.1 ± 0.5	3.1
17	1810 ± 46	0.281400	0.000825	0.028746	0.281372 ± 0.000012	-9.2 ± 0.4	3.1
18	1746 ± 39	0.281444	0.000957	0.030086	0.281412 ± 0.000011	-9.3 ± 0.4	3.0
23	1827 ± 14	0.281410	0.001284	0.048377	0.281366 ± 0.000013	-9.1 ± 0.5	3.1
24	1803 ± 40	0.281512	0.001384	0.051763	0.281465 ± 0.000020	-6.1 ± 0.7	2.9
1804–1738 Ma Capricorn Group							
Mooline Formation							
GSWA 143475: sandstone							
1	1804 ± 18	0.281352	0.000434	0.017725	0.281337 ± 0.000015	-10.6 ± 0.5	3.2
6	1857 ± 18	0.281436	0.000236	0.010635	0.281428 ± 0.000009	-6.2 ± 0.3	2.9
11	1992 ± 18	0.281542	0.000367	0.012776	0.281528 ± 0.000011	0.5 ± 0.4	2.6
12	2286 ± 17	0.281253	0.001161	0.037446	0.281202 ± 0.000010	-4.4 ± 0.3	3.1
13	1984 ± 18	0.281546	0.000409	0.014479	0.281531 ± 0.000008	0.4 ± 0.3	2.6
15	2514 ± 31	0.280863	0.001509	0.062128	0.280791 ± 0.000009	-13.8 ± 0.3	3.9
17	2389 ± 17	0.281233	0.001892	0.088807	0.281147 ± 0.000015	-4.0 ± 0.5	3.2
22	1840 ± 18	0.281458	0.001090	0.039091	0.281420 ± 0.000012	-6.9 ± 0.4	3.0
23	1998 ± 18	0.281526	0.000564	0.021071	0.281505 ± 0.000009	-0.2 ± 0.3	2.7
26	2109 ± 18	0.281299	0.000921	0.038370	0.281262 ± 0.000012	-6.3 ± 0.4	3.1
31	2710 ± 17	0.280752	0.000750	0.024728	0.280713 ± 0.000011	-12.0 ± 0.4	3.9
36	2135 ± 18	0.281253	0.001247	0.045792	0.281202 ± 0.000013	-7.9 ± 0.5	3.2
40	2293 ± 18	0.281233	0.001133	0.034350	0.281184 ± 0.000011	-4.9 ± 0.4	3.2
41	2007 ± 18	0.281272	0.000853	0.026660	0.281239 ± 0.000012	-9.5 ± 0.4	3.2
43	1975 ± 20	0.281409	0.000611	0.025067	0.281386 ± 0.000010	-5.0 ± 0.3	2.9
49	2539 ± 16	0.280994	0.000841	0.029570	0.280953 ± 0.000012	-7.4 ± 0.4	3.5
55	1988 ± 17	0.281463	0.001013	0.034691	0.281425 ± 0.000009	-3.3 ± 0.3	2.8
58	2449 ± 17	0.281222	0.001597	0.066764	0.281147 ± 0.000008	-2.6 ± 0.3	3.2
59	1787 ± 19	0.281484	0.001749	0.067772	0.281425 ± 0.000010	-7.9 ± 0.3	3.0
63	1781 ± 18	0.281473	0.000834	0.032404	0.281445 ± 0.000011	-7.3 ± 0.4	2.9
GSWA 148925: coarse lithic sandstone							
1	1808 ± 9	0.281619	0.001747	0.077895	0.281559 ± 0.000020	-2.6 ± 0.7	2.7
2	1777 ± 11	0.281595	0.001542	0.073248	0.281543 ± 0.000009	-3.9 ± 0.3	2.7
3	2547 ± 12	0.281277	0.000863	0.024608	0.281235 ± 0.000010	2.8 ± 0.4	2.9
4	2762 ± 10	0.281177	0.000784	0.031874	0.281136 ± 0.000012	4.2 ± 0.4	3.0
5	1844 ± 19	0.281618	0.000712	0.030119	0.281593 ± 0.000012	-0.6 ± 0.4	2.6
6	2653 ± 6	0.281169	0.000265	0.011138	0.281156 ± 0.000010	2.4 ± 0.3	3.0
7	2727 ± 4	0.280956	0.001141	0.050757	0.280896 ± 0.000011	-5.1 ± 0.4	3.5
8	1800 ± 14	0.281508	0.001008	0.046033	0.281474 ± 0.000009	-5.9 ± 0.3	2.9
9	1811 ± 18	0.281531	0.000450	0.021704	0.281516 ± 0.000013	-4.1 ± 0.5	2.8
10	1813 ± 12	0.281485	0.000921	0.036522	0.281453 ± 0.000015	-6.3 ± 0.5	2.9
11	1793 ± 14	0.281480	0.001393	0.053293	0.281433 ± 0.000011	-7.5 ± 0.4	3.0
12	1946 ± 13	0.281533	0.000000	0.030000	0.281533 ± 0.000010	-0.4 ± 0.3	2.6

Analysis no.	$^{207}Pb/^{206}Pb$ date (Ma)			$^{176}Hf/^{177}Hf$ measured	$^{176}Lu/^{177}Hf$ measured	$^{176}Yb/^{177}Hf$ measured	$^{176}Hf/^{177}Hf$ initial			$\varepsilon Hf_{(i)}$			T_{DM2} (Ga)
13	1982	±	13	0.281268	0.000504	0.024057	0.281249	±	0.000010	-9.7	±	0.3	3.2
14	1976	±	10	0.281392	0.001050	0.051700	0.281353	±	0.000019	-6.1	±	0.7	3.0
15	2618	±	23	0.281166	0.000083	0.003045	0.281162	±	0.000012	1.8	±	0.4	3.0
16	1796	±	29	0.281528	0.000288	0.012212	0.281518	±	0.000010	-4.4	±	0.4	2.8
17	3282	±	7	0.280567	0.000462	0.018155	0.280538	±	0.000012	-4.9	±	0.4	3.9
18	1974	±	18	0.281519	0.000550	0.020816	0.281498	±	0.000012	-1.0	±	0.4	2.7
19	1787	±	19	0.281496	0.000389	0.017839	0.281483	±	0.000013	-5.8	±	0.5	2.8
20	1762	±	12	0.281618	0.001195	0.051979	0.281578	±	0.000010	-3.0	±	0.3	2.6
1786–1610 Ma Bresnahan Group													
GSWA 143472: silicified sandstone													
1.1	1762	±	19	0.281518	0.000865	0.035279	0.281489	±	0.000010	-6.2	±	0.3	2.8
2.1	1779	±	19	0.281529	0.000816	0.027305	0.281501	±	0.000009	-5.3	±	0.3	2.8
3.1	1774	±	19	0.281569	0.000421	0.015582	0.281555	±	0.000010	-3.6	±	0.4	2.7
5.1	1769	±	19	0.281583	0.000542	0.020896	0.281565	±	0.000008	-3.3	±	0.3	2.7
14.1	2690	±	17	0.281048	0.001553	0.052605	0.280968	±	0.000012	-3.4	±	0.4	3.4
15.1	1808	±	20	0.281418	0.000789	0.027682	0.281391	±	0.000009	-8.6	±	0.3	3.0
27.2	1943	±	18	0.281632	0.000446	0.016409	0.281616	±	0.000010	2.4	±	0.4	2.4
28.1	1776	±	18	0.281557	0.000517	0.021520	0.281540	±	0.000010	-4.1	±	0.3	2.7
29.1	1991	±	19	0.281597	0.000616	0.029211	0.281574	±	0.000021	2.0	±	0.7	2.5
30.1	2641	±	17	0.281131	0.000553	0.023345	0.281103	±	0.000009	0.3	±	0.3	3.1
44.1	1782	±	19	0.281503	0.001421	0.047448	0.281455	±	0.000011	-6.9	±	0.4	2.9
45.1	2021	±	20	0.281593	0.001545	0.051772	0.281534	±	0.000010	1.3	±	0.3	2.6
1799–1620 Ma Mt Minnie Group													
GSWA 143473: sandstone													
14	1762	±	35	0.281289	0.001773	0.048698	0.281230	±	0.000019	-15.4	±	0.7	3.4
17	1810	±	19	0.281326	0.000754	0.020884	0.281300	±	0.000020	-11.8	±	0.7	3.2
20	2359	±	18	0.281220	0.000245	0.007067	0.281209	±	0.000027	-2.5	±	0.9	3.1
21	1784	±	19	0.281369	0.000469	0.018758	0.281353	±	0.000014	-10.5	±	0.5	3.1
22	1791	±	19	0.281362	0.001088	0.029576	0.281325	±	0.000018	-11.3	±	0.6	3.2
23	1779	±	19	0.281290	0.001087	0.030275	0.281253	±	0.000022	-14.2	±	0.8	3.4
26	1774	±	20	0.281411	0.000271	0.007550	0.281402	±	0.000043	-9.0	±	1.5	3.0
34	1792	±	19	0.281341	0.001011	0.038079	0.281307	±	0.000013	-12.0	±	0.5	3.2
35	1787	±	19	0.281386	0.000876	0.024166	0.281356	±	0.000020	-10.3	±	0.7	3.1
36	1796	±	19	0.281357	0.000868	0.023537	0.281327	±	0.000017	-11.1	±	0.6	3.2
37	1789	±	19	0.281420	0.000513	0.021004	0.281403	±	0.000012	-8.6	±	0.4	3.0
40	2701	±	17	0.280785	0.000774	0.034029	0.280745	±	0.000009	-11.1	±	0.3	3.9
45	2536	±	35	0.281064	0.000964	0.039806	0.281017	±	0.000015	-5.2	±	0.5	3.4

NOTES:
Lu–Hf isotopic data for detrital and magmatic zircons from potential sources regions including the Northern Capricorn Basins and the Gascoyne Province. Geochronology data available at <www.dmp.wa.gov.au/Geochron>.

This Report outlines the depositional and deformation history of the 1679–1067 Ma Edmund and Collier Basins of the Capricorn Orogen. The Edmund Basin formed during the 1680–1620 Ma Mangaroon Orogeny by the normal reactivation of pre-existing, major, crustal-scale faults to produce a half-graben architecture. Regional-scale extension has been calculated at ~7–8%. Paleocurrent directions indicate sediment supply largely from the north, but the age and Hf isotopic composition of detrital zircons from the Edmund Basin indicate derivation mostly from the Gascoyne Province to the south. These zircons represent multicycle detritus, having been recycled through various sedimentary basins in the southern Pilbara region. The architecture of the 1171–1067 Ma Collier Basin is still poorly known, but the age and isotopic composition of detrital zircons indicate that the sediments were sourced directly from the underlying rocks of the Edmund Basin. Total regional-scale shortening during all post-depositional orogenic events is calculated at ~21%. The Edmund and Collier Basins contain a wide range of mineral occurrences including the stratabound polymetallic Abra deposit and supergene Ilgarari and Butcherbird deposits. Many of these are associated with major crustal-scale faults that have been reactivated multiple times.

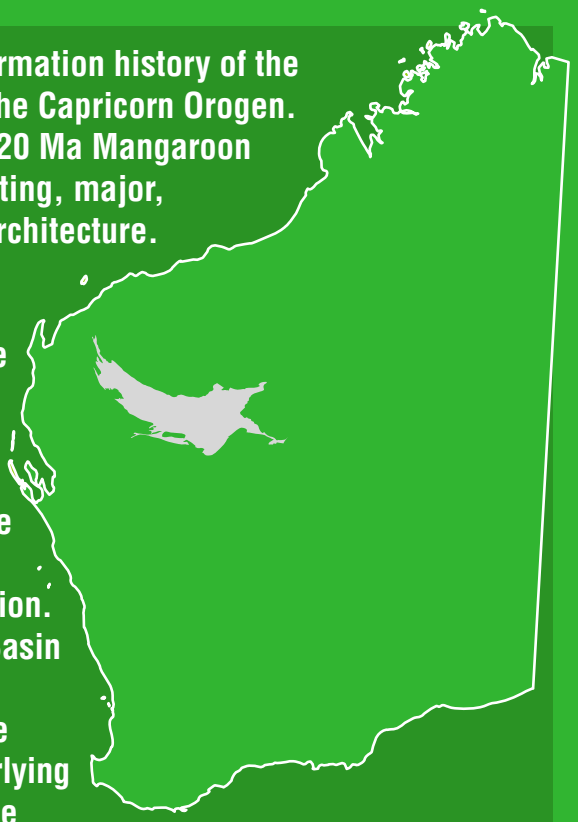

Further details of geological products and maps produced by the Geological Survey of Western Australia are available from:

Information Centre
Department of Mines and Petroleum
100 Plain Street
EAST PERTH WA 6004
Phone: (08) 9222 3459 Fax: (08) 9222 3444

www.dmp.wa.gov.au/GSWApublications

CUTTEN et al.

DEPOSITION, PROVENANCE, INVERSION HISTORY AND MINERALIZATION OF THE PROTEROZOIC EDMUND AND COLLIER BASINS, CAPRICORN OROGEN

REPORT 127